# Combination of infrared synchrotron radiation with optical near-eld microscopy techniques

Miguel Silveira

Thèse

présentée par

Miguel Patricio da Silveira

pour obtenir le grade de

Docteur de l'Université Joseph Fourier - Grenoble I

Physique de la matière condensée et du rayonnement

# IRS SNOM

# Apport du rayonnement synchrotron infrarouge aux techniques de microscopie en champ proche optique

Directeurs de thèse:

Dr. Fabio Comin et Prof. Serge Huant

Membres du Jury:

| | |
|---|---|
| Dr. Bruno Masenelli | Rapporteur |
| Prof. Antonio Cricenti | Rapporteur |
| Dr. Fabio Comin | Examinateur |
| Prof. Serge Huant | Examinateur |
| Prof. Joel Chevrier | Examinateur |
| Dr. Paul Dumas | Examinateur |

Grenoble, 15 dècembre 2009

# Abstract

My project is concerned with the development of an infrared aperture-less scanning near-field optical microscope (SNOM) that will use the synchrotron radiation of the ESRF as source of infrared light. This radiation has two main particularities well-suited to spectroscopic studies: this is a white source of light covering the near infrared band from 5 to 15 $\mu m$ where tunable laser sources are still under development and it is very bright and stable, both in time and space [DPGO05]. Once developed, the microscope will be applied to the infrared spectroscopy - essentially vibrational - and diagnosis of materials and of local nanostructures which are of current interest to the micro and nanoelectronic industry [RCB$^+$02].

As my project is very instrumental, the beginning was dedicated to the conception of a microscope system, starting with nothing and having all the needed materials at the end of the first year.

The second year was dedicated to the integration and implementation of the experimental setup, to the understanding of its functionalities and to trials for validating the new tool.

Afterwards we were fully committed to researching and understanding this unique tool. We have started with some preliminary results and then it would essentially be a question of allocated experimental time until obtaining the results that we had aimed for.

Our setup is unique and therefore the works we have for reference are from groups using the same techniques operating under very different conditions [WFA03; FWA05a; FWLA04; RGEH05; Hil04; GAS$^+$00b; Suk04; TKH04]

Our main difficulty is in detecting a weak signal, which we had expected to succeed. I will show later some calculations that made us believe so. One of our reference groups managed to do it in simpler conditions than ours, but it is worth recalling that it took them 3 years to adjust their setup sensitivity, thereby confirming that these are very hard techniques.

Our starting idea was of using synchrotron radiation as illuminating source in the infrared range because of its characteristics. This is a white light source, with all the wavelengths present at the same time, allowing us to perform spectroscopy, meaning that we will obtain chemical information of the sample [Hil04; MGCS04]. This is the big novelty comparing with the

other works. It turned out that the light is rather weak which makes the search for the signal a difficult task.

Our setup should then be tested with a laser, which is several orders of magnitude more powerful than the synchrotron radiation, and what might be a good debugging tool. This seems a good alternative to better understand what are the critical points that must be improved in our system.

The lasers to use could be visible, infrared ($CO_2$), or tunable. For spectroscopy, the tunable lasers are not only less stable but they are also more restricted in the spectral range to the very near infrared part of the spectrum than the synchrotron radiation.

The ESRF synchrotron facility is my home lab, and I have worked in collaboration with the CEA-LETI for the development of this tool.

# Résumé

Mon projet porte sur l'élaboration d'un microscope optique en champ proche (SNOM) sans ouverture fonctionnant dans le domaine de l'infrarouge et utilisant le rayonnement synchrotron de l'ESRF comme source de lumière infrarouge. Ce rayonnement a deux particularités bien adaptées aux études spectroscopiques: c'est une source de lumière blanche couvrant la bande du proche infrarouge de 5 à 15 $\mu m$ alors que les sources lasers accordables sont encore en développement. Il est très brillant et stable, à la fois dans le temps et dans l'espace. [DPGO05] Une fois élaboré, le microscope sera appliqué à la spectroscopie infrarouge - essentiellement vibrationelle - et le diagnostic des matériaux et des nanostructures qui sont d'intérêt actuel pour l'industrie micro et nanoélectronique [RCB$^+$02].

Comme mon projet est trés instrumental, le début a été consacré à la conception de tout un système de microscopie, à partir du zéro et avec tout le matériel nécessaire disponible à la fin de la première année.

La seconde année a été consacrée à l'intégration et la mise en œuvre du dispositif expérimental, à la compréhension de ses fonctionnalités et à des essais de validation du nouveau outil.

Après nous nous sommes pleinement engagés dans la recherche et la compréhension de cet outil unique. Nous avons commencé par quelques résultats préliminaires, puis cela a été essentiellement une question de temps expérimental alloué pour obtenir les résultats que nous avions visés.

Notre configuration est unique et donc les travaux que nous avons pour référence sont ceux de groupes utilisant les mêmes techniques d'exploitation dans des conditions trés différentes [WFA03; FWA05a; FWLA04; RGEH05; Hil04; GAS$^+$00b; Suk04; TKH04].

Notre principale difficulté est de détecter un signal faible. Je montrerai plus loin quelques calculs qui nous y ont fait croire. Notre groupe de référence a réussi à le faire dans des conditions plus simples que les nôtres, mais il est utile de rappeler que cela leur a pris 3 ans pour adapter leur sensibilité à l'installation, ce qui confirme que ce sont des techniques trés dur.

Notre idée de départ était d'utiliser le rayonnement synchrotron comme source de lumière dans l'infrarouge en raison de ses caractéristiques. Il s'agit d'une source de lumiére blanche, avec toutes les longueurs d'onde

présentes en même temps, nous permettant d'effectuer une spectroscopie, ce qui signifie que nous obtiendrons une information chimique sur l'échantillon [Hil04; MGCS04]. Telle est la grande nouveauté en comparison avec les autres travaux. Il s'est avéré que la lumière est assez faible ce qui rend la recherche du signal difficile.

Notre installation doit alors être testée avec un laser, qui est de plusieurs ordres de grandeur plus puissant que le rayonnement synchrotron, et qui pourrait être un bon outil de débogage. Cela semble une bonne alternative pour mieux comprendre les points essentiels qui doivent être améliorés dans notre système.

Les lasers à utiliser pourraient être visible, infrarouge ($CO_2$), ou accordable. Pour la spectroscopie, les lasers accordables sont non seulement moins stables mais ils sont aussi plus limités dans la gamme spectrale sur la partie infrarouge proche du spectre, que le rayonnement synchrotron.

Le synchrotron de l'ESRF est mon laboratoire d'accueil, et j'ai travaillé en collaboration avec le CEA-LETI pour le développement de cet outil.

# Contents

# Introduction

## L'état de l'art

Microscopie à sonde locale est largement connue et développée. C'est un concept très polyvalent permettant de nombreuses configurations différentes, spécifiques pour chaque type de recherche.

Pour ce projet, il a été décidé que la bonne configuration SNOM sans ouverture serait similaire à celle utilisée par les groupes effectuant des recherches avec des objectifs similaires comme Y. de Wilde ou T. Taubner [WFC+06; TKH04]. Ce que nous avons en commun avec les groupes visés est l'utilisation d'un microscope à force atomique combinée à un éclairage infrarouge, dans le but d'obtenir en même temps, l'information topographique et information de l'infrarouge de l'échantillon.

Ce qui différencie ce projet à partir des travaux d'autres groupes est qu'ils se tournent pour contraste infrarouge car ils utilisent la lumière monochromatique. Leur prochaine étape est d'essayer de présenter les capacités spectroscopiques dans leurs techniques de microscopie, ce que nous essayons déjà [WFC+06].

## Objectifs

La spectroscopie infrarouge a été largement utilisé pour caractériser chimiquement les matériaux et surfaces à l'échelle micrométrique. La réduction de l'échelle de micro à nano, assurez phénomènes physiques et chimiques inaccessible par microscopie infrarouge classique, qui est limitée par la diffraction et a une résolution de quelques micromètres dans l'infrarouge. Opérant en champ proche devrait permettre d'atteindre des résolutions de la taille du sommet de la pointe, c'est-à moins de 100 nm. Cela présente un intérêt particulier pour la biotechnologie, la microélectronique et microtechnologies. Dans ce contexte, l'objectif de ce projet est de combiner la lumière à large bande infrarouge produits par un synchrotron avec un microscope à champ proche optique fonctionnant à la fois en microscopie et dans les modes de spectroscopie.

Afin d'atteindre cet objectif, un microscope prototype a été développé

et installé à la source de rayonnement infrarouge ESRF.

Une première étape de ce projet était de montrer que le rayonnement synchrotron infrarouge a brillance suffisante pour être utilisées en microscopie en champ proche optique. Cela requiert l'espace éclairé sur l'échantillon d'avoir une densité d'énergie permettant un signal exploitable sur bruit.

Une deuxième étape était de faire de ce prototype, un dispositif de balayage avec la sensibilité requise et une résolution spatiale de ce type de microscopie tout en conservant la possibilité d'effectuer la spectroscopie. Cela permettrait à la caractérisation de nouveaux matériaux et des structures produites par les nanotechnologies modernes.

Développés par spectroscopie infrarouge (IRS) scanning near-field optical microscope (SNOM) devrait avoir une résolution inférieure à 100 nm et une sensibilité compatible avec l'analyse locale de l'etat des liaisons chimiques .

**Sommaire**

Le long de ce document, les bases nécessaires pour comprendre le développement de cet instrument sera décrite. Cela comprend une partie dédiée à la microscopie à force atomique (AFM), un autre à la microscopie optique et une courte présentation de rayonnement synchrotron. Ensuite, le développement de l'instrument est présenté en détail, suivi par les perspectives et les conclusions.

# Introduction

## State Of The Art

Local probe microscopy is widely known and developed. It is a very versatile concept allowing many different configurations, specific for each kind of research.

For this project it was decided that the right apertureless SNOM configuration would be similar to the one used by groups doing research with similar goals as Y. de Wilde or T. Taubner [WFC+06; TKH04]. What we have in common with the referred groups is the use of an Atomic Force Microscope combined with infrared illumination, with the purpose of obtaining at the same time topographic information and infrared information from the sample.

What differentiates this project from the other groups work is that they look at infrared contrast since they use monochromatic light. Their next step is to try and introduce spectroscopic capabilities into their microscopy techniques, what we are already trying [WFC+06].

## Goals

Infrared spectroscopy has been widely used to chemically characterize materials and surfaces at the micrometric scale. The scale reduction from micro to nano, make physical and chemical phenomena unreachable through classical infrared microscopy which is limited by diffraction and has a resolution of a few micrometers in the infrared. Operating in near-field should allow to reach resolutions of the size of the tip apex, that is, less than 100nm. This is of particular interest to biotechnology, microelectronics and other microtechnologies. In this context, the aim of this project is to combine the broad-band infrared light produced by a synchrotron with a near-field optical microscope operating both in microscopy and in spectroscopy modes.

In order to achieve this goal, a prototype microscope was developed and installed at the ESRF infrared beamline.

A first step for this project was to show that the synchrotron infrared light has enough brilliance to be used in near-field optical microscopy. This

requires the illuminated spot on the sample to have an energy density allowing an exploitable signal to noise ratio.

A second step was to make of this prototype a scanning device with the required sensitivity and spatial resolution for this kind of microscopy while conserving the possibility to perform spectroscopy. This would allow the characterization of new materials and structures produced by modern nanotechnologies.

The developed infrared spectroscopic (IRS) scanning near-field optical microscope (SNOM) should have a resolution smaller than 100nm and sensitivity compatible with local chemical bonds state analysis.

## Thesis Outline

Along this document the fundamentals needed to understand the development of this instrument will be described. This includes one part dedicated to atomic force microscopy (AFM), another to optical microscopy and a short presentation of synchrotron radiation. Afterwards the development of the instrument is presented in detail, followed by the perspectives and conclusions.

- Therefore on the first chapter, the atomic force microscopy principles are presented as well as the modes of operation. Then follows a discussion about the force sensor to be used. The objective of this chapter is to justify the technological choices of the AFM to develop, since it is going to be coupled with light and operate as on optical microscope;

- The second chapter is dedicated to optical microscopy, from classical microscopy to the subwavelength regime. The optical nearfield will be presented as well as the way it can be used in optical microscopy. Afterwards, the particular case of white light illumination which leads to spectroscopic capabilities is explored;

- The third chapter is dedicated to the particularity of this project, the synchrotron as infrared light source. It will briefly describe the way the light is extracted since it is not very common to use synchrotron infrared. The characteristics of this light are presented;

- The fourth chapter is the longest and describes all the development of the instrument. From the production of the tips that are probably the most important detail, to the integration of the whole system in the synchrotron. Also the conception and design of the AFM is detailed along with its performance results. To conclude, the experiments and preliminary results are presented;

- The fifth and last chapter describes new experiments done with lasers in an effort to better understand this delicate system. A new mechanical prototype is presented and the setup configuration for laser experiments that was used;
- Finally some conclusions are formulated about the work done and the results obtained.

# Chapter 1

# AFM

## 1.1 Résumé

Sur ce premier chapitre, les principes de la microscopie à force atomique sont présentés ainsi que les modes de fonctionnement. Suit alors une discussion sur le capteur de force à utiliser. L'objectif de ce chapitre est de justifier les choix technologiques de l'AFM à se développer, car elle va de pair avec la lumière et de fonctionner comme un microscope optique.

**Contents**



## 1.2 Introduction

Imaging individual atoms can be done by using X-ray or electron scattering techniques for example, but real space imaging was only achieved in 1981 by Binnig and Rohrer [BRGW82] with their invention, the scanning tunneling microscope (STM). They were awarded the Nobel Prize in Physics

for this in 1986. This microscope with its spectacular lateral resolution was extensively used in surface science with great impact. Nowadays it became a rather standard tool.

Although successfull, the STM is limited to conductive samples in order for the tunneling to occur from or towards the tip, depending on the bias. It was noticed that when the tip to sample distance was small, other forces would be sensed. Soon, these forces started to be used in the so called atomic force microscope (AFM), invented by Binnig in 1986. The big advantage is that while the STM requires surface preparation and ultra high vacuum environment, the AFM can image virtually any flat surface in ambient conditions. Consequently there are many AFMs in use in laboratories all around the world. Nevertheless, to reach the atomic resolution vacuum is required.

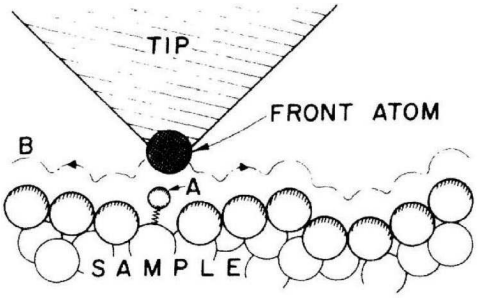


Figure 1.1: *Scanning tunneling microscope (STM) or atomic force microscope (AFM). Source [BQG86]*

## 1.3 Principle

The AFM and the STM are only different on the working principle. The use of a sharp tip close to the sample is common in both microscopies as illustrated in figure 1.1. The sharp tip is mounted on a $xyz$ piezo scanner capable of very small displacements in the three directions. In the case of the STM, the tip is metallic and there is a tunneling current flowing between sample and tip when the distance is of a few atomic diameters. This current is used as a feedback signal to control the distance in $z$. In the AFM, the metallic tip alone is replaced by a whole force sensor which can be equipped with an optical near-field probe, a thermometer or other kind of probes, giving rise to a large variety of scanning probe microscopes [Wic89].

On a simple AFM, the potential energy between tip and sample $V$ generates a $z$ component of the tip-sample force $F = -\partial V/\partial z$ and a spring constant $k = -\partial F/\partial z$. The AFM uses this $F$, or some derived entity, as the imaging signal.

Images can be obtained by scanning the probe in the $xy$ plane recording the $z$ position required to keep the $F$ signal constant, or keeping the $z$ position constant, recording the $F$ signal variation. A computer coordinates the scanning process, registers the signal and retrieves a 3D image, $z(x, y, F = const)$ or $F(x, y, z = const)$. The lateral resolution is proportional to the tip apex radius, therefore the smaller the tip the better resolution.

$F$ has got long and short range contributions of essentially electromagnetic origin. At close proximity to the sample, less than $1nm$, repulsive short range forces are dominant due to electron clouds interaction, or in other words, chemical forces. At $1nm$ or more, attractive long range forces are dominant like electrostatic, van der Waals and magnetic forces. If not in vacuum there will also be the presence of a viscous meniscus due to humidity.

## 1.4 Force Sensor


Figure 1.2: *AFM cantilever and tip - force sensor.*

The central element of a force microscope is the force sensor. In order to be sensitive to normal tip-sample forces it should behave like a spring in the $z$ direction. This is typically achieved with a microfabricated Si cantilever beam with a tip integrated [WBG91]. It has a specific resonance frequency $f_0$ and other important properties are the stiffness $k$, the quality factor $Q$, the variation of the resonance frequency with the temperature and which material the tip is made of. The stiffness is given by

$$k = \frac{E}{4}\omega\left(\frac{t}{l}\right)^3$$

where $E$ is the Young's modulus, $\omega$ is the width, $t$ the thickness and $l$ the length according to figure 1.2 [Che08]. The cantilever has a sharp pyramidal tip on its end and has low spring constant which leads to low resonant frequencies.

In order to detect the movements of the cantilever edge, a laser is focused on its top surface and the reflection is aligned with the center of a four quadrant photo diode like illustrated in figure1.3. In this way it is possible to determine the position and deflection of the cantilever at each moment and to feed this information to the piezo actuator that regulates the tip sample distance.

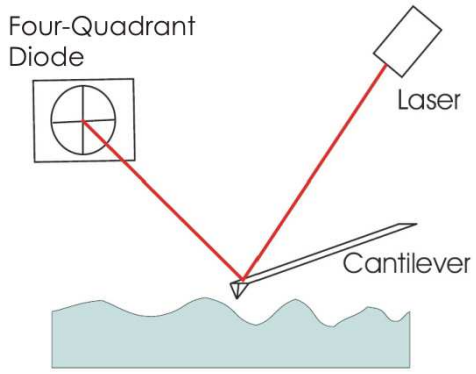


Figure 1.3: *AFM cantilever position detection.*

Some cantilevers have a deposited layer of piezoresistive material that allows measuring the deflection with an electrical signal.

## 1.5 Modes of Operation

As far as tip-sample distance control is concerned, there are several possibilities.

Considering the cantilever presented above and its stiffness $k$, when a force $F$ is applied, the resulting deflection $\Delta z$ is proportional to that force according to the Hooke relation $F = k\Delta z$. The amplitude of this deformation is measured as described before. Because of this optical system for detection, it is usually the sample that is displaced, both for scanning the surface and for the tip approach. An image is made by scanning the surface at constant force, measuring the cantilever deflection and adjusting the sample position $z$.

### 1.5.1 Static Modes

In this mode, also known as contact mode, the tip pushes the sample with a fixed force which is the value of the set point chosen for regulation. The forces involved here are the electronic repulsive forces from the Lennard-Jones potential. Samples are likely to deform if the cantilever is stiff and pushing hard, so this is a soft contact technique.

A profile at constant force can be obtained and corresponds to a total constant density of states, which is the closest to the topography. The cantilever deflection is used to feedback the circuit that controls the scanner, responding to the topography by keeping the deflection constant.

Otherwise, the profile can be acquired at constant-height where the cantilever deflection signal can generate directly the topography. This method is faster because there is no response time of the feedback circuit.

This mode quantifies the surface roughness with a high precision.

### 1.5.2 Dynamic Modes

In the dynamic modes of operation, the force sensor is deliberately vibrated. There are essentially two methods: the amplitude modulation (AM) and the frequency modulation (FM). In AM-AFM, introduced by Martin *et al.* [MWW87], the force sensor is driven at a fixed amplitude and at a fixed frequency, different from the resonance frequency. When the tip is close to the surface, elastic and inelastic interactions change the vibration phase and amplitude. These changes are used as feedback signal. The amplitude change is rather slow and becomes slower with higher quality factors of the resonator. This was improved when Albrecht *et al.* [AGHR91] introduce the FM-AFM where the change in frequency happens in the timescale of a single cycle.

In this method the force sensor with an *eigenfrequency* $f_0$ and spring constant $k$ is subjected to a positive feedback which enforces a constant oscillation amplitude $A$ [AGHR91; DZS92]. The frequency $f$ is determined by $f_0$ of the force sensor and the phase shift $\varphi$ between the excitation signal, input and the force sensor signal, output. When $\varphi = \pi/2$, the loop oscillates at $f = f_0$. Forces between tip and sample cause a change in $f = f_0 + \Delta f$ as illustrated in figure 1.4. By measuring the frequency shift $\Delta f$, the tip-sample force gradient can be determined.

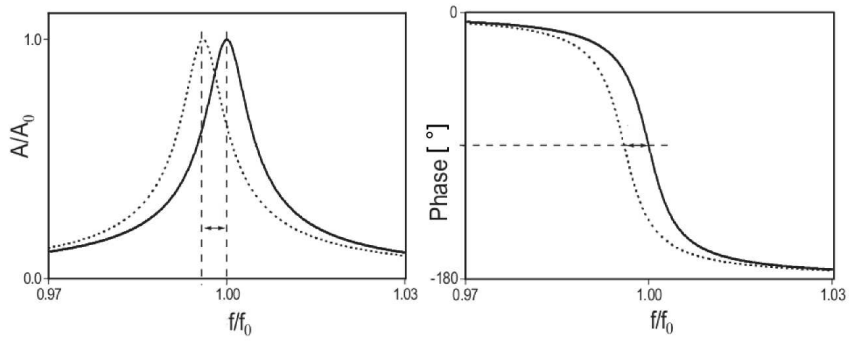


Figure 1.4: *Frequency shift observed during FM-AFM mode.*

Moreover, the oscillation amplitude depends on the excitation frequency and on the damping acting on the force sensor. If the excitation frequency is the same as $f_0$ then the amplitude is maximized, since this is the resonance condition. As for the damping, if the excitation energy is the same and the amplitude is smaller, the Lorenz curve that represents the resonance curve of the oscillator, will be broader.

## 1.6 Tuning Fork

In the 1970's the watch industry introduced the quartz tuning fork (TF) as frequency standards in clocks [Wal85; Mom97]. Readily after the invention of the AFM, these tuning forks were used as force sensors. For example, Karrai [KG95] used one on a scanning near field optical microscope (SNOM). Tuning forks are the preferred solution for SNOM microscopes because they allow to easily hold an optical fiber perpendicular to the surface, making it oscillate in the parallel direction for measuring the interaction with the surface and thus controlling the sample-probe distance. Karrai and others [KG95; RIS$^+$99; HGM02] have demonstated its use for low temperatures. Many home made AFMs were designed to use the TF. [Gie98; SCZC07; SJH02; RvHRW99; LA06; HKRF04].

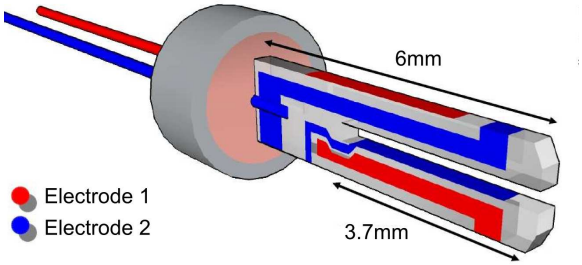


Figure 1.5: *Crystal quartz Tuning fork and electrical contacts distribution.*

In figure 1.5 a quartz tuning fork and its electrical contacts are illustrated. The tuning fork comes inside a metallic cylinder which is readily removed in order to give access to the TF. The tuning forks are good for use as force sensors because of the high quality factor ($Q$) despite the high stiffness values due to their geometry. They have specific oscillation modes where the two prongs are coupled and vibrate in a symmetric fashion and resonate at specific *eigenfrequencies*. The large geometry allows a wide selection of tips to be mounted with simple tools and no micromachining is needed.

Because of quartz piezoelectricity the electrical contacts can read an electrical signal after mechanical deflection. Alternatively the contacts can be used to electrically excite the vibration movement on the tuning fork. These contacts are strategically positioned to favour the use of piezoelectricity.

### 1.6.1 Excitation

There are several ways of exciting the tuning fork and it can happen that the excitation is being made by two different processes at the same time, if they overlap or there is an interference. The possibilities are:

- acoustic excitation, through air;

- electric excitation, by applying an ac voltage to the contacts;
- electromagnetic excitation, through the deposited electrical contacts working as antennas;
- mechanic excitation, by propagation of vibrations through the support, originated on a distant source.

Acoustic excitation is efficient for very small oscillation amplitudes, but on the other hand, the source of excitation needing a rather high voltage to actuate, it can induce electromagnetic excitation, which requires adequate shielding. It is also very sensitive to setup conditions [Rod09].

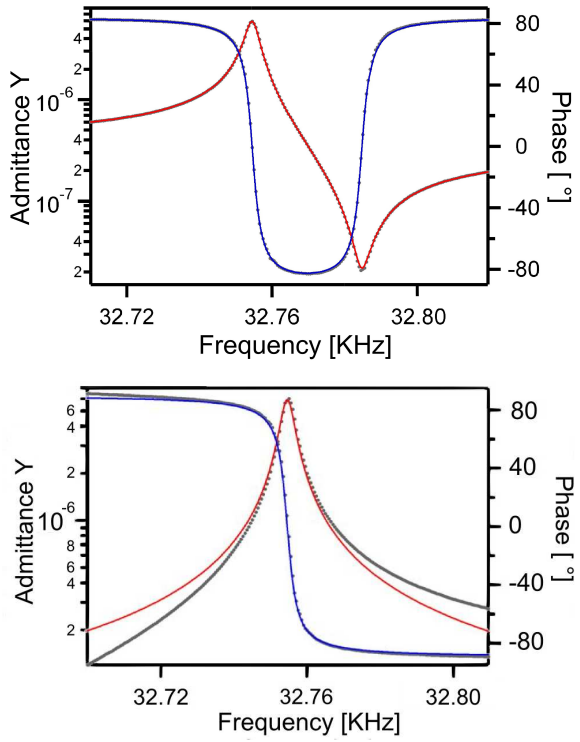


Figure 1.6: *Tuning fork electric excitation: asymmetric response and symmetric response with compensation circuit.*

Electric excitation is a popular way of exciting the tuning fork. It was the choice we made at the beginning of this project. When a voltage is applied to the electrical contacts a capacitance appears between the contacts with the quartz as the dielectric medium. In this way the response signal will be the addition of two currents: the current due to the capacitance, always present, plus the current generated by the oscillations due to the piezoelectric effect. The resonance curve is then distorted as illustrated in the first graph

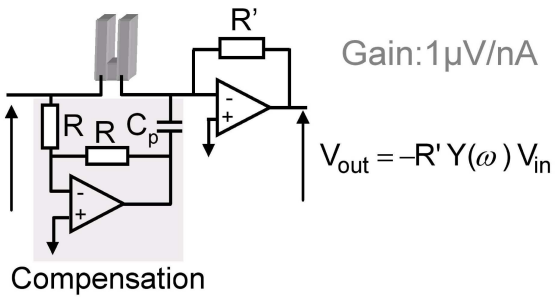


Figure 1.7: *Electrical circuit used to compensate for the tuning fork capacitance, with another tuning fork.*

of figure 1.6 where an anti-resonance appears. On the second graph the distortion was compensated by incorporation of an electrical circuit where another tuning fork is used to compensate exactly for the capacitance, as illustrated in figure 1.7. The same current is generated but with opposite phase. The distortion is canceled but an insignificant non horizontal base line persists.

Electromagnetic excitation appears in general only as contamination and interference. It has the same distorting behaviour of the electric excitation but even more accentuated. This means that all signals traveling through wires close to the tuning fork should be well shielded.

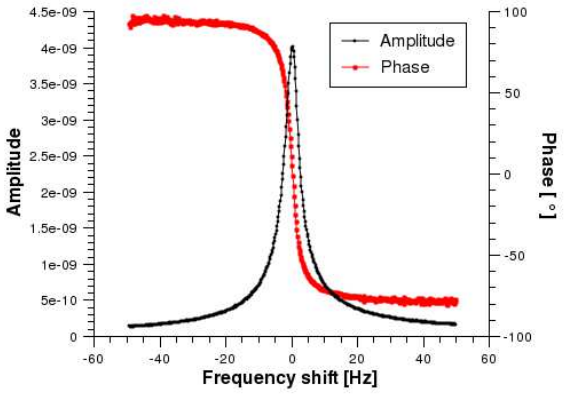


Figure 1.8: *Amplitude and phase signal read when using mechanical excitation.*

Mechanical excitation is the method adopted later in this project and is achieved by inducing a mechanical vibration to the tuning fork through its holding support. For this purpose, a dithering piezo is usually glued on the tuning fork's mount. In this process the only signal present in the tuning fork

contacts is the current generated by piezoelectric effect, purely proportional to the oscillations, as illustrated in figure 1.8. Another advantage of this method is that the dither piezo can be glued far away from the tuning fork, so that a higher voltage is needed to excite the tuning fork, obtaining therefore a better resolution in the tuning fork oscillating amplitude.

### 1.6.2 Detection and Signal Calibration

When a tuning fork vibrates, the quartz is stressed. Across the crystal, electric charges are separated inducing a voltage. These conditions generate an ac current that can be measured and related to the tuning fork motion. A transimpedance amplifier is used, converting the current into a voltage with amplification. If one wants to have a precise knowledge about the vibration amplitude, the applied tension for the excitation should be calibrated with the measured signal.

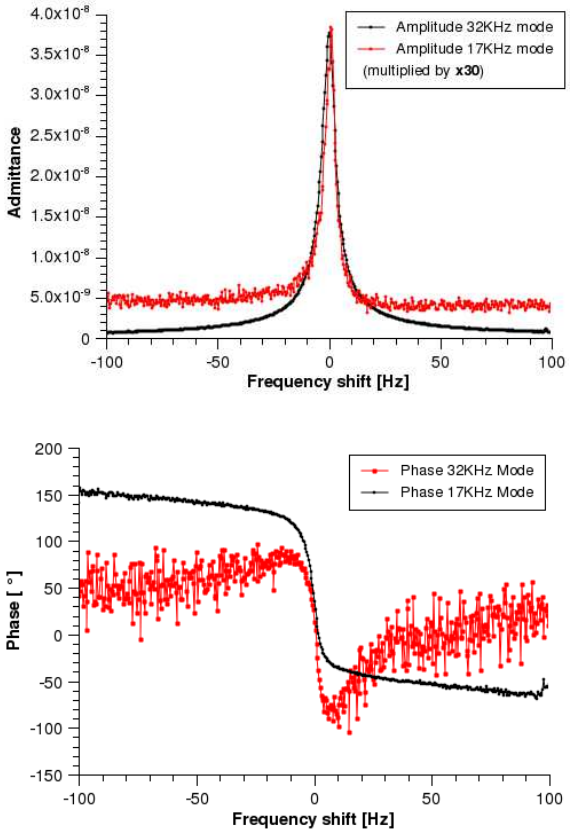


Figure 1.9: *Comparison between amplitude and phase of the two oscillating modes - 32KHz and 17KHz.*

The tuning fork has two fundamental oscillating modes that can be easily used. As illustrated in figure 1.9 one can see that they have different signal intensities. When comparing both cases, one signal has much lower amplitude and much noisier phase. This is due to the distribution of the electrical contacts being optimized for the other mode. Nevertheless, they are perfectly useable and usefull.

One of the modes has the resonance frequency at $17.87KHz$ and the prongs vibrate in the direction parallel to the tuning fork width, the smaller dimension. The other mode has the resonant frequency at $32.768KHz$ and the prongs vibrate perpendicularly to the previous mode. This is the optimized and more commonly used mode. These frequencies change whenever the tuning fork's characteristics change, for example by gluing a metallic tip to one of the prongs. The same will happen when during operation, the tuning fork will feel an interaction with the sample and change its vibration.

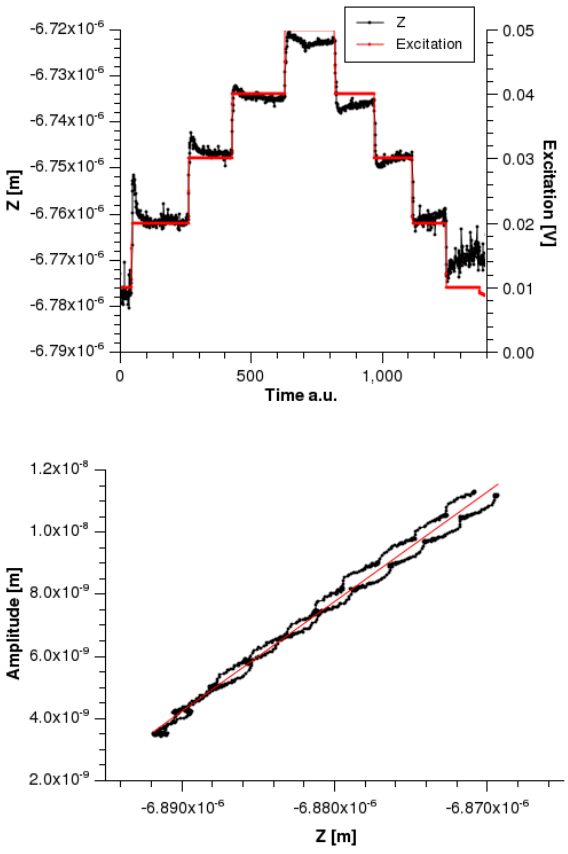


Figure 1.10: *Calibration procedure. First a comparison between the excitation signal and the Z response; second, a plot of the detected amplitude vs the displacements in Z.*

The method used for calibration consists in changing the excitation signal step by step and observe the change in $Z$, which represents the sample position with respect to the tip lowest point while it oscillates. Each step observed in $Z$ will then correspond to the change in vibration amplitude since the tip and sample are kept in distance regulation. If the measured amplitude is plotted against the $Z$ signal, the slope will give the calibration factor for the amplitude in $[mV/nm]$, because of the transimpedance amplifier. Both graphs are illustrated in figure 1.10. It is clear the piezo response to the change in excitation applied to the tuning fork. On the second graph the amplitude is actually a signal measured in $mV$ that is directly converted to $nm$ since the relation factor is set to the unity, after $10^{-7}$ amplification of the signal. Plotted against the real displacement in $Z$ the slope of the linear regression will directly give the calibration, the factor that will correctly convert the signal in $mV$ after the amplifier into $nm$.

This will allow to know the amplitudes involved when using the tuning fork.

#### Amplitude Linearity

In this project the chosen mode of operation is the tapping mode and with high vibration amplitudes because of optical reasons that will be discussed in the next chapter. There is the possibility of having to use the tuning fork with high amplitudes, near 100 nm [TKH05a].

An experiment was performed by Nicolas Chevalier and Frederico Martins [CRB+06] where the tuning fork would be excited to an extreme while observing the amplitude behaviour at the same time. The amplitude was measured with a Fabry-Perrot cavity, which is a technique that uses the interference between an incident laser beam and its reflection, in this case on the tuning fork's prong [Mar08]. The current generated by the tuning fork vibration was also measured which configures another way of calibrating the tuning fork's output signal with the oscillating amplitudes. As illustrated in figure 1.11 one can see the tuning fork's impressive linearity until amplitudes of about $1\mu m$.

This confirms the tuning fork as a good AFM force sensor when large oscillation amplitudes are required.

### 1.6.3 Shear Force

The two oscillation modes are usefull for addressing an important question for this project. The developed instrument is a local probe optical microscope (SNOM), which typically uses the tuning fork as force sensor but with an optical fiber attached [KG95]. The principle consists in oscillating a sharpened optical fiber parallel to the surface and approaching it to the surface until an interaction is felt by damping the oscillation. This interaction

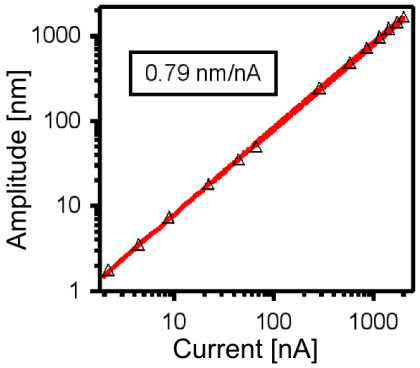


Figure 1.11: *Tuning fork oscillation amplitude linearity observed until* $1\mu m$ *with optical detection. Reading output current provides another calibration method.*

depends on distance and according to some authors [GAS+00a; KT00], it is felt about $20nm$ away from the surface, this is therefore a non-contact technique. Then the distance can be kept constant by maintaining the intensity of the interaction. This is the so-called shear force mode.

This mode is very relevant because optical fibers are fragile and replacing them on an AFM setup requires some considerable work.

Shear force is not fully understood since there is no clear physical explanation for it. Other authors [GBSU95] proposed that the probe was indeed having some contact with the surface. Other authors even explore the possibility of force fields acting on the parallel movement of the tip.

There are in fact dissipative and elastic forces acting on a particle moving parallel to a surface. The issue is the exact distance at which these forces start to be felt. Other than the friction on a surface, these forces can actually be felt at a distance from the surface but the magnitudes involved are very small and should not be strong enough to be felt by a tuning fork. These forces were probed with other more sensitive instruments than in Stipe *et al.* paper [SMS+01].

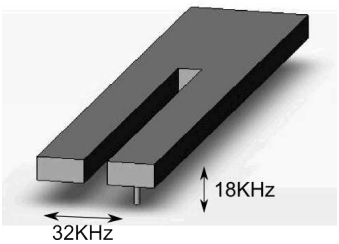


Figure 1.12: *Position of the tuning fork when both modes of vibration were simultaneously used.*

What are these forces that are used in SNOM ? Is there some tapping after all as described in the paper by Gregor *et al.* [GBSU95] ? This is where the two modes described above become usefull. By mechanically exciting the tuning fork with the two resonance frequencies at the same time, both modes vibrate at the same time. Using the tuning fork in the position illustrated in figure 1.12 and if one of the frequencies is nearly the double of the other, it will make the tip describe an eight-shaped horizontal figure.

Approach experiments were carried out in order to shed some light over this discussion. The sensor, tuning fork plus tip, was slowly approached to the surface, the movement perpendicular to the surface would do the distance control by tapping the surface, an understood method. At the same time and independently, when the movement parallel to the surface would start registering an interaction, signaling the presence of a shear force, one would know at what distance it happened with some precision. The modes were calibrated as described above, in order to ensure the control over the vibrations amplitude. These experiments were performed on gold and silicon samples, with different tip radius, different amplitudes, vacuum and air and the result was always exactly the same. Some results are presented in figure 1.13, where different amplitudes were used.

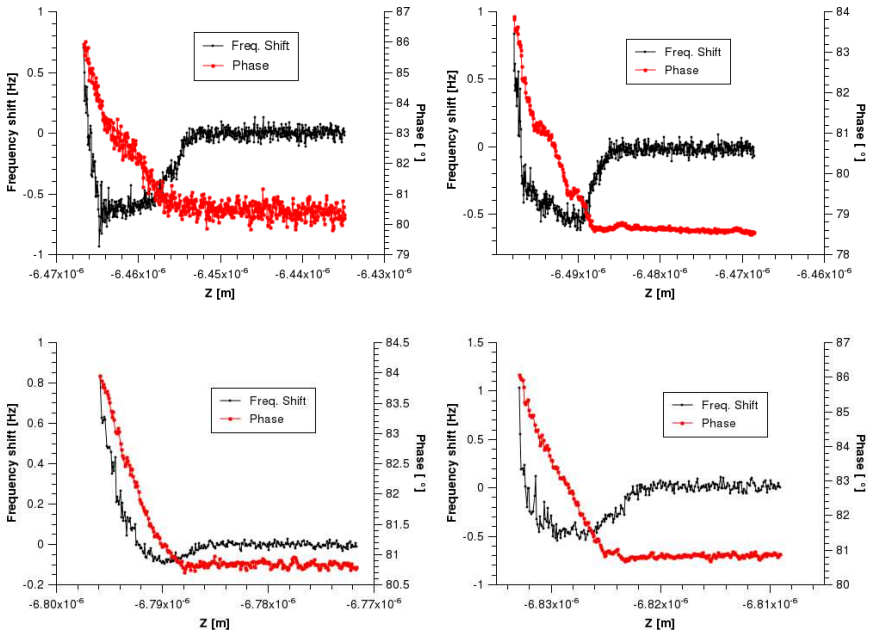


Figure 1.13: *Approach curves. Amplitude of tapping mode and phase of the shear mode, acquired simultaneously.*

The two first graphs are of the same oscillation amplitude in the tapping mode, 3 $nm$ and of different shear oscillation amplitudes, 1 and 10 $nm$

respectively. The other two graphics have the same shear oscillation amplitude 5 $nm$ and different tapping amplitudes, 10 and 3 $nm$ respectively. The smaller amplitudes bring noisier signals. It is always visible that the phase, corresponding to the shear mode, only changes after the tapping mode starts interacting with the surface, in the attractive part of the Lennard-Jones potential

These results lead to the conclusion that contact is essentially the cause of attenuation of the shear mode vibrations, in the range of the tuning fork sensitivity. Therefore, using the shear force for non-contact microscopy should be carefully thought of [GSPH00].

This is one of the reasons why the metallic tip working in tapping mode is the choice for this project.

## 1.7 Instrumentation

The conception of a local probe microscope implies the overcoming of some subtle instrumental difficulties. They have to do with the probe, the *ensemble* for tip-sample relative movement, with great precision. Moreover, the regulation system, the isolation from external vibrations are also very important.

### Scanning Devices

A local probe microscope has necessarily a system for positioning the probe relatively to the sample with a better precision than the desired resolution for the instrument. For atomic resolution it is needed a lateral precision of $0.1nm$ and $0.01nm$ for the vertical direction. Piezo electric motors are suitable for this with a typical a range of a few microns. These are of easy implementation and allow high frequency scans with good resolution. On the other hand, their behavior is not linear with the applied voltage, they present hysteresis, creep effects and they drift with time. Nevertheless these disadvantages can be corrected, compensated, or just minimized.

### Vibrations

In order to obtain the best possible resolution, the system should be isolated from external mechanical vibrations. The microscope can be isolated from external sources and should be of the more rigid conception possible. A tip usually works just a few nanometers away from a surface and the amplitude of external noise can easily be much larger. The more disturbing and more present noises are the natural vibrations of buildings, the vibrations caused by walking people, machines working or even acoustic vibrations because the frequency range is the same.

A cover can be installed to prevent the acoustic vibrations, a heavy base and elastic absorbers do the rest of the filtering plus the fact that rigidity of the microscope is the most important, preventing parts from resonating.

### Approach

An approach system is essential to bring the tip close to the sample into the dynamic range of piezo actuator. This system should have a travel of few milimeters and a resolution of at least half of the piezo travel. This system has to be a rigid connection between the tip and the sample.

### Control and Regulation

In order to regulate the measured physical quantity by the probe, an electronic system is needed to control the tip-sample distance. Usually this regulation is of the kind proportional, integral, differential (PID). The analog signal specific from the probe is sampled by a analog-digital converter (ADC). The DAC feeds the signal to a digital signal processor (DSP). The software that operates the DSP makes all the calculations for a PID regulation, whose result is sent to a digital-analog converter (DAC). Finally the output is sent to the piezo actuator. The same processor operates the $x, y$ coordinates and sends to a computer the regulated $z$ signal, for each coordinate pair. The computer can then produce an image. This computer is also the interface with the user.

# Chapter 2

# Spectroscopic Infrared SNOM

## 2.1 Résumé

Le deuxième chapitre est consacré à la microscopie optique, de la microscopie classique au régime sub-longueur. Le champ proche optique seront présentés, ainsi que la faon dont il peut être utilisé en microscopie optique. Par la suite, le cas particulier de l'éclairement de la lumière blanche qui conduit à des capacités spectroscopiques est explorée.

### Contents

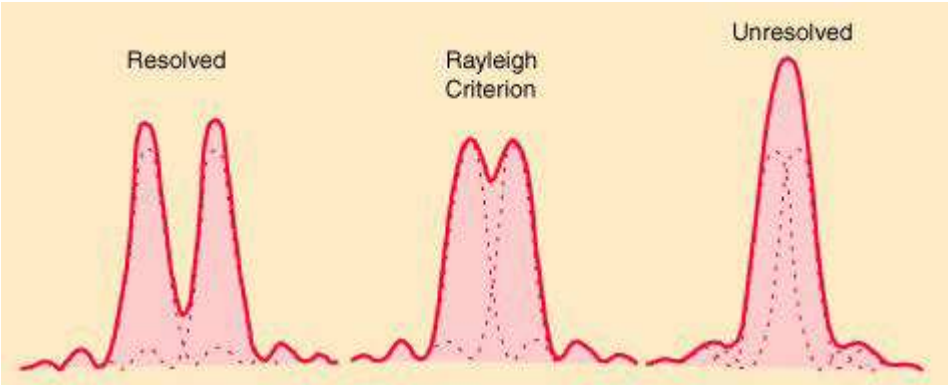


Figure 2.1: *Diffraction criteria.*

Microscopy is the ensemble of techniques for viewing objects and features that are too small to be seen by the naked or unaided eye. There are three well-known branches of microscopy, optical, electron and scanning probe techniques. In this work, the intention was to combine two of these techniques, the optical with the scanning probe technique. The latter is introduced in the last chapter and its combination with the optical technique will be presented here. This results in what is commonly designated by Scanning Near-field Optical Microscope, the SNOM.

We start by understanding the limitation in resolution of the classical optical microscopes.

## 2.2 Classical Microscopy Resolution

In microscopy, resolution describes the shortest distance between to objects where they can still be distinguished as separate entities by an instrument. This follows from the Abbe theory of image formation [Abb73]. Abbe came up with the so called Point Spread Function (PSF) which gives the intensity profile in the image plane due to a point source in the image plane. The resolution limit was pointed out by Rayleigh as the distance between two points for which the first intensity maximum of the Airy pattern of the first point coincides to the first intensity minimum of the Airy pattern of the second point.

The wave nature of light and the way it propagates, make lens-based microscopes limited in terms of resolution due to diffraction, which is given by the Rayleigh criteria,

$$D = 0.61 \frac{\lambda}{n \sin \theta} \tag{2.1}$$

where $D$ is the resolution, $\lambda$ is the wavelength of light, $n$ the refractive index of the medium between sample and objective and $\theta$ is the vertical half-angle

in which an object can be seen by the objective. [Ray79]. The $n \sin\theta$ is also known as the numerical aperture (NA), characteristic of an objective. This means that for the visible spectrum the maximum attainable resolution will be around 300nm, which is not enough if we want to characterize materials and structures produced by the nowadays technologies applied to nanosciences. In order to increase the resolving power of an optical microscope, we have to decrease the light wavelength using ultra violet or x-ray radiation for example, or we can use an objective with higher numerical aperture.

### 2.2.1 Confocal microscopy

Still in the context of seeking for a better resolution and contrast, I would like to say a few words about confocal microscopy since it is also an integrating element of the instrument developed in this project. The image obtained by a conventional microscope forms blurry images from features that are slightly out of the focal plane. Confocal microscopy was invented by Minsky and patented in 1957, and it introduces depth resolution by means of a pinhole, as illustrated in figure 2.2. In this way the amount of out-of-focus light reaching the detector is much smaller. [Vis93; MJT+96; Rad06] In fact, this contribution decreases proportionally to $1/z^2$, where $z$ is the distance to the focal plane. This creates the sectioning effect, when just a thin slice of the sample is imaged.

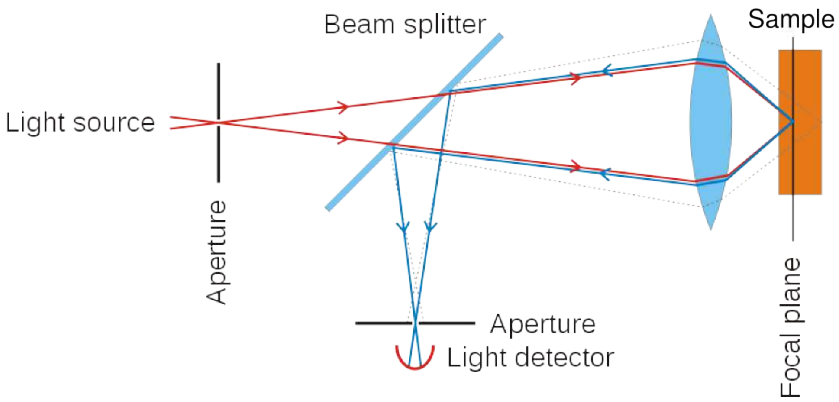


Figure 2.2: *Confocal Principle.*

The PSF now is the product between the PSF of the illuminating beam and the PSF of the detection pinhole, which brings an important increase in resolution of a factor of 1,4. [Min88]. Since this improvement comes from a filtering process, it is understood that this technique results better with powerfull illuminating sources like lasers.

Nevertheless, there is still the diffraction limit. If we wish to attain a better resolution, we have to tackle the problem with a different approach. One good idea is to simply inspect the light that does not propagate but remains trapped to the surface. This light can be detected if perturbed by the presence of a sharp object, which will make this wave propagate to a detector placed in the far-field at a large distance.

The details about this trapped light and about how can we detect it will be extended in the following sections.

## 2.3 Near-field

It has been long known that the surface limiting a solid body modifies locally the physical properties of many materials. [Zan88]. This produces specific surface phenomena like spontaneous polarization, electronic work function, electronic surface states, surface polaritons, surface enhanced optical properties, etc.

Outside a given material, the near-field can be defined as the extension of the field existing inside this material. It results from the imposition of a continuous variation of field amplitudes and energies across the interfaces. In most cases, the amplitude of the near-field decays very rapidly along the direction perpendicular to the interface giving rise to the so-called evanescent wave characteristic of the near-field.

In the next paragraphs I am going to describe a bit more in detail how this near field arises, following the treatment of [Jac99]. Let us start by considering the propagation of a monochromatic electromagnetic wave in vacuum pulsating at $\omega$, coming from $z < 0$ and traveling in the positive $Z$ direction. We can try to determine the field $E(x, y, z, t)$ all over $z > 0$, taking a known field at $Z = 0$ as a starting point:

$$E(x, y, z, t) = E(x, y, z)exp(-i\omega t). \tag{2.2}$$

This field is solution to the Maxwell's equations. We start from the wave equation

$$\nabla^2 E - \frac{1}{C^2}\frac{\partial^2 E}{\partial t^2} = 0 \tag{2.3}$$

where $c$ is the speed of light in vacuum. The 2-dimensional Fourier transform of this field in the plane of the object $z = 0$ is:

$$E(x, y, z) = \iint E(\alpha, \beta, z)exp[i(\alpha x + \beta y)]d\alpha d\beta \tag{2.4}$$

with $\alpha$ and $\beta$ the spatial frequencies of the field. This field satisfies the Helmholtz equation, which gives:

$$\frac{\partial^2 E(\alpha,\beta,z)}{\partial z^2} + \gamma^2 E(\alpha,\beta,z) = 0 \tag{2.5}$$

with

$$\gamma^2 = \frac{\omega^2}{c^2} - \alpha^2 - \beta^2 \tag{2.6}$$

which gives a general solution of the kind

$$E(\alpha,\beta,z) = A(\alpha,\beta)exp(i\gamma z) + B(\alpha,\beta)exp(-i\gamma z) \tag{2.7}$$

If we only take the field propagating in the positive $z$ direction, the term $B(\alpha,\beta)$ must be $\emptyset$. Moreover, for $z = 0$ the field is known and therefore $A(\alpha,\beta) = E(\alpha,\beta,0)$. We can now write:

$$E(x,y,z) = \iint E(\alpha,\beta,0)exp[i(\alpha x + \beta y + \gamma z)]d\alpha d\beta. \tag{2.8}$$

The field can therefore be regarded as a superposition of plane waves propagating in the direction determined by the wave-vector:

$$k = (\alpha,\beta,\gamma). \tag{2.9}$$

The wave propagation in the half-space $z > 0$ depends on the value and nature of each spatial frequency $\alpha$ and $\beta$ of the plan $z = 0$. Since $\gamma$ is himself a function of the spatial frequencies associated with the object (equation 2.6), two cases can be distinguished:

1. $\gamma$ *is real*: in this case, the spatial frequencies $\alpha$ and $\beta$ verify the relation:
$$\alpha^2 + \beta^2 \leq \frac{\omega^2}{c^2} = \left(\frac{2\pi}{\lambda}\right)^2. \tag{2.10}$$
Plane waves associated with electric field **E** represent radiative waves propagating towards the growing $z$. These waves are detectable in the far-field, at distances much bigger than the wavelength.

2. $\gamma$ *is an pure imaginary number*: on the contrary, in this case the spatial frequencies verify:
$$\alpha^2 + \beta^2 > \frac{\omega^2}{c^2} = \left(\frac{2\pi}{\lambda}\right)^2 \tag{2.11}$$
Here we are considering the high spatial frequencies. The electric field (expression 2.8) shows up a term $exp(-\gamma z)$. We are then talking about evanescent waves, that remain confined at the surface plane $z = 0$ and cannot be detected beyond a typical distance of $1/\gamma$. Within this zone is the near-field, where evanescent waves prevail. Out of this zone, it is called the far-field and there are only propagating waves.

When an object is illuminated, it generates two different types of waves by diffraction: the propagating waves associated with the low spatial frequencies and the evanescent waves associated with the high spatial frequencies of the object. These evanescent waves are the only ones that contain therefore, the high spatial frequency information corresponding to the object small details. These waves decay exponentially in $z$, meaning they can only be detected in the near-field. Propagation can be considered as a low-pass filter preventing all waves of high spatial frequency in the field from propagating.

### 2.3.1 Optical Near-field

Optical nonfluctuating near-fields are not permanent and must then be generated by external illumination. One simple way of doing this is by illuminating the sample by external reflection which will generate an electromagnetic field $(E_0, B_0)$ above the sample, critically dependent of the incident angle. Another way to illuminate a sample is by Total Internal Reflection (TIR). In this case, the light coming through the transparent sample illuminates the surface from below and reflects back into the sample, with an angle larger than the total reflection angle. In this way we obtain an excitation field above the surface in the form of evanescent surface waves.

Figure 2.3: *Total Internal Reflection and Total Reflection illumination methods.*

In either case there are evanescent waves created, but while the TIR technique has an almost pure near-field at the surface, the external reflection has also reflected light mixed in. This can be challenging for some detection techniques where the signal-to-noise ratio is very low because of all the background. This difficulty can be minimized by modulating the distance between tip and sample, something very handy in the case we want to use a tuning fork based AFM, as the tuning fork is already made vibrating for the purpose of distance control. Other important difficulties are related with the polarization of light, which becomes a relevant factor in intensity distribution.

Anyway, this is just what we need, an optical field trapped on the surface rich on information about the surface. We can then try to detect it. If we now bring the AFM technique together, we have the means to control the distance between a sharp tip and the surface. This can be achieved with a

very high spatial resolution and also in the lateral displacement of this tip. We can then think of the possibility of detecting an optical signal at a very confined area with respect to the wavelength. This is a way of doing subwavelength optical microscopy without dealing with the diffraction limit.

### 2.3.2 Applications in microscopy

For any spectroscopic technique the light source is of primary importance. Also, in optical methods little sample preparation is needed. Biological samples can be more conveniently characterized and identified [Mic00]. In near-field microscopy, sensor-sample distance control is so fine that the systems used for control can also be used to obtain topographical images. Since there's a wide range of choice in terms of illuminating sources, and they can be easily changed, local spectroscopy has become a subject of great interest. With the adequate sensor, surface plasmons can be studied. Because of the highly localized information in these fields, it is possible to detect single molecules, or features in molecules like the presence of cromophores. cromoph] Mainly test samples are used, but with the rapid development of near-field spectroscopies, physical mechanisms taking place in the subwavelength size range can be studied. Another important application is related to the miniaturization of technologies and the optical communication devices, transferring information inside subwavelength structures.

## 2.4 SNOM principles

The concept of SNOM was born in 1928 by the brain of the Irish scientist [Syn28]. He proposed to use a small aperture to image a surface with subwavelength resolution using optical light. For the small opening he suggests using either a pinhole or a quartz cone coated with metal expect for at the apex. The large difficulty here is the alignment and accurate displacement of both sensor and sample surface.

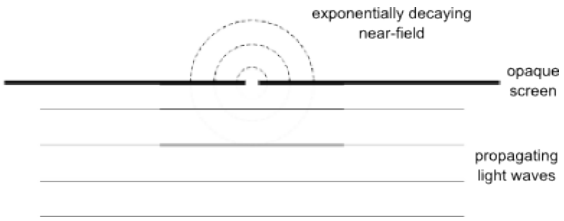


Figure 2.4: *The idea of Synge: when normal, propagating light passes through a sub-nanometric aperture in a opaque screen, a near-field is created behind the screen.*

Synge suggested the use of a strong light source behind a thin, opaque metal film with a 100nm hole, working as a small source. He recommended

that the aperture should be closer to the surface than the aperture diameter. The goal was to reconstruct a point by point image of the sample after detecting the transmitted light at each position. He even suggested later, in 1932, to use piezoelectric actuators as a way to scan the aperture at a few nanometers from the surface with great precision. In 1956 the near-filed imaging principle was for the first time demonstrated with acoustic waves. The first publications on applications of SNOM technique started only in 1984. Since then the technique has known a large developments.

### 2.4.1 Imaging principle

The imaging in SNOM is based on dipole-dipole interactions between the sensor tip and sample [Oht98]. The tip apex and the sample are considered to be very small spheres. Since the sample and apex size is much smaller than the wavelength, we can ignore the interaction of the spheres with light and consider imaging based on the interaction between two dipoles.

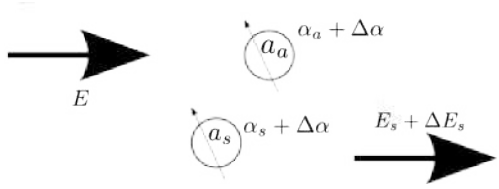


Figure 2.5: *Dipole interaction.*

The electric field $E(t)$ will induce an electrical dipole moment $m$ on the particle of interest according to $m = \alpha E$, where $\alpha$ is the polarizability. The presence of another dipole will cause an interaction between dipoles. This interaction will result in a change in polarizability of the dipoles. The interaction is reciprocal and so, the modulation of the polarizability will be the same for both dipoles. The amount of coupling between the probe and the sample depends on the size of the spheres. At the same time, the coupling between dipoles decreases rapidly with the distance. The polarizability of the spheres depends on their size and on their the refractive index $n$. In standard near-field microscopy, the detected intensity $I_{det}$ is composed by the near and the far-field parts:

$$I_{det} \propto \mid E_s + \Delta E_s \mid^2$$

$$\mid E_s + \Delta E_s \mid^2 \propto ((\alpha_a + \Delta\alpha) + (\alpha_s + \Delta\alpha))^2 E^2$$

where $E_s$ and $\Delta E_s$ are the constant and the modulated electric fields scattered by the coupled dipoles. $\Delta\alpha$ represents the near-field signal while the indexes $a$ and $s$ refer to each of the two spheres like illustrated in figure2.5.

### 2.4.2 Tip size: contrast vs resolution

From the previous model of the coupled dipoles, it follows that the resolution in near-field microscopy is determined only by the tip apex size. All the other features and dimensions of the tip are going to affect the image contrast. If we increase the size of one sphere we obtain a higher intensity, since the interaction volume is bigger, but also a smaller resolution. The size of the apex will define at the same time the resolution and the contrast. It has been found that the contrast will be optimal when the apex size is similar to the size of the feature to observe, independently of the refractive index of both sample and probe. If we increase the size of the apex, the contrast will decrease since the constant signal, or in this case background signal, is proportional to the tip size. Likewise, if we decrease the apex size we will be decreasing the modulated signal, the near-field signal. The shape of the tip should be sharp so that the dipole coupling just behind the apex can be minimized, avoiding extra background signal. Since classical optical theories cannot fully describe the tip-sample interactions, the optimization of the probe is based on experience [GD96]. The issue about decreasing the tip size is that the optical throughput will also decrease rapidly. There are a few techniques to go around this difficulty.

### 2.4.3 Electromagnetic waves

The theoretical knowledge about scattering of electromagnetic waves at the mesoscopic scale(0.1-1$\mu m$) remains limited, in particular in the case of SNOM. For the theoretical treatment, the Maxwell's equations are used and ideally the detailed solution should be achieved. In some cases a numerical approach works better , depending on the approach of matching electromagnetic boundary conditions at the interfaces [GD96]. The problem still remains for the near-field, since these are macroscopical approaches of the mesoscopic problem, like in the diffraction theory. They are suited for modeling the response of particles bigger than 10nm, in the visible region of the spectrum.

The first theory to consider the interaction between sample and probe, is the microscopic self-consistent approach, that is based on diffraction theory but considering the existence of a probe. Another theory is the scattering theory, also called field susceptibility, or even Green dyadic which is used to resolve diffraction by small apertures.

When any of these two techniques is applied to real size probes, the problem of the computer memory capacity limitation arises. As an alternative, the Finite-Difference Time-Domain (FD-TD) method is less demanding in terms of computer capacity and several models have been successfully studied with it [Chr95; FK96].

### Diffraction theory

This theory uses the Maxwell equations as a starting point to a macroscopical approach of the optical near-field. The theory can describe near-fields above a surface if no probe is present. Diffraction theory can be used to determine the field distributions above specific objects [LBBC95]. When objects that scatter light are nanometric size, the diffraction theory cannot be used, but it still indicates that a better contrast and better image of the object can be obtained if the light is p-polarized, instead of s-polarized. This can be used as an advantage in setups that allow you to set your preferred polarization of incident light.

### Photon Tunneling

Photon tunneling is comparable to electron tunneling through a potential barrier. It is an exchange of energy between two media through a gap of low refractive index. If the gap is too large, there will be no photon exchange but an electric field will penetrate the gap beyond the solid interface. This electric field decreases exponentially along $z$ with a characteristic distance of:

$$d_p = \frac{\lambda}{2\sqrt{(n\sin\theta)^2 - 1}}$$

This gives the measure for the distance over which there is a significant electromagnetic field, for the case of total internal reflection. When the angle of incidence inside the material is the closest to the critical angle, the penetration depth is the longest, reaching several wavelengths [Moe95]. If a second body of high refractive index comes close to the first within the penetration depth, transmission will occur.

### Self-consistent Approach

In this case, the total system is seen as a set of polarizable spheres. Mutual interactions between all dipoles are taken into account through field operators that are inserted in the diffraction theory equations. This results in the self-consistent approach that describes the optical interaction between a thin dielectric tip and a surface illuminated by internal reflection [GC90]. This approach has confirmed that p-polarized light enhances contrast and gives a better image of a structure than s-polarized. P-polarized light induces dipoles perpendicular to the surface. This brings importance to the position of the tip relatively to the source dipole [GC90].

The scattering of electromagnetic fields by small structures and features on the structure can be formulated by means of the Green dyadic function (GDF). It can be used to study electromagnetic fields on the region of perturbations and the far-field generated by these perturbations. This approach consists in analyzing the perturbation of a reference system.

#### Finite-difference time-domain (FDTD)

This method can be used with realistic probe sizes thanks to manipulations with Maxwell's equations. The equations are considered as a set of finite difference equations in both time and space. There is also a simplification of dividing the space in discrete cubic cells, each one with its own complex dielectric constant. This method reduces drastically the CPU and memory need when comparing with the previous methods [Chr95; FK96].

#### Multiple-Multipole Method (MMP)

Solving Maxwell's equations for systems with tip-sample geometry with near and far fields is so complicated that numerical methods have to be used. This MMP method uses a semi-analytical approach in multiple connected homogeneous, isotropic and linear media. The field in each domain is described by a series expansion of known analytical solution of the Maxwell's equations. The basis functions for these expansions are multipoles with different origins and solutions like plane waves or waveguides modes. It has been successfully used to study light propagation and confinement in several 3D systems [PNHH96; NPH95].

### 2.4.4 Aperture SNOM

As explained before, the SNOM is a scanning near-field optical microscope, which can be seen as a generic AFM used as an instrument to study optical near-fields. The sensor is a tip and its control is in fact very similar to the one used in standard AFM microscopy. The tip can oscillate either parallel or perpendicular to the surface and when approaching the surface will soon start to dissipate energy due to interactions with potentials present in the surface. This loss of energy determines the signal that will be used for distance control. In this way, the sensor can be safely kept inside the near-field. Since this technique has emerged, many configurations have been tried and used.

The two most used SNOM techniques are the aperture SNOM and the scattering type SNOM, aSNOM and s-SNOM respectively. The main difference resides in the near-field sensor [Kar06]. The aSNOM uses an optical fiber with a sharp tip, which usually has a metallic coating all along the fiber leaving only a small transparent aperture at the apex, figure 2.6 a). This apertures can have around 50-150nm diameter and this will be approximately the attainable resolution with this kind of sensor. The aperture collects the evanescent light and guides through the waveguide to the detector.

This is the technical breakthrough into the subwavelength optical microscopy. We can now see details in an optical image smaller than the wavelength itself.

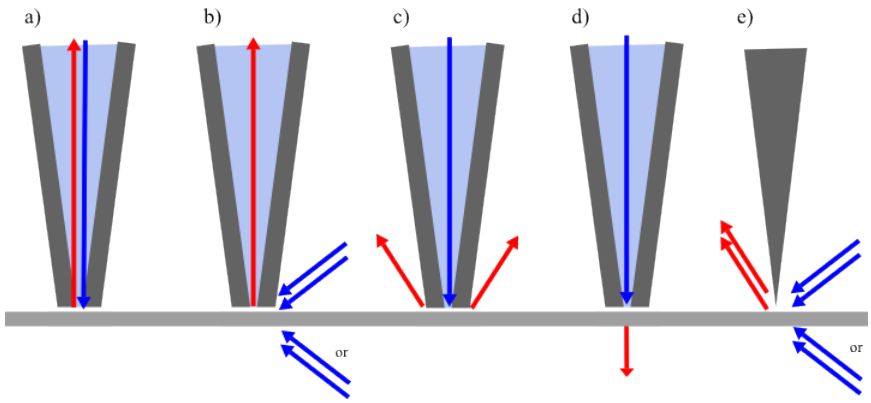


Figure 2.6: *Different modes of illumination. Different kinds of tip: from a) to d) they are optical fiber tips, with metal coating and small aperture; e) is a metallic opaque scattering tip.*

This technique presents different approaches to generate and detect the near-field. The sample can be illuminated through the fiber with light emission at the aperture and then the reflected light can be collected through the same aperture and finally detected, like described in figure 2.6 a). Otherwise the sample can be illuminated sideways from the exterior, focusing the light spot on the sample under the tip apex, followed by detection close to the surface like before, figure 2.6 b). Another approach is detection in the far-field after illuminating the sample through the tip, figure 2.6 c). In figure 2.6 d) we can see the case of a transparent sample where after illumination from the tip, the collection happens under the sample in the so-called transmission mode. To finalize we can look at figure 2.6 e), where we can see the scattering tip, illuminated from the far-field, and detected again in the far-field. The tip is opaque and works just a scatterer. In both cases presented with external illumination, it can be considered the TIR illumination, from under the sample.

### 2.4.5 Scattering SNOM

For this technique, the near-field sensor is opaque, homogeneous and made of dielectric, semiconductor or metallic material. This kind of probes can be much sharper than the aperture ones, which means an even better optical resolution than the aSNOM. This is actually one of the reasons for the success of this technique, as it is possible to produce atomically sharp tips.

In this case, the illumination is always from the exterior, focused on the sample surface for higher density of photons near the tip apex. Also in the Total Internal Reflection (TIR) configuration, where the near-field is generated at the surface of a prism if illuminated by internal reflection.

The tip will interact with the evanescent waves when brought close to the surface within the range of the near-field. It will then act as a source as it scatters the photons into the far-field [TKH05b]. A high numerical aperture objective has to be used to collect as many photons as possible.

This technique is less efficient then the aSNOM. Since the tip is sharper, the zone of interaction is smaller producing less detectable photons. Detectable photons are also less since the detection is done far and the solid angle is small. Nevertheless there are very good results with this technique, usually by means of intense sources like lasers, Free Electron Laser (FEL) [VMS+04]. The limit in intensity is the thermal stability of the sample. It can successfully be used to image and study surface plasmons and other surface effects [WFC+06].

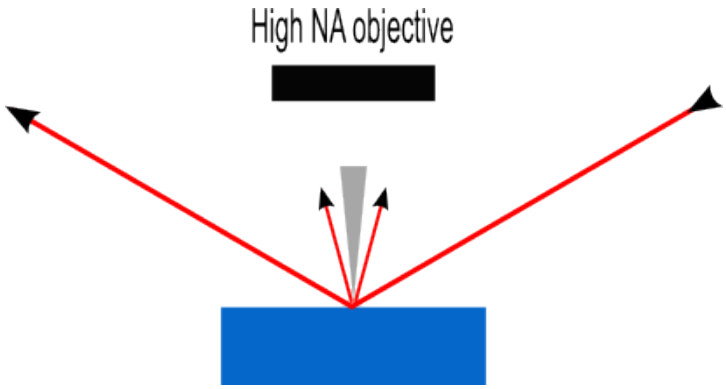


Figure 2.7: *Simple optical configuration of a scattering SNOM.*

### Signal detection

One important drawback with this technique is the optical background noise and thus the low signal to noise ratio (S/N). Therefore, the signal generation and its detection chain must be optimized and if possible, the use of parallel techniques that can help in the detection of a signal is necessary.

For example, the signal can be filtered by means of a lock-in amplifier that can extract the signal coming from the near-field only, if the tip oscillates as in a normal AFM operation mode. Better filtering of the near-field signal is achieved by setting the lock-in amplifier to operate at $2\omega$, higher harmonic frequencies present only in the near-field. The intensity is though much weaker [FWA05b]. Another well known method is the heterodyne detection. Heterodyne detection is done by interferometry and it can make a very weak signal detectable [KK00].

## 2.5 Infrared Spectroscopy and SNOM

Optical spectroscopies are used to obtain information about matter from its interaction with radiation. Depending on the frequency of the incident radiation the interaction will be with different kinds of energy levels in the matter. The kind of information obtained, depends on the setup sensitivity and the kind of sample. Two different analysis can be done: qualitative where we can identify a substance through its spectral signature, depending on the used energy levels; or quantitative where we can quantify the presence of a substance still through its spectral signature.

### 2.5.1 Energy levels in a molecule

From quantum mechanics, the energy of a molecule is quantized in different levels characterized by a set of quantum numbers. Also, a molecule can be schematically considered as composed by atoms where electrons ensure their chemical bonding, for the case of the covalent bond. The Born-Oppenheimer approximation decouples both the movement of nuclei and electrons, which are much lighter, thus, managing to decouple both energies. In a first approximation, $E$ can be described as the sum of the separate energies

$$E = E_e + E_v + E_r$$

where $E_e$ stands for the electronic energy, $E_v$ the nuclei vibrational energy and $E_r$ the molecule rotational energy and where $E_e >> E_v >> E_r$.

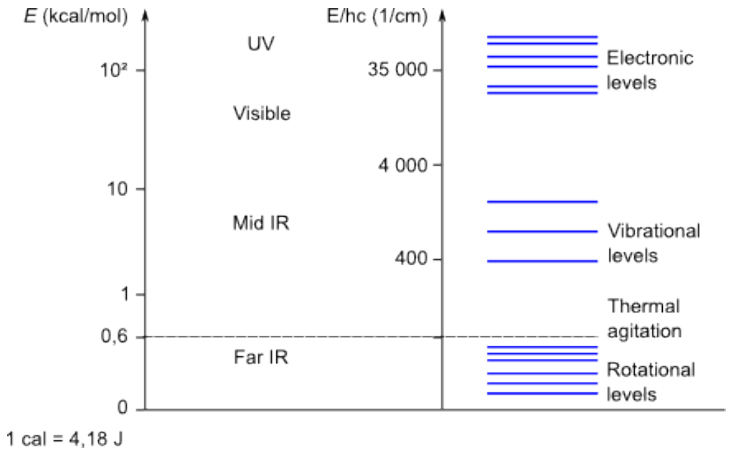


Figure 2.8: *Values of electronic, vibrational and rotational contributions in a molecule.*

A more detailed description can show some coupling between these energy components. Figure 2.8 shows a scheme with the energy bands corresponding to the different contributions.

The electronic energy $E_e$ depends on the number of electrons and shape of the molecule. The energy $E_v$ is due to the vibration of the nuclei of the molecule and depends on their masses (m and M) and on their relative position. These vibrations can be described through the harmonic oscillator model in which two masses connected by a spring can represent adequately a covalent bond. Let us simply consider the case of a diatomic molecule. The vibration frequency of such an oscillator depends on the atom masses and the bonding force through the value of its stiffness constant $k$. If we consider the oscillator as harmonic, the elongation is proportional to the force and according to Hooke law, the vibration frequency $v_0$ is the given by

$$\nu_0 = \frac{1}{2\pi}\left(\frac{k}{\mu}\right)^{1/2}$$

where $\mu = mM/(m+M)$ the reduced mass of the oscillator connecting the masses $m$ and $M$.

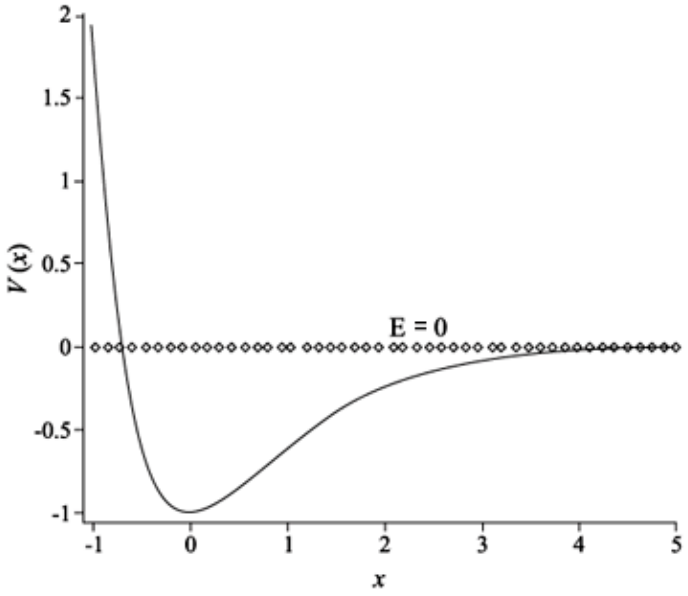


Figure 2.9: *Anharmonic Potential.*

The energy of such an oscillator is quantized and depends on the integer $v$, the vibrational quantum number:

$$E_v = \left(v + \frac{1}{2}\right) h\nu_0$$

with $\nu = 0, 1, 2....$ The potential well associated with a diatomic molecule is similar to the harmonic oscillator, but only for small movements in respect

to the equilibrium position between the nuclei. For large separation distances the molecule can dissociate and this is incompatible with the strictly harmonic vibration hypothesis, but still valid and natural for the anharmonic vibrational case 2.9. The elastic force is not only proportional to the distance and there is a new parameter $x_e$ of anharmonicity, where

$$E_v = \left(v + \frac{1}{2}\right) h\nu_0 - \left(v + \frac{1}{2}\right)^2 x_e h\nu_0$$

gives the anharmonic oscillator energy levels. One important difference between harmonic and anharmonic is that now, the selection rules allow transitions that are normally forbidden.

Other than the vibrational movements, the molecule can rotate. The polyatomic molecule case is more complicated since the energy takes into account some inertia momenta.

### 2.5.2 Interaction of Radiation with Matter

Due to radiation interaction with matter it is possible to change the energy state of a molecule into a state of higher energy. The radiation has an associated energy proportional to its frequency. As shown in figure 2.8 if the incident radiation has low energy, then in microwaves or far IR region, only the rotational energy of the molecule will be affected. If the energy is higher, up to the near IR region, the obtained spectrum is a complex superposition of vibrational and rotational transitions. Raman spectroscopy, is a second order effect that involves transitions to rotational states and the light scattered from the sample is shifted in wavelength from that of the incident radiation.

In our case we are interested in radiation in the infrared zone where the wavelength is around the micrometer. Fundamental vibrations and associated rotational-vibrational structures can be probed. This is the infrared spectroscopy domain.

In fact, the interaction of radiation with matter can be roughly divided in three classes of phenomena: absorption, diffusion and emission. Absorption and diffusion will dissipate energy from an incident beam when it goes through a material, unlike emission which corresponds to a loss of thermal energy, emitted by a material.

#### Absorption

We have just seen that a certain material has several levels of energy. If an incident beam has the adequate energy, there is the probability for photons to be absorbed by the sample taking it to an excited state of energy. This probability depends also on the polarization states of the beam, and of

the selection rules that will determine if the absorption is allowed. In order for the absorption to happen at all, it is necessary that:

$$h\nu_0 = \Delta E$$

where $\nu_0$ the incident beam frequency, $h$ the plank constant, $\Delta E$ the difference between two energy levels. Macroscopically speaking, the attenuation of the beam after crossing the sample can be expressed as:

$$I_t/I_0 = exp(-Kd)$$

with $I_0$ the intensity of the incident beam, $I_t$ the intensity of the transmitted beam and $K$ the absorption coefficient of the sample. According to the electromagnetic theory, the presence of an absorption band leads to existence of a complex refractive index.

**Diffusion**

Diffusion includes all the phenomena in which the radiation changes its propagation direction when crossing a material. Diffusion can be either elastic or inelastic, in which case the beam will loose energy and consequently change wavelength.

Elastic diffusion can originate from the presence of local changes in the refractive index, or by diffraction on grain edges or particles. The effect will be stronger when obstacles have a size comparable to the wavelength of radiation.

**Emission**

All bodies in equilibrium at a certain temperature radiate electromagnetic energy. The intensity and distribution of radiant energy within the range IR-Visible-UV is governed only by the temperature of the emitting body. The total radiant energy emitted by the body is proportional to the fourth power of its absolute temperature, like stated by the Stefan-Boltzmann law.

The rate at which the body radiates, depends as well on the nature of the emitter. The Kirchhoff law states: *At thermal equilibrium, the emissivity of a body (or surface) equals its absorptivity.*

This theorem is sometimes informally stated as a poor reflector is a good emitter, and a good reflector is a poor emitter. If it is a perfect black body, all absorbed light will be radiated. Generally, bodies are "grey" since they reflect a part of the incident radiation, bringing emission down to a lower value but still proportional Plank's law for the black body. For a given temperature $T$, this law can be described, as a function of the frequency $\nu$ by the expression:

$$I(\nu, T) = \frac{2h\nu^3}{c^2} \frac{1}{e^{\frac{hc}{kT}} - 1} \tag{2.12}$$

with $k$ the Boltzmann constant and $c$ the speed of light.

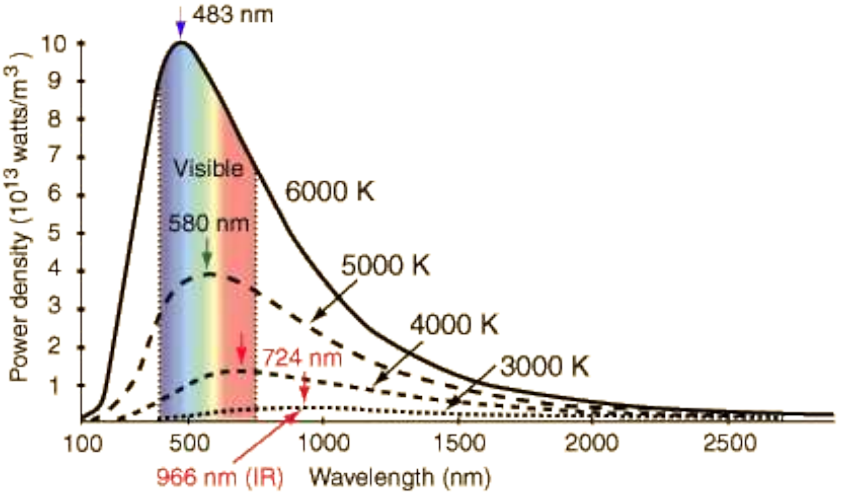


Figure 2.10: *How black body emission changes with temperature.*

The area under each line for each temperature that are shown in figure 2.10, correspond to the intensity of the emitted radiation. The function $I(\nu, T)$ has a peak for $h\nu = 2.82kT$. It falls off exponentially at higher frequencies and polynomially at lower.

The wavelength corresponding to the maximum emitted radiation is related to the temperature by Wien's law which states that there is an inverse relationship between these two.

We can note that for low temperatures, the maximum emission is in the infrared. That is why this kind of radiation are frequently designated as thermal radiation.

### 2.5.3 IR Spectroscopy

We can distinguish two kinds of optical spectroscopies: those that involve changes to electronic states, particularly in the visible and UV region; and vibrational spectroscopies, infrared and Raman. Not all molecules have high rates of absorption in the visible-UV but all molecules vibrate and are active in vibrational spectroscopies. A consequence of this is that vibrational spectroscopies are more selective.

Raman spectroscopy can probe vibrational states, but by different selection rules from those of the infrared spectroscopy. There can occur absoption of infrared radiation only if the vibration of the considered mode can induce a change in the electric dipole moment of the molecule. Raman diffusion can only be seen if the concerned vibration can change the molecular polarizability. These two types of vibrational spectroscopies can probe

vibrational energy levels by recurring to different mechanisms, which often give complementary information for a detailed vibrational characterization.

Infrared spectroscopy is based on the fact that molecules have specific energy levels of rotation and vibration. For the case of vibrations, the resonant frequency can be related to the strength of the bond and the mass of the atoms as described in figure 2.8 and thus, can be associated with a particular type of bond. While a simple diatomic molecule can stretch, more complex molecules combine different vibration modes which lead to characteristic frequencies of infrared absorption for specific chemical groups. In analyzing these absorption characteristics, details of a molecular structure can be obtained. For example, the $CH_2$ group, usually found in organic compounds can vibrate in six different ways. The infrared spectrum is obtained by analyzing the light coming from the sample, revealing how much energy was absorbed at each wavelength. This technique works essentially on samples with covalent bonding.

### 2.5.4 Instrumentation

There are two common methods to obtain an absorption spectrum of a sample. One can use a monochromatic beam shifting its wavelength over time, or by means of Fourier Transform Spectrometer that can analyze the whole spectrum at once.

In any case, the beam is usually split into two branches: one goes through the sample, and the other works as reference. Afterwards both are reflected to the detector, so that the two signals can be compared. The main reasons to use this technique are that it prevents fluctuations from affecting the data and that undesired effects can be cancelled out. In the first case, of the sweeping monochromatic source, the recorded signal is the difference between the intensities of the reference beam and the beam that passes through the sample. Both beams will arrive alternately to the detector.

In the second case the source is not monochromatic. Both beams will arrive together to the detector and form an interferogram, from which a Fourier Transform can be directly extracted. This method is also faster, which can be of importance in terms of noise and stability.

Optical spectrometers have the following elements in common: a source of radiation; a wavelength selecting device; a sample positioning system; a detector and recorder. It is the optimization of all these elements that allow to obtain a quality spectrum.

#### IR sources and detectors

Commercial IR sources are usually made of a ceramic piece heated up to about $1000K$. According to the curves in figure 2.10, this means it can radiate from 5000 to 300 $cm^{-1}$.

There are other kinds of sources such as lasers which the case of IR is often a $CO_2$ laser, that can be very intense, emitting a $10.6\mu m$ wavelength beam.

Another source is the Free Electron Laser (FEL) which can be tuned into different frequencies, it is intense but each time wavelength changes it takes some time to stabilize [VMS$^+$04; CGB$^+$98]. This can be an inconvenient if there is an interest in having fast measurements.

A source that only recently has been used is the IR from synchrotron radiation. It is naturally a continuous source, it is very stable, but intensity is a limitation. The use of this source is the main objective of this work and will be discussed further ahead.

A detector is described by its sensitivity, spectral bandwith and quantum efficiency. The sensitivity quantifies the smallest detectable signal by the detector. The quantum efficiency is the ratio between the induced current and the incident flux.

There are defined kinds of noise common to all detectors: detection noise, due to variations on the signal flux and the dark current, that is the current that goes through the photosensitive device.

Detectors can be of thermal or quantum nature. The thermal detector is sensitive to the heat generated by the absorption of a photon. The quantum detector is sensitive to the photons directly and has a faster performance. This is the case of the Mercury Cadmium Telluride (MCT) detector, the kind of detector used in this work. It uses a photoconductor and is Nitrogen cooled.

### Fourier Transform IR

As a brief introduction to the FTIR spectrometer, one can say that the FTIR is the essential part of the IR spectrometry system. This instrument is capable of separating all the frequencies present in a white beam. It has got an internal source of IR, an incandescent SiC bar, but in our case it works with an external source. The light inside the instrument is processed in an interferometer, where usually one of the paths changes length generating an interferogram. Most of the commercialized devices are based on a Michelson interferometer, schematized in figure 2.11.

The Michelson interferometer is composed by two perpendicular flat mirrors, one fixed (Mf) and the other moving (Mm). There is also a beamsplitter (Bs) positioned at 45° with respect to the incoming beam. For the infrared domain they can be made of KBr or $CaF_2$ depending on the desired transmission band. As light goes through the interferometer, the moving mirror changes the length of the optical path in one of the branches, generating an interferogram at the detector (D) after the two branches have been recombined. The interferogram represents the variation of the signal intensity over the displacement $\delta$ of the moving mirror, or the phase. For a monochromatic

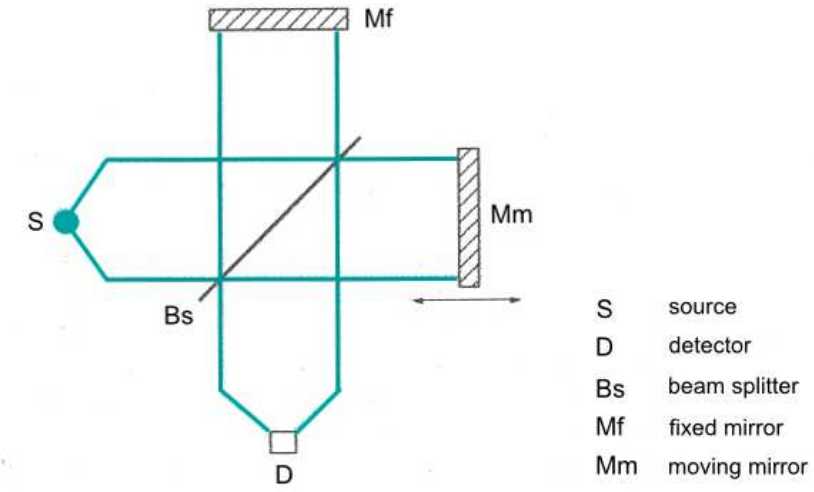


Figure 2.11: *Michelson interferometer.*

source an interferogram is a simple cosine, but for a continuous source the interference pattern of all the present waves is also an oscillation but with an intensity maximum at the center, and decaying rapidly on the sides.

The light that comes from the sample has a different spectrum due to interactions and this is collected by the detector and fed to the FTIR's electronic module. With the help of a computer interface we can control different parameters such as the mirror(Mm) speed, the number of scans or even some mathematical parameters for the Fourier Transform operation. The interferogram or the spectrum can be displayed on the computer at each mirror pass or after data acquisition.

### 2.5.5 IR SNOM

If instead of analyzing macroscopic samples we wish to analyze small regions of a given sample, an optical microscope may be introduced in the system, typically a confocal microscope as described in section 2.2. This is called micro spectroscopy. With this technique, it is possible to obtain a chemical mapping of a sample with the lateral resolution of the microscope.

In classical microscopy the resolution is limited and is proportional to the wavelength of the illuminating light. If we want a better resolution, a way of overcoming this obstacle is to adopt a Scanning Probe Microscopy (SPM) technique by means of a sharp tip in the SNOM configuration. The resolution is easily around 50nm. For the case of IR, since waves are longer than in the visible region of the spectrum, compared with classical microscopy, the increase in resolution is much more significant. In respect to spectroscopy, this technique sounds very promising but there are still some difficulties.

The photon density under the tip has to be high enough to generate a detectable signal, as illustrated in Figure 2.12. The source has then to be rather intense which is the case for lasers, but lasers are monochromatic and spectroscopy has to be made for certain frequencies only. Laser technology is rapidly developing and there is already the possibility to produce tunable lasers. Other used source for IR microspectroscopy is the Free Electron Laser (FEL)[CGP+98]. The FEL is tunable but is unstable in intensity and position which at such a reduced size region of interest becomes critical.

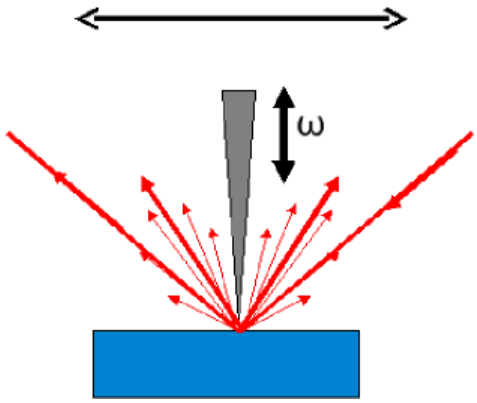


Figure 2.12: *Scheme of a SNOM.*

There is also the synchrotron as source for IR microspectroscopy. The source is continuous and very stable. It works very well with classical optical microscope and the possibility to use a SPM technique should be explored. This is the objective of this thesis, the development of a IR SNOM for spectroscopy recurring to synchrotron radiation. This source is presented in the next chapter. Afterwards, the developments towards the integration of a SPM will also be shown.

# Chapter 3

# Synchrotron IR

## 3.1 Résumé

Le troisième chapitre est dédié à la particularité de ce projet, le synchrotron comme source de lumière infrarouge. Il décrira brièvement la manière dont la lumière est extraite car elle n'est pas très courant d'utiliser synchrotron infrarouge. Les caractéristiques de cette lumière sont présentés.

**Contents**



This chapter briefly presents the synchrotron IR radiation. We will describe the method of extracting this light, used at the European Synchrotron Radiation Facility (ESRF) in Grenoble, France. We will also introduce the characteristics and main uses of this light.

At present, at the ESRF, IR microspectroscopy is performed in a dedicated end station. Here is shown the available equipment and we discuss the possibility of increasing the lateral resolution of the existing system by integration of a SPM.

## 3.2 Synchrotron IR Light Production

In order to adequately use the infrared light, its origin and path until the microscope should be understood. At the source, the light is produced by a dipole acting on the high energy electrons of a synchrotron storage ring, as represented in figure 3.1.

The synchrotron operates in many different modes. They have different time structure in respect to photon emission, but at very high frequencies,

where the differenc is irrelevant for this project. Only the number of photons, intensity of the beam, is important.

The electrons are deflected, emitting radiation tangentially to the storage ring, from the high energy x-ray to the infrared. This radiation is confined to a small beam with high brilliance. Brilliance is a measure typical from synchrotron technology which defines roughly the photon intensity per solid angle. These units are used in opposition to the photon intensity of a radial source that with identical intensity has much smaller brilliance, since it radiates in all directions.

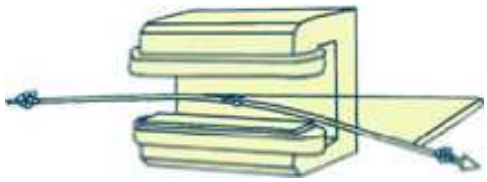

Figure 3.1: *The dipole generating synchrotron radiation.*

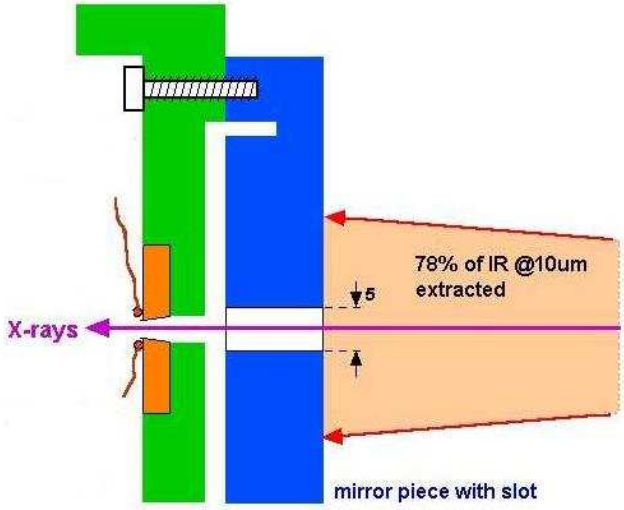


Figure 3.2: *Schematic view of the IR extraction mirror.*

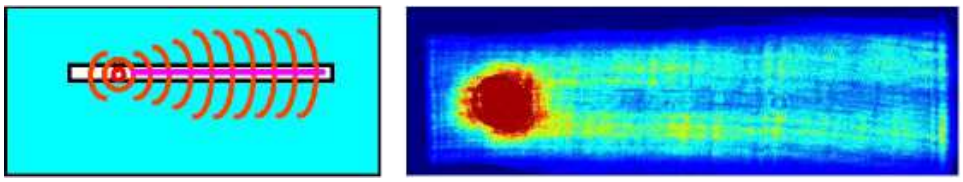

Figure 3.3: *Theory and image of the reflection on the extraction mirror.*

How is then the infrared extracted? The method used at the ESRF

consists in a mirror that deviates only the infrared into a series of optical elements. These elements will focus the divergent beam and guide it until the end station by successive reflections with almost no losses.

To do this, a property of synchrotron radiation becomes relevant that is: longer wavelengths have higher divergence. Therefore, at a certain distance away from the light generating dipole, the IR will illuminate a larger surface spot than will the shorter wavelengths like UV and X-ray radiation. This is the principle used for the IR extraction.

In practice there is a slotted mirror that will reflect the IR into a perpendicular direction, so that it can be extracted away from the shielded tunnel where the accelerated electrons run. This mirror is designated M1 in figure 3.4.

To ensure that the extracting mirror does not get damaged by x-rays or the heat load, the mirror has a small gap through which the high energies, of lower divergence, will pass through and hit an absorber further away. In this way only the wavelengths of interest will hit the mirror and be reflected. With a $5mm$ gap, one quarter of the IR will be lost along with the higher energies. Therefore, approximately 75% of the infrared present in the beam will be extracted and used. The extracting mirror is represented in figures 3.2 and 3.3 [Sch05].

The light is guided to the end station where the FTIR and confocal microscope are installed. Along the optical path, some mirrors are elliptically shaped so that the beam focusing remains under control. There are two focal points. As shown in figure 3.4, one is between mirror M5 and M6, where there is an optical bench that can be used to study and characterise the beam. The second focal point is located right at the beginning of the granite table where the instruments sit. First, the beam goes into a mirror box (MB1) where the beam is tailored before use. In practice, in this box, the beam is made parallel and its position adjusted to perfectly couple with the FTIR. Since the synchrotron is a dynamic machine, the beam can occasionally be found at a slightly different position. This mirror box will easily correct this change by means of its motorised mirrors.

Since the beam comes directly from the electrons storage ring vacuum environment, all the optical path is also kept under ultra high vacuum (UHV), despite the presence of a diamond window separating both vacuums. This also avoids the beam absorption by air. After mirror M5, a valve can be closed in order to give access to the first focal point, where the pipes can be opened for inserting diagnosis devices in the optical path.

This infrared light covers a large range of wavenumbers in the infrared domain, from 1000 to 4000 $cm^{-1}$, plus visible light. The visible part of the beam is very useful for visual alignment purposes although it does not coincide precisely. Before the light reaches the microscope, it goes through the Fourier Transform Infrared Spectrometer (FTIR). The FTIR will modulate the light creating a continuous source interferogram. An example of a

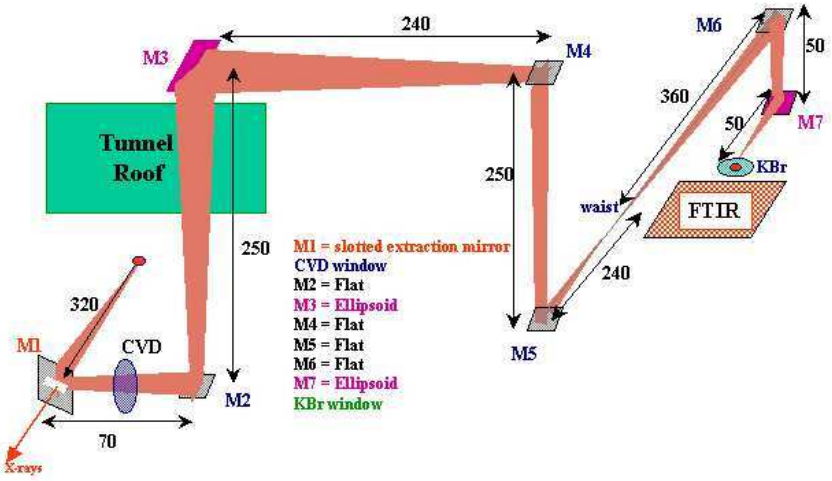


Figure 3.4: *Optical path of light.*

continuous source interferogram is shown in figure 3.6. This interferogram allows coding the wavelengths contained in the beam.

In the microscope, after the light has interacted with the sample by transmission or total reflection, it reaches the detector. The detector signal comes back to the FTIR where it is processed by Fourier Transform and the spectrum is finally obtained. To increase the signal to noise ratio, several spectra are usually acquired for each point.

On figure 3.5 there is an example of a spectrum where the water absorption peak is evident near 2400 $cm^{-1}$.

Again in figure 3.5, a difference between two source intensities is illustrated. One is the synchrotron and the other is the globar, internal source available inside the FTIR, magnified 40 times here.

The synchrotron beam integrated flux was measured, with different filters at 3, 5, 8 and 10$\mu m$ with around 0.01% bandwidth. This is plotted in the graph in figure 3.7. The order of magnitude is $10^{11}$ photons per second for this source measured with each filter.

Polarization measurements were also carried out. It was seen that the light has a complex polarization state probably due to reflections occurring all along the optical path since the synchrotron radiation is partially polarized. Namely, mirrors M3 and M7 illustrated in figure 3.4 that are elliptical, change the polarization state. One measurement is plotted in the figure 3.2 graph indicating that this needs further investigation. Polarization states are of great importance for the kind of experiments we aim to perform..

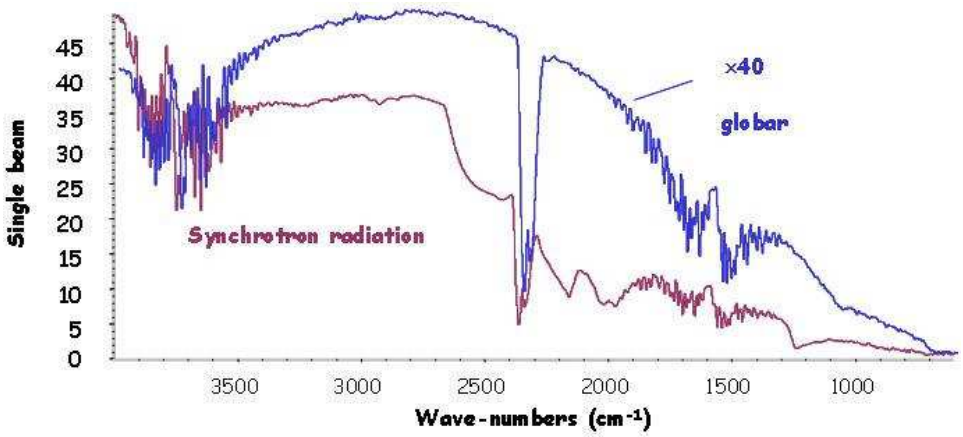


Figure 3.5: *Synchrotron IR spectrum.*

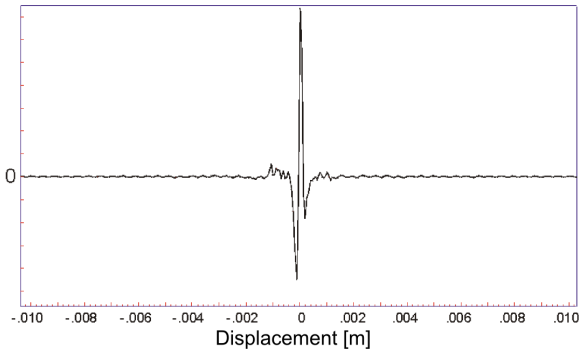


Figure 3.6: *Example of a continuous source interferogram.*

### 3.2.1 Synchrotron IR Spectroscopy - uses

At present the existing confocal microscope coupled with the FTIR has permitted research with the infrared microspectroscopy technique.

The areas of interest range from archeology to cosmetics passing through any other field where chemical identification is needed. Chemical mapping is also achieved simply by scanning the sample.

## 3.3 IRS SNOM

To increase the lateral resolution of the existing technique, a SNOM can be integrated. The principles of this technique will be presented in detail during the next chapter.

Comparing the intensities of the various kind of sources available for use in microspectroscopy, a laser is, for example, much stronger and generates much more photons than the synchrotron radiation in the IR. There is even

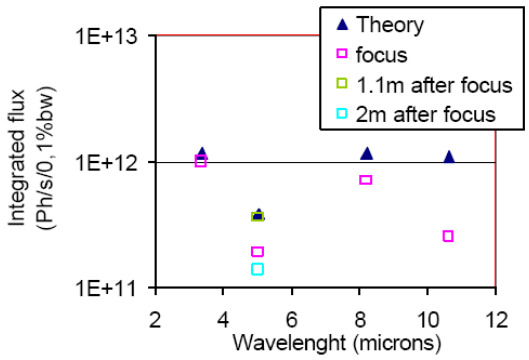


Figure 3.7: *Measured integrated flux of the IR beam.*

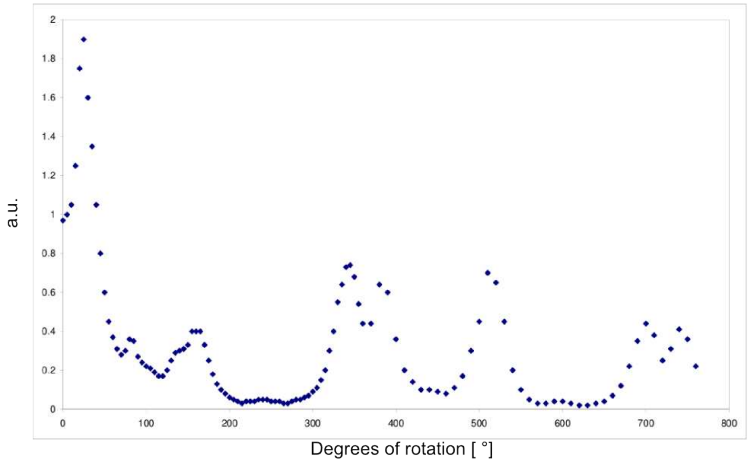


Figure 3.8: *Polarity of the IR beam measured after the FTIR spectrometer.*

the doubt if the photons available in the synchrotron beam are enough. The density of photons under the tip might be lower than the required. This means that there would not be enough scattered photons, and the detector may not have the sensitivity to detect a signal. This is even more significant for non linear effects happening on the sample, such as the second harmonic generation, because the intensities are much lower that the linear part of the signal.

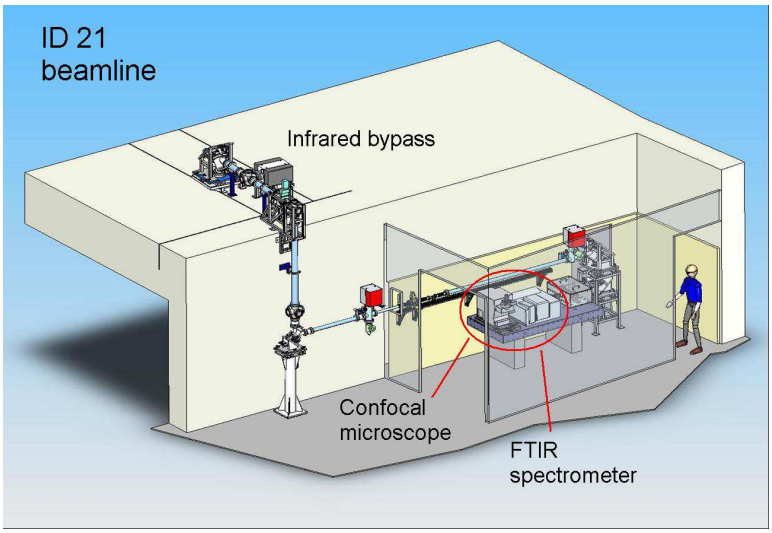


Figure 3.9: *Schematic view of the transfer line.*

Figure 3.10: *End station for the IR beam.*

# Chapter 4

# Development Of The Instrument

## 4.1 Résumé

Le quatrième chapitre est le plus long et il décrit tout le développement de l'instrument. De la production des trucs qui sont probablement le détail le plus important, à l'intégration de l'ensemble du système dans le synchrotron. Aussi la conception et le design de l'AFM est détaillé avec ses résultats de performance. Pour conclure, les expériences et les résultats préliminaires sont présentés

### Contents



This project is part of an Agence National de Recherche (ANR) project, that involves various partners: Université de Technologie de Troyes, responsible for studying the effect of extracting an optical near-field with a metallic

tip; École Polytechnique, responsible for studying the role of polarization in this process; ST Microelectronics, the industrial partner and in Grenoble, the synchrotron (ESRF) and CEA-LETI, responsible for developing the prototype in a first stage of the project. In this development part there were 3 people involved, two from LETI and myself from the ESRF and therefore Iwill often refer to this group during this chapter.

In this chapter, all the development work will be presented with support from the previous chapters. Here will be discussed the implementation of the AFM, its integration with the infrared light from the synchrotron, which makes it a special kind of SNOM, and other alternatives that had to be redesigned throughout this project.

In order to develop a SNOM that operates with the infrared produced by a synchrotron, some technological choices had to be made. Its integration has to be carefully studied not only mechanically, but also functionally including the definition of alignment procedures, signal detection and signal processing. All of these steps will be detailed in this chapter.

Since this project consists in the development of an instrument, it is of very practical and technological nature. The process of development goes necessarily through identifying difficulties and overcome them. In order to debug some of these difficulties auxiliary techniques have to be introduced. In particular for this project, alternative light sources were used, leading to different experimental setup configurations. These are discussed later within this chapter.

## 4.2 Introduction to the IR SNOM

To overcome the limitation imposed by the diffraction limit, we can no longer observe the emitted light by the sample by means of a classical optics, but instead we have to take advantage of the presence of a standing wave at the sample surface called the evanescent wave. This evanescent wave does not propagate, staying trapped at the surface and can be generated by grazing incidence illumination or by total internal reflection. This is the case for all scattering SNOM microscopes, with external illumination. Typically for the SNOM a laser source is used. This is where the main difference is. What is being developed here is also a SNOM, but with a different source, the synchrotron light, a continuous source.

The evanescent wave is originated at the interface between two media and decays exponentially with distance. Most of its intensity is present close to the surface, decaying exponentially away from the surface. This wave contains information relative to the sample, which in the IR domain corresponds to the chemical bonding information. If an object or irregularity is present, this evanescent wave is scattered. The scattered light will come from such a small area, just the size of the object. If we can chose this scatterer object

size, with our continuous source we should obtain spectroscopic information with the desired lateral resolution. This can be of nanometric scale which represents a breakthrough over the diffraction limit. Optical information is obtained from an area smaller than the illuminating wavelength. Of course, the smaller the object is, the less light will be scattered. If on top of all this we can control the positioning of this object we should be able to build a chemical map, point by point, by acquiring a spectrum at each position.

The AFM sounds like the perfect tool for this function. It works thanks to a sharp tip whose position relative to the sample, can be controlled very well in the three directions $xyz$, with very high resolution - close to the nanometer. Not only the AFM would be responsible for the topographic imaging of the sample with lateral resolution of a few tens of nanometer but it would also be used at the same time for scattering the light with similar lateral resolution. Since the image is formed by scanning the sample surface, a chemical mapping can be done by acquiring a spectrum at each point during the scanning of normal AFM operation.

Since the AFM tip oscillates at a certain frequency ($\omega$), the light reflected or diffused on the sample and surrounding objects can be filtered out by using a lock-in amplifier set at the same frequency. In this way the light originated by the presence of the tip alone can be acquired.

The first steps into the development of the SNOM were the definition of the components that should integrate the system. There was already an available confocal microscope coupled with a FTIR spectrometer at the synchrotron. After some discussion it was decided to use the available setup and to adapt to it. Otherwise a new optical microscope would have to be designed and mounted which would be much more complicated and time consuming.Therefore, a prototype AFM should be designed and incorporated into the existing microscope, and the optical part of the system would be complete. Some adaptations to the beam path had also to be introduced so that the sample could be alternatively illuminated from the side.

Other than this, an instrumentation system had to be implemented in order to operate each component and to coordinate the activity of all the components together.

In parallel with the development of the prototype, the production of the tips was also developed. It was chosen to use metallic tips to be used in a scattering SNOM type configuration. The objective was to obtain quality sharp tips in a consistent way. This objective was reached and moreover, the tips could be done in a very short period of time and with a not expensive method.

In figure 4.1 we can see how the system was structured:

- there is an AFM which roughly consists in a sample mounted on a $xyz$ scanner, a force sensor equipped with a metallic tip over it, the control electronics and a computer;

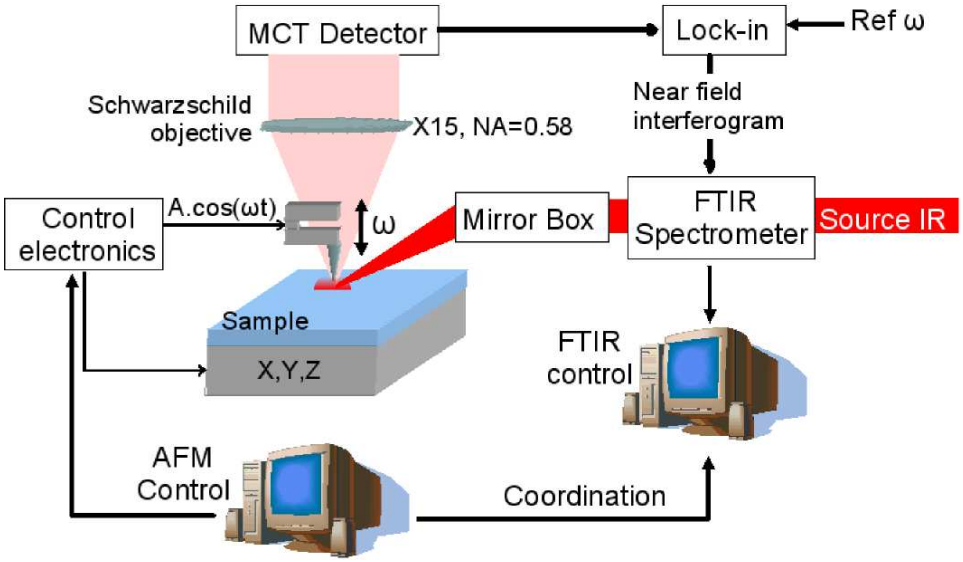


Figure 4.1: *Scheme of the synchrotron IR SNOM setup*

- the sample and force sensor are installed under an objective and the respective infrared detector of a confocal microscope;

- the sample is illuminated by infrared beam generated by a synchrotron, that passes through a FTIR spectrometer and is focused and sent onto the sample by a set of mirrors designated here by the mirror box. Another mirror box exists and consists in a set of mirrors interfacing between the source and the experiment and is not mentioned here in detail;

- the signal from the detector is filtered by a lock-in amplifier. The filtered signal is sent to the spectrometer for analysis;

- there are two computers: one to operate the AFM, through its control electronics, and another that operates the FTIR and confocal microscope. The first computer will also be responsible for the coordination between AFM movements and spectra acquisition. So that a spectrum can be obtain at each point of a topographical image.

Lets now see in detail the development of each of these elements in the system, the encountered difficulties and adopted solutions.

## 4.3 AFM Conception and Mechanical Design

### 4.3.1 Constraints and Needs

For integrating the AFM into the confocal microscope, one has to know this microscope and imagine how to make it working with our requirements. An image of the confocal microscope is presented in figure 4.2. There is a rotating objective selector with several different objectives installed. Two of them are reflective lenses and are the ones with fewer losses, compared with refractive lenses. We can see a motorised platform that is used for positioning and scanning the sample in the three directions. The resolution in this platform movement is about $10\mu m$ since that is the maximum resolution a confocal microscope with infrared can have. It also does not hold big loads since it was designed to hold samples. We can see that the microscope can also perform transmission microscopy which in our case could be useful with transparent samples.

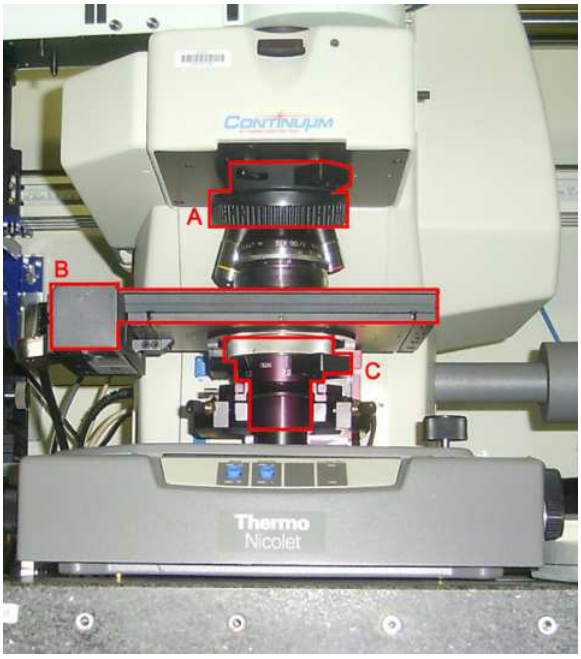


Figure 4.2: *View of the confocal microscope: A - objective selector; B - motorised platform; C - transmission objective.*

A few questions can be asked such as: can the motorised platform be used, can the objective be used in an off-axis position, can we change where the illumination comes from and how?

If the motorised platform can be used, we have already the $XYZ$ stage for positioning under the objective. This is not the case since this element is designed for holding samples only and seemed to be quite unstable if loaded

with the AFM for example.

If the angle of the objective could be changed, we would expect to capture more photons, since the emission in the vertical direction is not the most intense when a metallic tip is used to scatter a near-field wave .

If we could change the illumination we could improve the generation of the near-field wave on the sample since the vertical illumination, done through the objective, is not the most favourable. There would be a component of the electric field perpendicular to the surface.

Two fundamental aspects had also to be taken into account. One, is the space or volume available under the objective. Second, the bulkiness of the AFM itself. It has to fit and keep the desired characteristics at the same time. Therefore, motors and scanners had to be carefully chosen. The size could not compromise the range.

One of the requirements set for the microscope was that it should work with large samples unlike typical AFM microscopes. We are talking about centimeters range. This is not usual because this brings mechanical instability due to long lever arms.

It was also decided that both the sample and the tip should be provided with most possible degrees of freedom, for the positioning and scanning movements, since the operating procedures had still to be defined.

Another requirement was that the setup could be easily moved between different laboratories so that other sources could also be tried.

### 4.3.2 Solutions and development

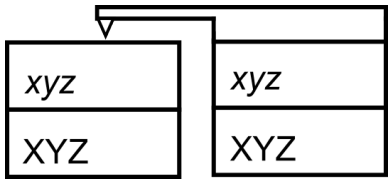


Figure 4.3: *Simple scheme of the movements required for the AFM to operate.*

The principle chosen for the AFM is illustrated in figure 4.3. Sample and tip are sitting on independent towers able to move independently. Below we have the positioning systems for both the sample and the tip, which can be done separately, and on top, the scanners also for both sample and tip. This will allow different approaches to the SNOM operation. We can chose for example to illuminate a specific point on the sample and do a scan over with the tip. Another possibility would be to fix the tip on a certain point, that can be the interception with the illuminating beam and then let the sample scan under it.

Here one major difficulty becomes evident, and would only be assessed with experience. The two approaches described above have to consider, not only the focal point of the illuminating beam but also the focal plane of the objective. The characteristics of a confocal microscope is that this plane is very thin, limiting the detection volume to a very confined volume. So far it is still not clear which would be the best approach.

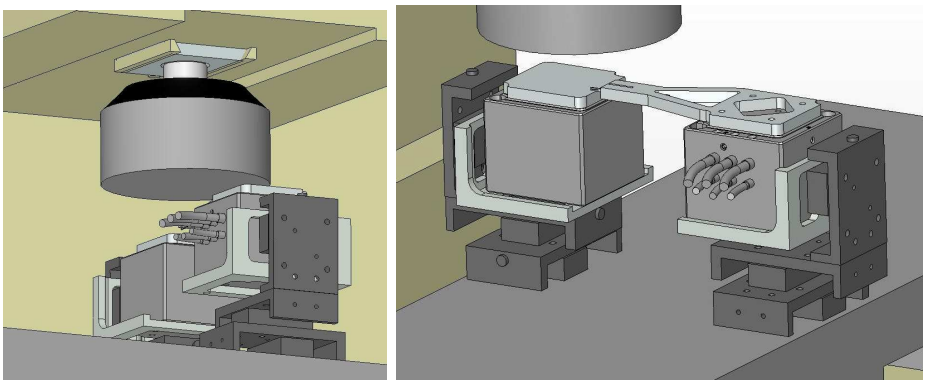

Figure 4.4: *Drawings of the first prototype installed under the objective - two different views.*

For the realization of this theoretical conception the motors and their configuration were finally selected. Before ordering the AFM motors, the integration into the confocal microscope had to be simulated to make sure that the mechanics were all correct, since every millimeter counted. By means of a 3D graphics design software I did the final drawings of the SNOM to be installed in place. This can be seen, with the sample correctly centered under the objective, in figure 4.4.

Figure 4.5: *From left to right - three inertial translation tables assembled together; piezo scanner with* 1*nm resolution in closed loop.*

Since the simulation showed no problems, motors and control electronics

were ordered. For positioning, they are inertial translation tables with $30mm$ travel, $200nm$ steps and the ability of supporting a $400g$ load. They can be assembled together to form a set of three capable of moving in the three directions, as illustrated in figure 4.5. In the same figure is shown one of two scanners capable of closed loop operation with around $1nm$ resolution and $38\mu m$ range in the three directions. Each one weights 130 grams, so they could easily carry the positioning motors.

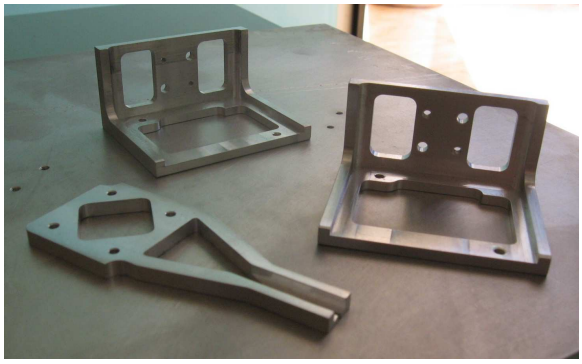

Figure 4.6: *Pieces designed to couple the piezo scanners with the translation tables, plus the force sensor holder.*

In order to couple the translation motors plus the scanner, in the tower configuration represented in the 4.3 scheme, some adaptation pieces were designed by me, as well as the arm that will hold the force sensor over the sample. These pieces are perforated and have large holes in order to decrease the load on the motors as can be seen in figure 4.6.

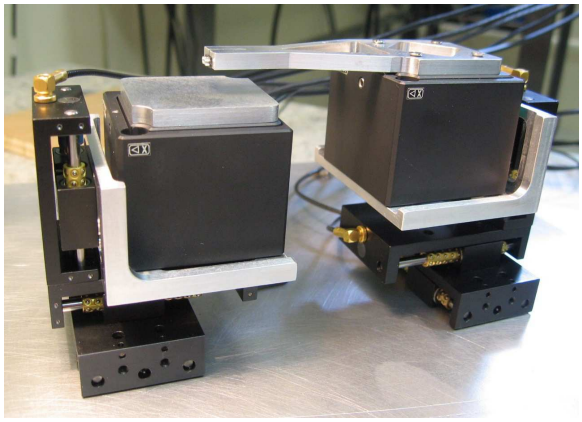

Figure 4.7: *Illustration of the first AFM prototype.*

The whole assembled prototype is shown in figure 4.7. At this point, the control electronics and computer had already arrived and the AFM tests

could begin. The first tests went on, unfortunately without success: the AFM was not able to regulate the tip-sample distance. There was too much mechanical instability.

After this experience, new ideas started to emerge and the prototype has been redesigned. Before introducing it, let us first look at the tips, something that at this moment was still under development.

## 4.4 Tips

The tip is a fundamental element in an AFM. It is the tip that determines the lateral resolution of the microscope. In commercial AFM microcopes, tips are usually part of a silicon cantilever and they are quite resistant to shock, suffering few damages when touching or even scratching a surface.

For the case of the SNOM, since it is an optical microscope, optical fibers are usually the adopted choice. These are usually not commercial and made by the user himself since it is one optical fiber with a tip at one end. The other extremity can either reach a detector or be used for laser injection. The optical fibers are tapered by mechanical pulling or chemical etching. Usually they are applied an opaque metallic coating on the sides for optical shielding, leaving a small aperture at the apex only. This coating can easily be removed by contact with a surface, forcing the microscope user to be extremely careful not to damage the probe, at the cost of having to remove the whole optical fiber. Optical fiber probes are therefore considered fragile.

In the case of this project, the scattering type of SNOM was chosen. The fundamental reason for this is that silica optical fibers have an absorption band in the infra red. Since we are not using a monochromatic laser, but the synchrotron white light instead, this absorption would probably be limiting the applications for this microscope.

The scattering tip that we use is a chemically etched tungsten wire. The tip is glued to a quartz tuning fork in what configures our force sensor. We have decided to produce our own tips following the method described by Kulawic *et al* [KNT$^+$03], which we have adapted. The publication describes a quite complete recipe, but nevertheless it does not have all the information needed for a successfull reproduction. I did an exhaustive study in order to understand the method and to be able to master it, since there are many variables involved.

There were two different kind of tuning forks, one had $3mm$ long prongs and the other $3.7mm$. The bigger one had also a bigger stiffness $K$, therefore less sensitive to a mass attached to it. There were also tungsten wires of two different diameters: $50\mu m$ and $125\mu m$, which would represent different loads on the tuning fork. Nevertheless the tungsten tips were always the shortest possible in order to minimize the mass load. We have always used the thinner wire, and the thicker wire, with the smaller tuning fork, and

bigger one, respectively. Eventually, the bigger option was not very much used with the AFM since it presented quality factors (Q) somewhat smaller and was therefore less sensitive. I had even designed two different tuning fork holders, for each of the options.

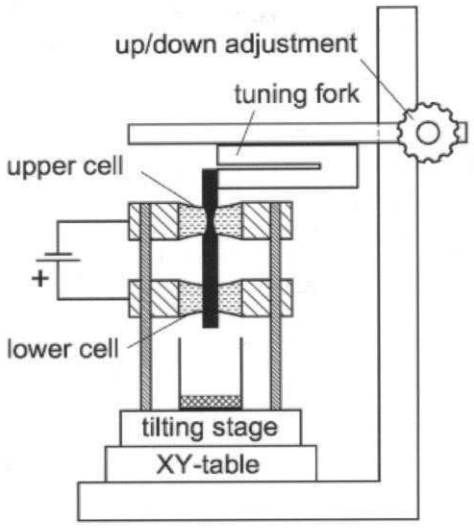


Figure 4.8: *The scheme used for production of the tungsten probes. Source: [KNT+03].*

In figure 4.8, is illustrated the scheme extracted from the publication that we have used for building our setup for producing the probes. Mr Kulawic's group also uses a quartz tuning fork just like we intend to do.

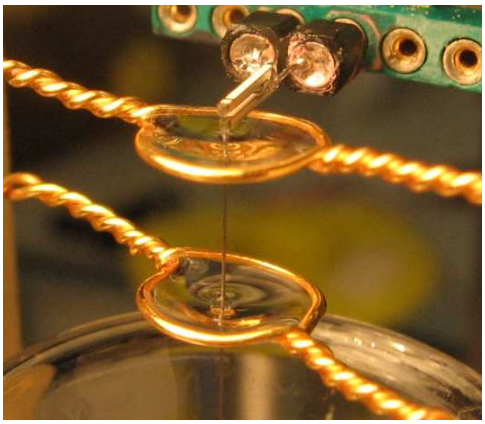

Figure 4.9: *Gold rings with suspended KOH drops and tungsten wire ready for etching.*

The process will now be described. To start, a short piece of tungsten

wire cut in advance is needed, also a quartz tuning fork and glue. The wire is glued to the end of a prong of the tuning fork and after a couple of minutes, when the glue is dry, the etching can be done. To do the etching, two drops of potassium hydroxide (KOH) at a concentration of 3M, a strong alkaline solution, are suspended in two gold rings. The gold rings, and therefore the drops, are kept at different electric potentials. Then the wire is dipped through both drops, like illustrated in figure 4.9, allowing an electrical current to circulate and electrolysis to happend, which is described by the simplified reaction:

$$W + 2H_2O + 2KOH \rightarrow 3H_2 + K_2WO_4$$

On the anode, the upper ring, is where the tungsten will be etched.

After etching for a while, the wire becomes so thin that the lower portion of it just falls down due to gravity alone. The electric circuit will then open up, since the wire is no longer connecting both drops, stopping any further etching. This leaves a nice uniform taper on the etched wire, now a nice tip on the prong of a tuning fork. This is showed on a sequence of pictures extracted from a movie made during the production of one tip, displayed in figure 4.10.

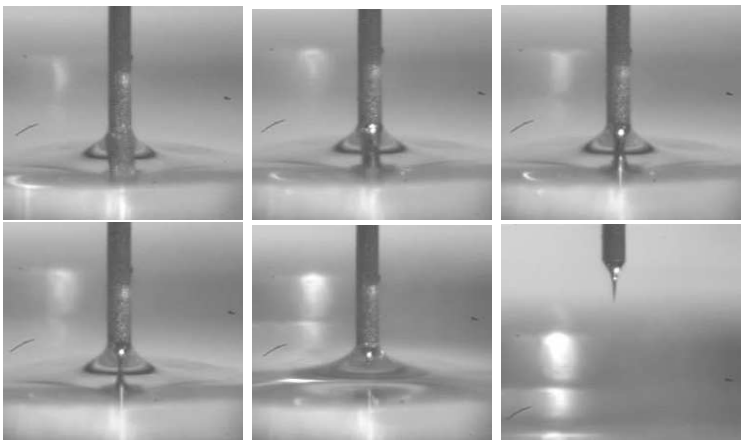

Figure 4.10: *Images taken during the etching of one tip.*

In order to achieve this success, I did many different experiments. Different applied electric tensions and different wire lengths were the two main variables. The length of the wire is important because the longer it would be, the heavier it would be and this would affect the moment of breaking during the etching. The voltage applied would determine the reaction speed. By examination of the results with an optical microscope and taking the best sets of results to a Scanning Electron Microscope (SEM), I have finally found the best combination between these two factors. Not only the result was good, but it was also reproducible.

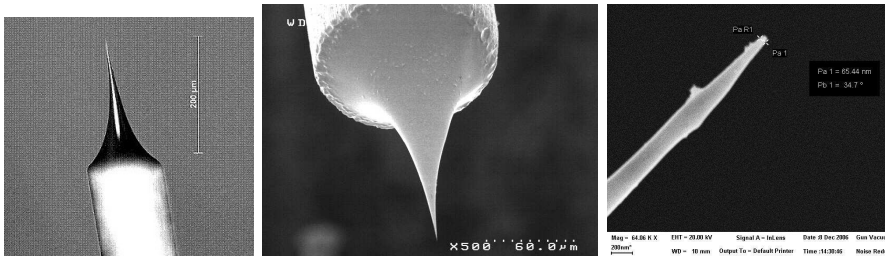

Figure 4.11: *Optical and SEM images of a good tip,* $200\mu m$ *long and* $65nm$ *diameter at the apex.*

In figure 4.11, the picture on the left hand side shows what would be considered a good tip on the optical microscope, and on the right hand side is a SEM image of a good tip, and the respective zoom in image. A measure was taken and indicates $65nm$ of apex diameter. The length of the taper is $200\mu m$. These measures are reproducible.

Our etching recipe was then to use a $2cm$ long piece of $50\mu m$ diameter tungsten wire, glued onto a small tuning fork. Apply $8V$ to the setup and after approximately 2 minutes the wire will breach.

For the big tuning fork and the $125\mu m$ diameter wire, the applied voltage would instead be $10V$ and the wire only $1cm$ long. The time was approximately the same.

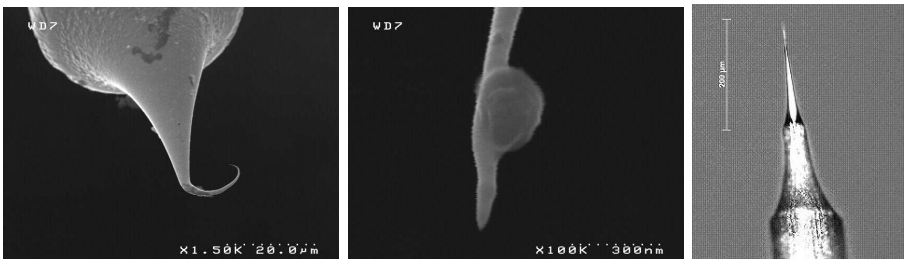

Figure 4.12: *Examples of defects found in tips.*

All this process is quite straightforward once fine tuned, but until then some defects were found to happen, as illustrated in figure 4.12. The first image on the left shows that the setup should be isolated from air drafts during the etching. When the wire was becoming thinner, the presence of air conditioning systems would make the hanging part of the wire balance. Putting a box covering the setup during the 2 minutes of the process would be enough. There is also no problem since the etching stops when the tip is made.

The next two images show defects that stopped appearing after some added precautions were implemented: cleaning the wire with ethanol before gluing without touching it again with the fingers; rinsing and cleaning well

the gold rings before and after, and rinsing the tip right after the etching is finished.

The figure 4.13 illustrates a force sensor ready for use. This is the place where we typically glue the tip, a good place if we want to use the tapping mode. It is clear that the amount of mass added is very small relatively to the size of the tuning fork. In the same figure, is presented an image done with that force sensor, where the grooves are $200nm$ deep.

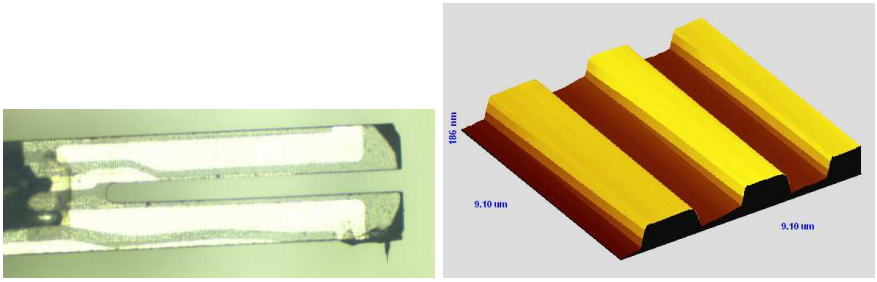


Figure 4.13: *Tuning fork with a tip and an image done with it.*

### 4.4.1 Variation

If we consider that our AFM is going to be used under an objective, the fact that the tip is situated under the tuning fork, will make it invisible. Regarding that the tip is not only part of the force sensor, but will also be the light scatterer, it is important that it can be seen by the objective.

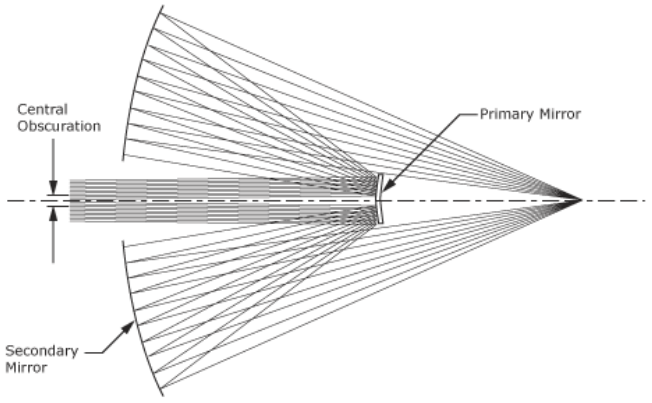


Figure 4.14: *Scheme of a Schwarzschild objective, reflective optics.*

The objective is a reflective objective in the Schwarzschild configuration as illustrated in figure 4.14. Although there is a blind section under the objective where the tuning fork can be placed with minimized interferences, the tip will anyway be hidden. Since I had good practice in producing tips,

Icame up with one solution that consist in extending the tip out from under the bulky tuning fork.

Figure 4.15: *New technique for producing a long tip.*

This is illustrated in the sequence of pictures in figure 4.15. The screen on the pictures was displaying the images from a telescope, which facilitates the job of handling and specially gluing such small objects. I started by bending the last 2 millimeters of a wire, precut with the right length of 2 centimeters as described in the tip making recipe. Then, as illustrated in the top left corner image, the wire is aligned with the tuning fork. Then, a single drop of glue is slowly approached to the bottom of the tuning fork until contact and then retracted. As we can see on the last image of the top row, a small quantity of glue stays on the tuning fork prong. On the bottom row, on the left, the wire is finally brought to contact and left there for a couple of minutes. Once the glue is dry, it can be dipped in the etching drop and the last picture shows the result.

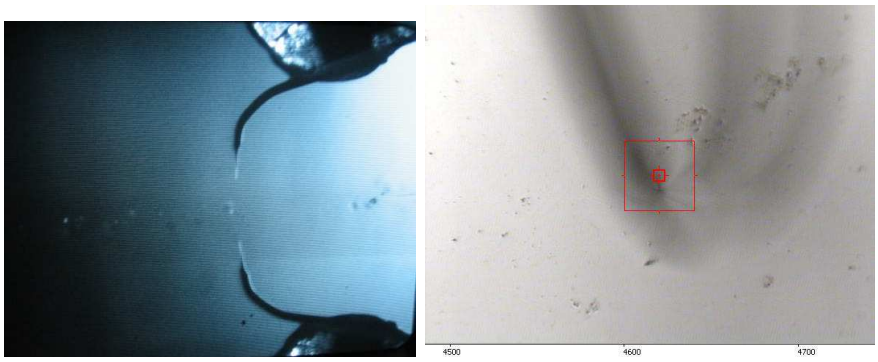

Figure 4.16: *Long tip ready for approaching a surface, and viewed by the objective.*

In figure 4.16, the picture on the left hand side illustrates one of these tips already close to a sample, just before the final approach. On the right

hand side, the tip is already touching the sample in tapping mode, viewed by the objective. This proves that this tip is a good idea since no tuning fork is on the way. We can slightly see a little bit of the wire. Note that although present, it seems transparent because it is in the blind volume of the objective. Moreover, the very tip can also be seen focused inside the red square since it is touching the sample and the sample is clearly focused. This is exactly what was needed.

One may now ask the question of how is the dynamics of such a system? I also did some calculations and reached an important conclusion. The extended wire with the tip cannot be longer than one millimeter and that is what we can see in the previous images. When these pictures were taken, I had already done this estimation.

The extended tip on the tuning fork configures a coupled oscillator. The excitation comes from the tuning fork that oscillates at approximately $32KHz$. The problem is simple: if we want the tip to oscillate in phase with the tuning fork, one has to simply ensure that the tip resonance frequency is higher that the excitation frequency. We can consider the following expression for calculating the tip resonance frequency:

$$\omega_0 = 2\pi f_0 = \frac{1,015T}{L^2}\left(\frac{E}{\rho}\right)^{1/2}$$

If we consider the diameter of the wire $T = 50\mu m$ and for the tungsten the constants $E(W) = 405GPa$ and $\rho(W) = 19250Kgm^{-3}$, it is easy to determine what is the resonant frequency for each length of wire. Note the proportionality with $1/L^2$.

| L [mm] | $F_0\left[10^4Hz\right]$ |
|---|---|
| 0,5 | 14,2 |
| 0,6 | 9,89 |
| 0,7 | 7,27 |
| 0,8 | 5,56 |
| 0,9 | 4,40 |
| 1 | 3,56 |
| 1,1 | 2,94 |
| 1,2 | 2,47 |

Table 4.1: *Table with tip lengths and respective resonance frequency.*

Table 4.1 shows the resonant frequencies for the respective tip length. We can see that for a $1mm$ tip the resonant frequency is $35KHz$, close to the tuning fork $32Khz$. Therefore the tip should always be the shortest possible but still visible by the objective.

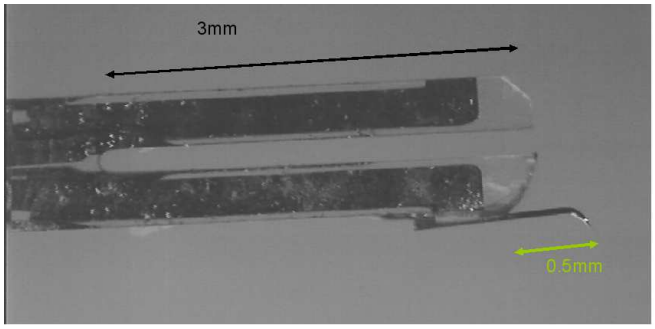


Figure 4.17: *Long tip well in the requirements.*

There is an example illustrated in figure 4.17. It looks long but it is indeed very well inside the defined parameters. We assume the glue has enough rigidity when dry.

### 4.4.2 Alternatives

Still on the force sensor manufacture, some variations were tried like gluing the tip in different places or with different orientations, so that other modes of vibration could be used, as illustrated on the scheme in figure 4.18.

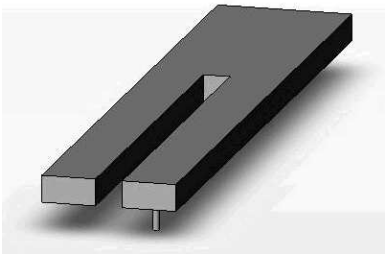

Figure 4.18: *Scheme of a tuning fork with a tip in position for other modes of oscillation.*

Figure 4.19: *Electrical contacts on the faces of a tuning fork.*

Usually the tip is glued closest to the edge of the tuning fork in order to minimize the damping of the oscillations. Taking into account the electrical contacts distribution of a tuning fork represented in figure 4.19 one can glue the tip close to one of the contacts using electrically conductive glue. This was made and for example, one could define the electric potential at the tip. If the potential of the sample could also be defined, many kinds of experiments could be performed.

## 4.5 Second AFM Prototype

As said before, the first AFM was not able to regulate the tip-sample distance. This was in part, or even mainly due to the way the force sensor was fixed to the holding arm. It was not rigid enough as fixation method. In figure 4.20 we can see the force sensor, the quartz tuning fork, decapsulated. In the first two images we can see that not only the capsule had been removed but also the ceramic base. The tuning fork was then held directly by its electric contacts. On the two images on the right hand side of the same figure, we see the tuning fork with the ceramic. This time, the tuning fork was tightly clamped between two screws on the ceramic base. This configures a much more solid mechanical structure and good results were obtained in this way as demonstrated further ahead.

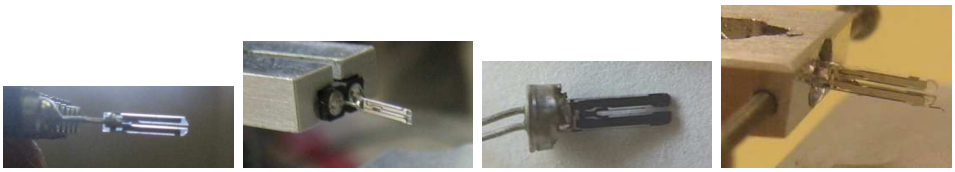

Figure 4.20: *Previous tuning fork fixation method vs new fixation method.*

At the moment of the first prototype we did not know what was exactly the problem, so it was decided to setup a more stable version. This time, based on more solid manual translation tables instead of the fully automated prototype. The motorized translation tables are less rigid, specially with those travel distances. Nevertheless, these were replaced by the same model but with the shortest travel, $8mm$ instead of $30mm$, at no extra cost. This would allow, after success, to change the AFM back to a fully automated version, on a more stable configuration.

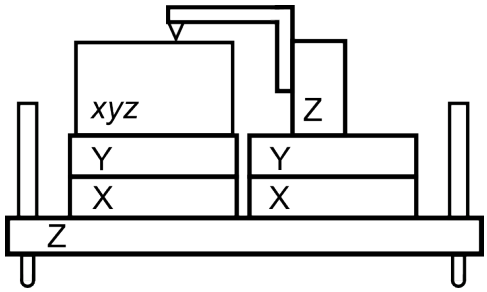


Figure 4.21: *Second scheme of the movements required for the AFM to operate.*

Another reason behind this new configuration is a better understanding of the needed operating procedures. This led to a better definition of the working protocol and therefore a change in the mechanics configuration.

This also led to the final design of the base, the fixed table that will hold the AFM when installed under the objective.

The generic concept is presented in figure 4.21, where you can see a much richer and complex system. The idea of bringing the sample to the objective's focal plane is now improved by having the whole AFM movement system on a common elevator base plate, keeping the two-tower principle. Now the sample has no longer an independent movement in the $Z$ axis direction, except for scanning.

The tip can be kept at a close distance from the sample while bringing the sample into the focal plane. The tip can also be approached and retracted independently and by means of a very useful remotely controlled motor. This makes the approach of the tip a much easier task than if it was done manually. The tip has no longer scanning capabilities since it would be an extra load on the vertical motor for the approach. This vertical movement was tested and proved to be repeatable, although with differences between the way up and way down. The $XY$ positioning tables are manual and stable for both tip and sample.

Figure 4.22: *Manual actuator and ESRF developed Microjack, the motorized actuator.*

The global vertical movement is manual and is controlled by three independent actuators. These actuators can be motorized later in the *microjack* configuration developed by the ESRF mechanical staff. These actuators, both manual and motorized are illustrated in figure 4.22. The actuators pass through the elevator plate touching the fixed base in three points. While manually operating, one has to adjust the actuators one by one, but when motorized, all can be moved at the same time avoiding the AFM from tilting. Nevertheless, this tilting of the AFM is very subtle to the naked eye. On the other hand, when looking at the image captured by the objective, because of the magnification, it becomes more important. That is why the motorization is considered.

The prototype was assembled and is shown in figure 4.23. This is the realization of the scheme presented in figure 4.21 just like it was used for AFM performance tests. The tests for this prototype were successfull and showed this was a good working AFM.

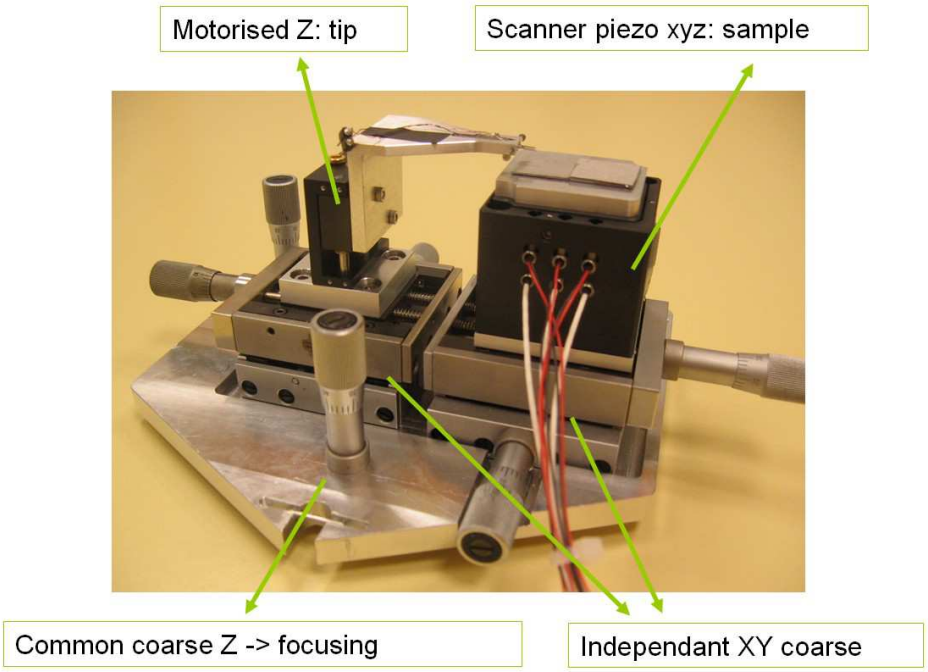


Figure 4.23: *The assembled second prototype.*

## 4.6 AFM Operation and Performance

As the AFM was built, the electronics and the computer have also been delivered. The infrared end station at the synchrotron was still undergoing preparative works for the SNOM and could not be used yet.

We started testing the stand alone AFM. This time, the mechanical configuration was clearly more rigid, and the force sensor was definitely better attached.

The Swiss made electronics from a company called Nanonis, consist in a control system and an oscillation controller. It is remotely commanded from a normal computer running a Nanonis software. This software is based on LabView, is very user friendly and can be adapted to ones needs. For example there is an extra module that does the automatic approach of the tip by controlling the coarse $Z$ motor as well as the scanner. Another important module for this project performs a spectroscopy mapping. It uses a grid and it can acquire an external signal, spectroscopic in our case, at each point of a topographic image. In this way we can obtain a topographical image superimposed with a spectroscopic mapping. In our case of the synchrotron infrared light, it would be the chemical mapping.

For now we had to learn how to approach the tip and keep it in regulation in at least one mode, the tapping mode. Then the scan control module,

which is also very rich in possibilities for scanning, had to be mastered too.

We were using electric excitation on the tuning fork. The amplifier had a compensation loop so that the resonance curve of the tuning fork would be symmetrical. Later, the mechanical excitation was preferred since no extra electronics were needed.

Finally we managed to keep the tip in control close to the surface in tapping mode. After trying it out and learning how to set the right parameters on the phase-locked loop (PLL, i.e., oscillation controller), set point and oscillation amplitude, some images started to come out. Then there was the difficulty of speed in acquiring images because the good quality factor of the force sensor was a limitation to it. A good oscillator has a long relaxation time. Therefore, any feature on the surface has to be slowly scanned so that the oscillator has time to relax and proceed the image acquisition with good quality.

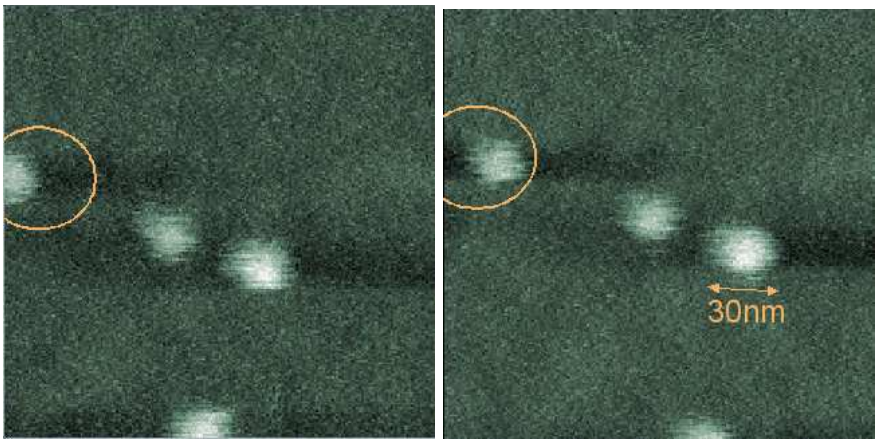


Figure 4.24: *AFM images of a* 250$nm$ *square, taken in 30 minutes each. It shows the AFM* 30$nm$ *lateral resolution.*

Once we were able to do good images it was time to evaluate the AFM performance in terms of stability, thermal drift, lateral resolution. A set of images done on silicon substrate with 5$nm$ silica particles is shown in figure 4.24. The particles measure 30$nm$ which is the lateral resolution of the AFM. The particles are in reality 5$nm$ big, but the convolution with the tip makes them look like 30$nm$. This is in agreement with our tips that typically have a diameter of approximately 60$nm$. The two images show a 250$nm$ square and were made at a speed of $50nms^{-1}$. They were taken one right after the other and each one took 30 minutes to be completed. If we focus on the particle with the circle around we can see that from one image to the other, it has moved, corresponding to a drift of 30$nm$ in 30 minutes.

The images in figure 4.25 are of a 1$\mu m$ square, taken at double speed of the speed used in the previous images, $100nms^{-1}$. They were also taken one

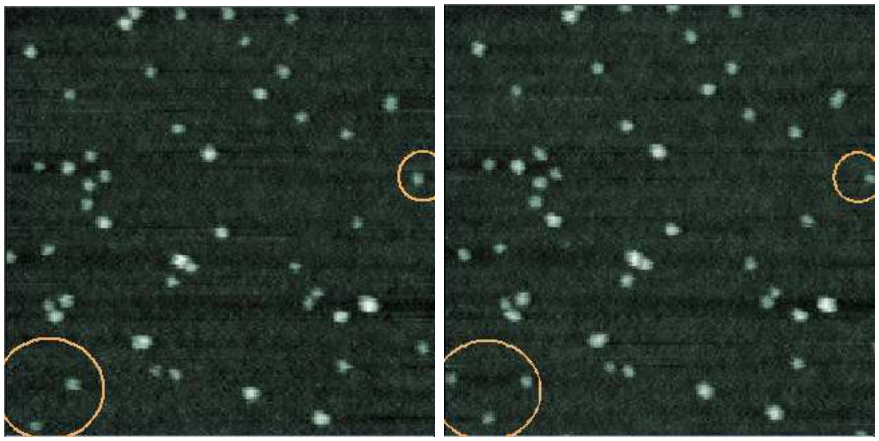

Figure 4.25: *AFM images of a* $1\mu m$ *square, taken in 1 hour each. It shows the 60nm per hour drift, confirming the 1nm per minute drift.*

right after the other and took 1 hour each to be completed. We can again see that the particles moved of about 60 *nm* in one hour, corroborating the precedent drift measurement of 1 *nm* per minute. This is of comparable quality to any commercial AFM.

The drift is an important issue in this project because we want to acquire a spectrum, or more, at each point of a map. The setup has to be very steady so that slow measurements can be made.

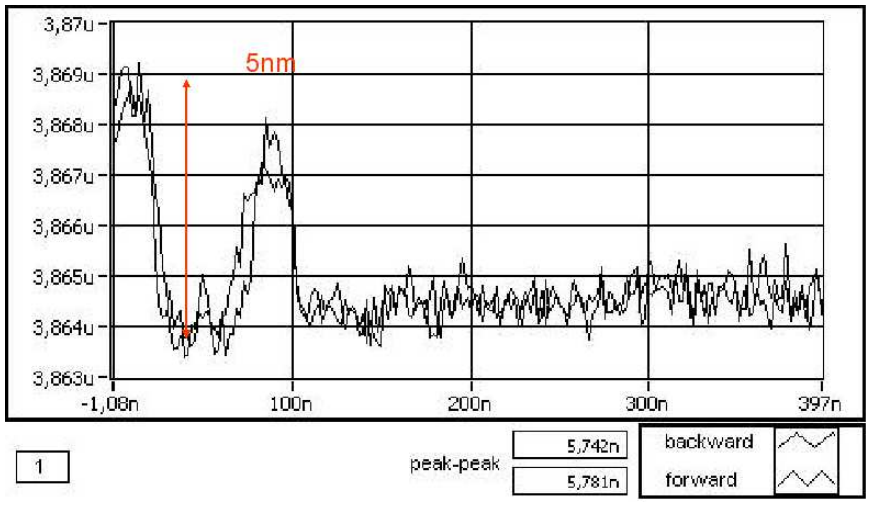


Figure 4.26: *Back and forward profile lines during the acquisition of images in figure 4.24, showing 5 nm high particles.*

In figure 4.26 are shown the backward and forward profile lines captured during the acquisition of the images in figure 4.24. The lines confirm the

size of the silica particles present on the sample, showing a 5 $nm$ height and again confirming the microscope's lateral resolution of 30 $nm$. Also here can be noticed the good signal to noise ratio.

The integration of the AFM in the infrared end station will be detailed in the next section, but here is the place to present its performance in the real working environment, the synchrotron radiation facility.

The synchrotron is a very noisy place for this kind of experiments. There are interferences from surrounding sounds, electricity and mechanical vibrations. The intensive presence of motors, vacuum pumps, electrical cables and many other devices can possibly interfer with the sensitive operation of an AFM microscope.

It was hard to even get the AFM to be in distance control. There was for example a nitrogen flux inside the microscope that had to be reduced since it was blowing into the AFM, but eventually it was possible to acquire images.

Figure 4.27 shows the comparison between two images of the same size acquired on the same sample. One is just the 3D image of one of the images in figure 4.25, done in a quiet lab, while the other was made in the infrared end station. The signal to noise ratio has clearly worsen but, fortunately, imaging of $5nm$ particles is still possible.

The force sensor in this case had a less good quality factor what helps in the case of presence of noises.

Two more examples of the AFM working in its real environment are presented in figure 4.28. The image on the left hand side is a $500nm$ square with a $200nm$ grain and was imaged at a speed of $200nms^{-1}$. The other image is a $2,5\mu m$ square where the sample was a 1 $\mu m$ width line pattern. The image was taken at fast speed, $400nms^{-1}$. This shows that the AFM does work well, including in noisy environments, like it will be needed.

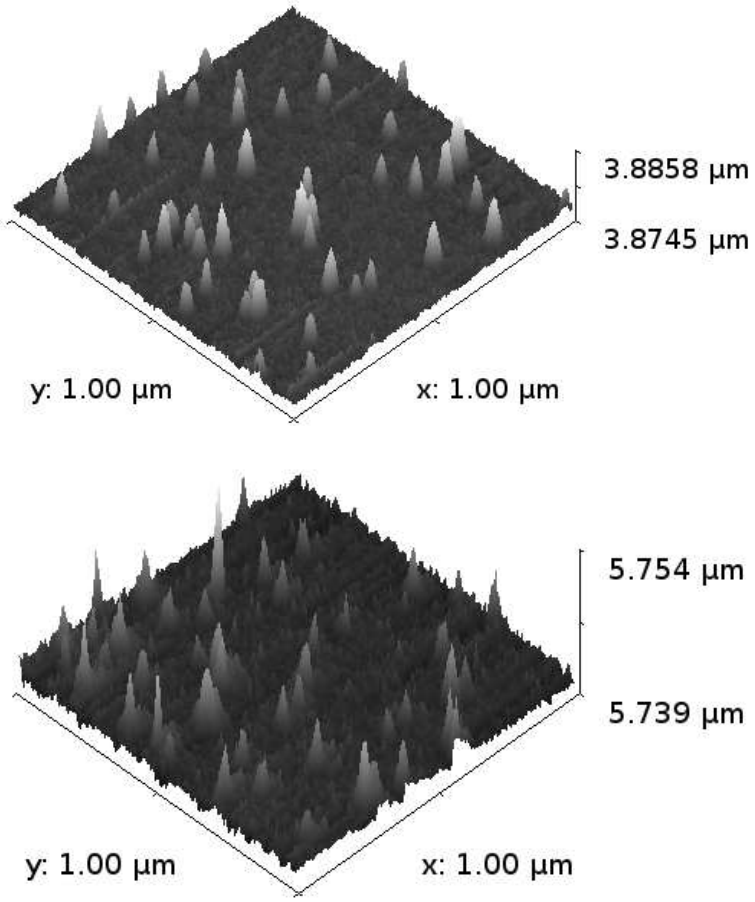


Figure 4.27: *Comparison of two images of the same sample in two different laboratories.*

## 4.7 Synchrotron Infrared End Station

The confocal microscope has to be prepared for each time the AFM is to be installed. One of the steps is the removal of the motorized platform since the AFM has its own positioning system and all the room that can be made available should be made available. The picture in figure 4.2, earlier in this chapter, shows these parts.

The confocal microscope is equipped with an objective selector. Since we only want to use one of the reflective objectives, we can remove this rather bulky selector. The chosen objective can be attached directly to the microscope by means of an adaptation plate designed by me, specifically for the occasion. Some centimeters are increased to the available height. This detail can be seen in the left drawing in figure 4.4 where the objective is

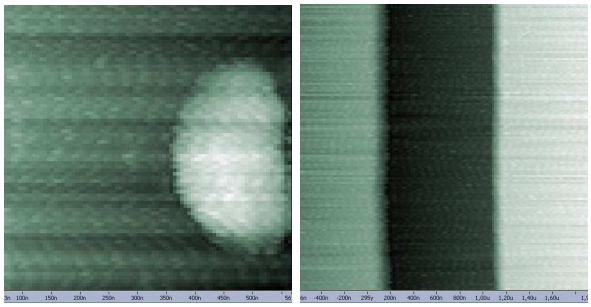

Figure 4.28: *AFM images made at the synchrotron setup, showing very reasonable stability.*

represented, screwed into the adaptation plate. The transmission objective is also removed reaching the maximum available volume. A little guide was made with pictures and instructions of how to prepare the microscope and the reverse as well, after removing the AFM. This guide can be found next to the Confocal microscope in the end station.

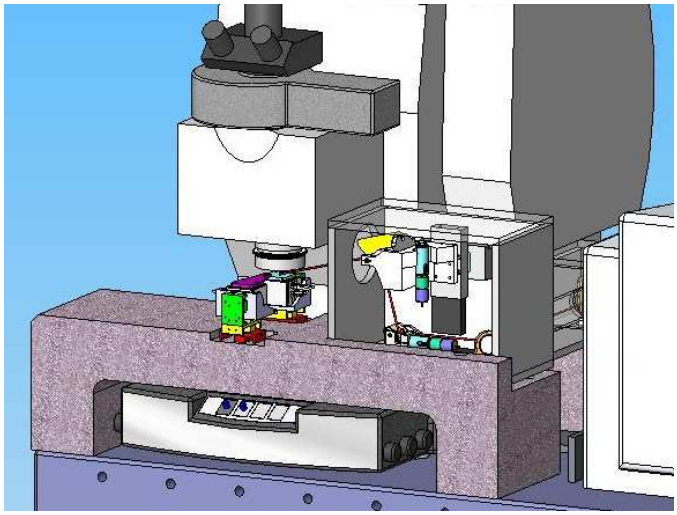

Figure 4.29: *First drawings with AFM and mirrorbox 2 integrated.*

The change in the beam path is part of the end station modifications and therefore was charged to ESRF staff. In particular a removable mirror box (MB2) was designed so that the beam would be intercepted, redirected, focused and finally illuminating the sample in grazing incidence for better generation of the near field. Thanks to the collaboration, the AFM drawings were integrated in the official drawings of the end station, like illustrated in figure 4.29. This would allow the mechanical engineering staff to properly design the mirror box 2 and the optical path of the beam, according to the SNOM needs.

The mechanical integration of the AFM in the microscope had to be carefully studied. Here is presented how the common elevator is the key element for this integration. As said before, this elevator has three actuators which are actually the contact point with the fixed table. It is very important to take advantage of having the three points. We can make use of an invention by Lord Kelvin. If there are three point on the AFM side, the base where the AFM sits will instead have a line, a point and a plane. This system gives a precision close to the micrometer when removing and putting back the AFM. The principle is illustrated in figure 4.30

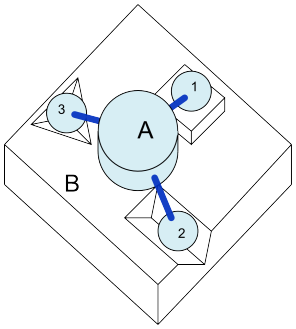


Figure 4.30: *Lord Kelvin's invented principle that allows the AFM "A" to be removed and put back on its base "B" with 1 μm precision. Point 1 sits on a plane, point 2 sits on line and point 3 sits on a point.*

The table that will hold the AFM is removable. The final version of this table is firmly bolted to the granite table and therefore very stable. It has the line, the point and the plane positioned in a way that when the AFM is placed, the sample holder sits centered, right under the objective axis. This is illustrated in figure 4.31. The elevator base was designed so that it could be secured by three springs to the fixed base. Since there is not much vertical space available, the AFM has also the sample holder on the objective focus with a little margin of half a centimeter on each direction. In this way, the sample cannot be thicker than one centimeter. The focal distance is $12mm$ like illustrated on the picture in figure 4.32.

Now that all the elements of the setup are there, we have started to learn how to operate the infrared beam, the mirror box 2, the microscope and the software that controls all the standard infrared microspectroscopy equipment. This includes choosing the FTIR and the microscope working parameters.

### 4.7.1 IR Beam and Signal Detection

The mirror box is also a removable part of the system. When installed, it intercepts the beam between the FTIR and the microscope with one mirror and sends the beam to the set of mirrors that will focus and position the

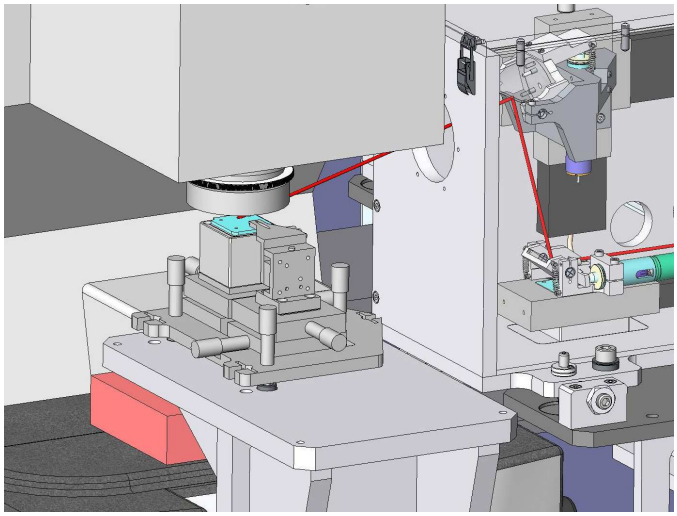

Figure 4.31: *Final drawing of the AFM on the definitive table and mirror box (MB2).*

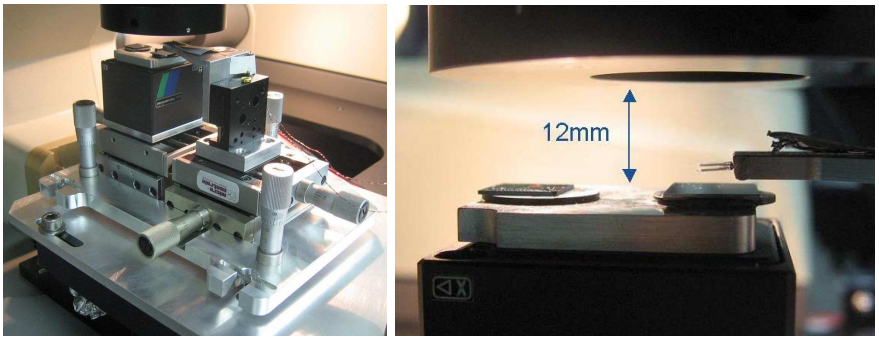


Figure 4.32: *Left: Final version of the AFM on the definitive table and mirror box (MB2); Right: Sample under objective at focal distance.*

focused beam on the sample. This set of mirrors is fully motorised. The possible movements are illustrated in figure 4.33. The last mirror is parabolic with a fixed focal distance of $203,2mm$.

In order to align the beam in the best possible way, the detector was used. By using a diffusive surface sample, the beam would scatter light in all directions. It was then possible to detect a signal whenever the most intense part of the beam would cross the objective axis. For this, we would move the motors in MB2 in a systematic fashion. First using the R1 rotation of the parabolic mirror, conjugated with its vertical translation with motor T3. Then, by moving motors T2 and T3 at the same time, the focused spot would travel on the sample surface and eventually be seen by the detector. In the end, by comparing the intensities, one could come back to the position

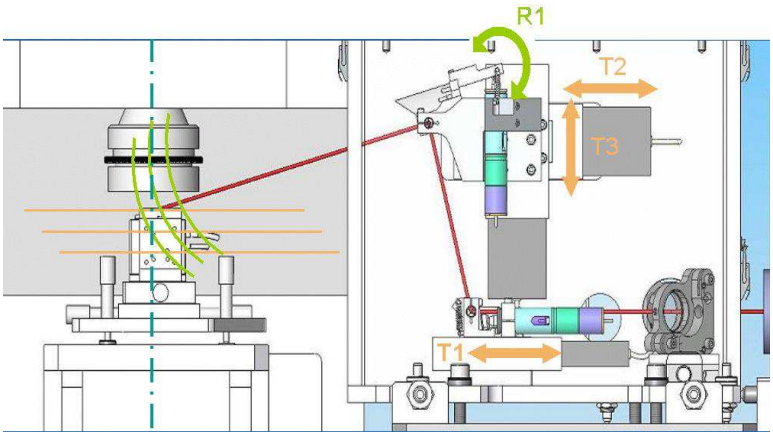


Figure 4.33: *Scheme of the possible movements for alignment of the beam focus with the objective.*

where the highest intensity was detected.

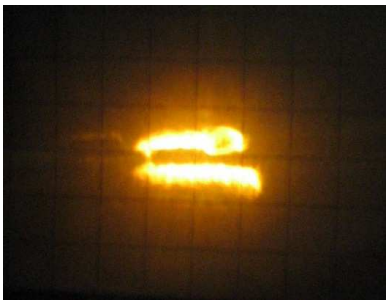

Figure 4.34: *The beam aspect before the FTIR. The image of the extracting mirror has almost 1,5 cm.*

There is a difficulty intrinsic to the way the IR beam is extracted. This is shown in figure 4.34 where the image of the extraction mirror can be seen. When the beam is focused by the parabolic mirror, under the objective, the same image can still be seen. It looks so big that we have to choose which of the two lines to use and which part of it. There were identified to peaks of intensity in the two lines. This means that a lot of photons will be out of the detection volume of the objective. The detector is only detecting the infrared photons and they are roughly coincident with the visible part of the beam. The detector also does not detect continuous signals and therefore in order to detect a diffuse signal from a sample, a chopper is used for modulation in combination with a lock-in amplifier. Otherwise, the AFM in operation is used, with the lock-in synchronized with the tip. This is how to do when finally looking for the wanted signal.

Just to start it is enough to do one point spectroscopy. This means that

the AFM does not have to scan the sample, and only approaching and retracting the tip is enough to keep it simple. Another important parameter is the amplitude of the tip oscillations. Some authors say that for the infrared, the optimal amplitude is of the order of $100nm$ [TKH05a]. This is for the case of the laser, and there is no information for the case of a white source.

When the sample is on the focus plane of the objective, the beam hits the sample surface in the objective axis, then the tip will be positioned in the center of axis as well. We can indeed detect the diffuse light modulated by the tip. But if we set the lock-in to filter the signal at $2\omega$, no signal is detected. If there was a detected signal, this meant that we were measuring a non linear effect, the second harmonic generation (SHG), and therefore a result of the evanescent wave. This signal is also expected to be much less intense than the signal at $\omega$.

At this point we can only say that the effect that we are looking forward to detecting, can be present but with lower intensity than the detector noise. The microscope has a second detector with a larger surface of detection, $250\mu m$ instead of $50\mu m$. This will allow more photons to be detected but with the drawback that noise increases by about a factor 10. Still, we have considered that there is not enough photon density on the focal point.

Since the interferometer inside the FTIR takes out half of the beam original intensity, it was decided to try and bypass over it. For this purpose, we have mounted a bypass with the help of mirrors and mirror mounts and for the first time we have detected a signal, during approach-retract experiments with big tuning fork amplitudes. the signal was not strong enough for $2\omega$ and it was not very consistent. Also the tip was already a bit damaged and probably a bit blunt, which probably helped.

In figure 4.35 is illustrated what was measured during two approaches of the tip to the sample, done at the same place of the sample, with the same amplitude. On the first, the contact happened at $1000s$ and on the second at near $800s$. The approaches were done at the same speed, so starting at the same distance, that corresponds to $200s$ before contact, the signal has a similar behaviour. Then, when changing place on the sample, the signal would have another profile, but still it would repeat itself if the same approach would be repeated. It is hard to propose an interpretation.

What we had so far is illustrated in figure 4.36, it is the generation of an evanescent wave and its extraction with a metallic tip. The problem is that the tip will also modulate all the light present at the surface. This complicates the detection because there is a lot of noise along with the signal we are looking for.

It would be great if we could have only the evanescent wave at the surface. Then I had the idea of illumination by total internal reflection in order to eliminate all the noise. There was some prisms available used for Attenuated Total Reflectance (ATR) that were immediately tested like illustrated in figure 4.37. One was made out of silicon and another made

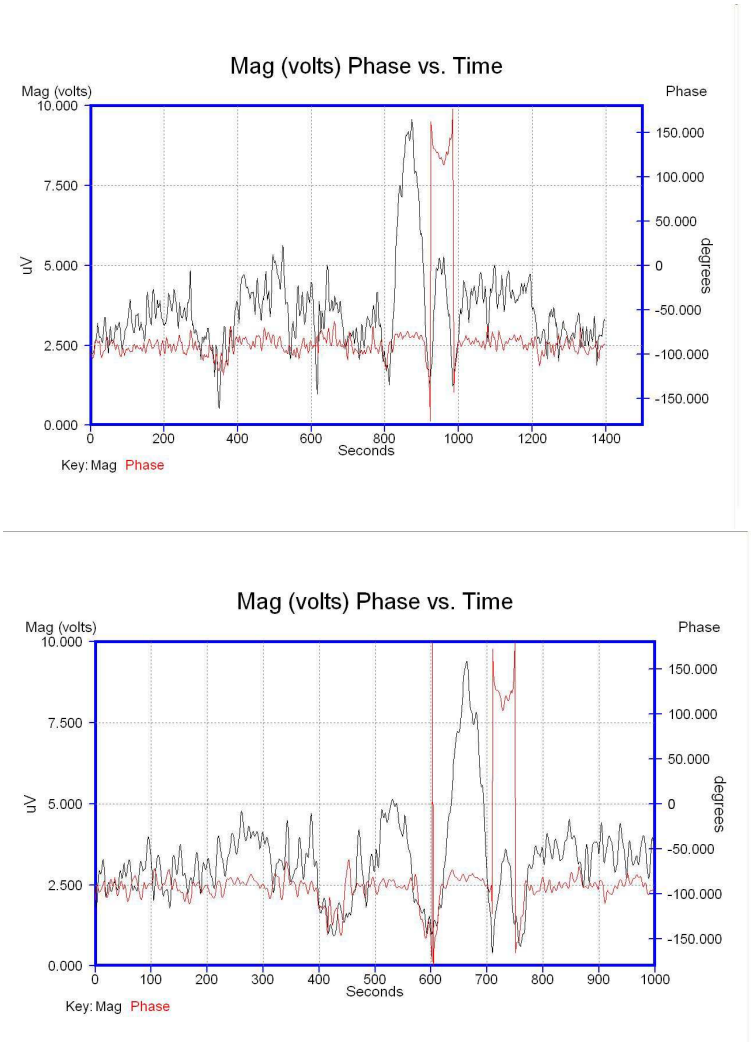


Figure 4.35: *Signal detected while approaching the tip.*

out of Zinc Selenide (ZnSe) a common material in infrared technology.

A simple calculation tells us that if a beam illuminates this prism in the perpendicular direction to the entry face, the reflections on the same side will have a $1cm$ period. This is helpful to know for when looking for the place of the internal reflection. It is enough to make a $1cm$ scan.

Because of the prism geometry, the MB2 cannot send the beam perpendicular to its face. The bypass had to be extended and bypass the MB2 too like illustrated in figure 4.38. Without MB2, it was noticed that the beam has a considerable divergence. Apparently the first mirror box, that shapes the beam, has one parabolic mirror mounted in the wrong direction. In order to minimize the effect of the divergence and make this idea usable,

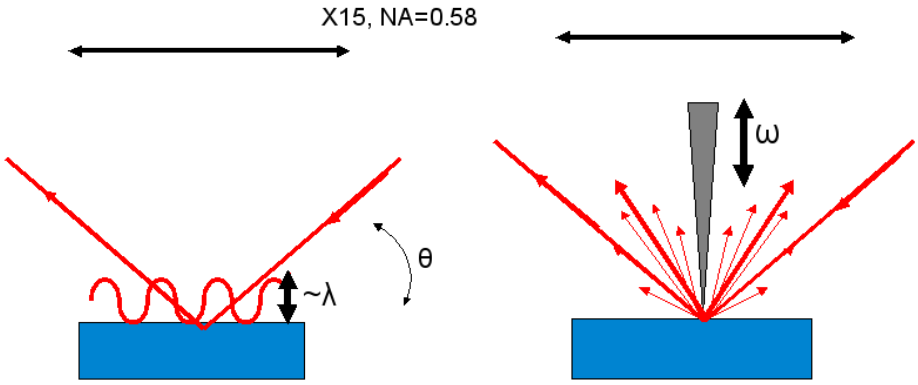


Figure 4.36: *The evanescent wave and its noisy extraction.*

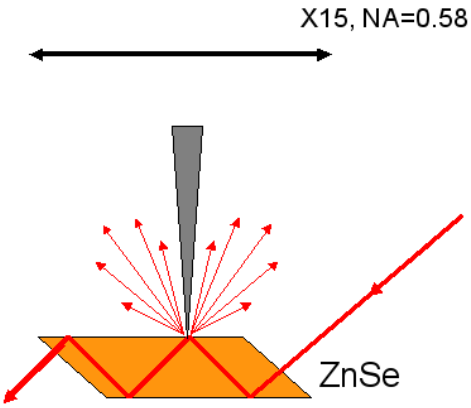


Figure 4.37: *The evanescent wave and a clean extraction due to internal reflection.*

a telescope was mounted with two parabolic mirrors with different focal distances which corresponds to the [EF] segment of the scheme. Although it was possible to decrease the size of the beam by approximately a factor 2 and send to the sample, this would still leave a larger spot than with the MB2.

On the picture in figure 4.39 we can see the successive internal reflections of synchrotron light on the ZnSe prism. This means that there is some light diffused at the surface probably due to the polishing state of the prism, and there is also the light emerging out of the last face. One can distinguish the two bands of the extration mirror.

The internal reflection can be seen by the microscope, in fact with little intensity, it cannot be detected. Nevertheless, it is enough to chose the prism position.We take the first reflection which has lost the least photons and position the tip over it in the center of the objective focus. The experiment

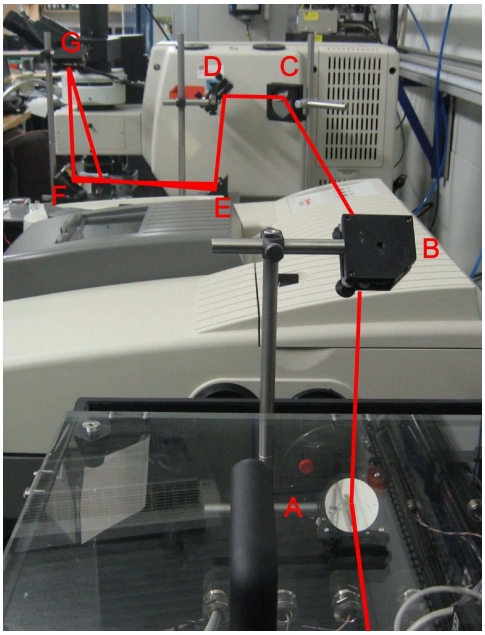


Figure 4.38: *Mounted bypass over the FTIR.*

seems better than any so far but still no signal was detected like this.

It needs to be said that during these approaches the tip is still and is actually the sample that does the vertical scan, from down to up until contact with the tip. This can be one of the problems since the sample is moving around the focal plane of the objective and decreasing the probability of making the signal reach the detector. This movement was rather under control, but still had to be chosen in which part of the approach the sample would be in focus. Usually it was chosen the moment of contact to be on focus. This lead to a change in the way the AFM would work when used with the lasers.

### 4.7.2 Signal estimation

At this point, there are doubts about that the system does not work because of a poor understanding of the setup or because of limited number of photons delivered by the source. An estimate can be done of the number of photons that could reach the detector and the minimum number of photons that can be detected.

The synchrotron infrared coming from the ultra high vacuum (UHV) pipes has to cross several windows. The windows have to exist for protection, separating different levels of vacuum. There are two diamond windows, they transmit 83% of the infrared each. There is also a KBr window that has a transmission of 96%. In the rest of the infrared system there are mirrors

Figure 4.39: *Successive internal reflections of synchrotron light on ZnSe prism.*

that have almost full reflectivity but there is still the interferometer that looses half of the intensity and also a mirror inside the microscope, before the detector that takes out another 50% of the intensity.

The intensity measurements were done in the optical bench, between the diamond windows and the KBr window, with three different filters at different wavelengths. There were measured between $10^{11}$ and $10^{12}$ photons/s/0.1%bw. This means that at the sample, there can be roughly $10^{11}$ ph/s/0.1%bw .

Trying to estimate the photons that will be extracted by the tip, one can consider that the tip has an average 60nm diameter, along the last micron and therefore $3\mu m^2$ surface. One micron because the near-field decays exponentially perpendicular to the surface and has in total approximately the size of the wavelength, a few microns in the infrared. When the beam was focused on the sample it was concentrated in a spot of about $300\mu m^2$. This makes a 100 times ratio. If the photons were homogeneously distributed, and the tip fully efficient, $10^9$ ph/s/0.1%bw would be extracted. Since the objective numerical aperture(NA) is 0.58, and $NA = n \sin\theta$, the collection angle is 70° and therefore only 40% of the photons are collected, if distributed homogeneously. The mirror inside the microscope cuts off another 50% which makes a total of $10^8$ ph/s/0.1%bw reaching the detector.

On the detector side, the given characteristic is the $D^*$ which is $5 \times 10^{10} cm\sqrt{Hz}/W$ for our detector. The Noise Equivalent Power (NEP) can now be calculated:

$$NEP = \frac{\sqrt{Ad\Delta f}}{D^*}$$

with the detector area $Ad = 6.25 \times 10^{-4} cm^2$ and bandwidth $\Delta f = 10^6 Hz$ which makes $NEP = 12.5 \times 10^{-9} W$. Still,

$$NEP = \frac{\Phi}{\sqrt{\Delta f} S/N}$$

where $\Phi$ is the radiation power that can be detected. If we let the signal to

noise ratio be close to one, then $\Phi = 1.25 \times 10^{-11} W$. Now, in order to obtain a flux in photons per second lets assume a $5\mu m$ photon with $E = 4 \times 10^{-20} J$. This gives a flux of $3 \times 10^8 Ph/s/\%0.1bw$.

This estimation gives the same order of magnitude between received and minimum detectable photons, with a lot of assumptions that can be very inaccurate. This strongly suggests that we are working close to our detection limit.

# Chapter 5

# Perspectives

## 5.1 Résumé

Le cinquième et dernier chapitre décrit de nouvelles expériences avec des lasers à faire un effort pour mieux comprendre ce système délicat. Un prototype de nouvelles mécaniques sont présentées et la configuration d'installation pour des expériences laser qui a été utilisée

**Contents**



## 5.2 Laser

Before any further research with the prototypes as they are, a few questions could be clarified. Namely, more information on the near field exaltation phenomena would be valuable, in order to understand in which direction our setup should be developed. It would also be good to understand if our setup has any elementary error and where are the weak or sensitive points.

An incursion in the world of lasers seemed to be an alternative. Lasers are much more powerfull than the synchrotron and the same kind of experiment could be carried out with a different source where the chances of success are much larger and is also a rather popular technique, the laser SNOM.

Lasers are in constant development and tunable lasers exist, in particular Optical Parametric Oscillator (OPO) are a recent technology. They are tunable and wavelengths can easily be changed.

### 5.2.1 Visible light laser experiment

There was the possibility of using a neighbour laser lab, in Institut Néel from CNRS. There were different lasers available as well as a space on a optical bench. LETI could lend an infrared confocal microscope similar to the one at the synchrotron.

It was decided that to start, we would try to perform a classic experiment of scattering SNOM microscopy with a He-Ne red laser. An identical Schwarzschild objective would be used. This would allow to practice the technique.

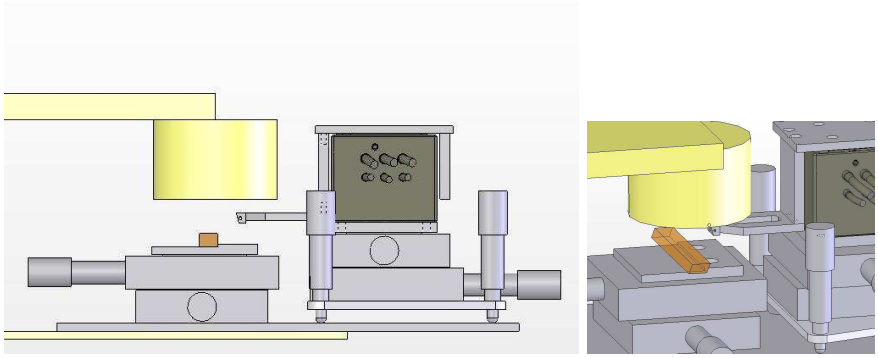

Figure 5.1: *Drawings for the new AFM design for laser experiments.*

A new setup required a new AFM prototype. Some changes were introduced to the new concept as can be seen in figure 5.1. For example, it was decided to scan the tip rather than the sample. In approach-retract experiments, the sample would now be permanently on focus and the tip would do the vertical movements.

The whole AFM could stay on the microscope sample holder, that in this case is manual and much more rigid. This would do the office of total elevator and sample focusing mechanism. The tip is mounted on a manual elevator system of three feet like in the second prototype, which allowed to remove and reposition the tip easily. This showed to be enough for the coarse part of an tip approach. A picture of this new designed AFM is illustrated in figure 5.2. The base plate is fixed to the microscope elevator so it is the sample holder.

We have learned about lasers and tested some. Then we prepared the setup on the optical bench and tried a red laser on the ZnSe prism. We were so far without a detector. There was no photomultiplier available.

Meanwhile we had been to Université de Technologie de Troyes (UTT), partner in the ANR project, and had arranged for an experiment during one week.

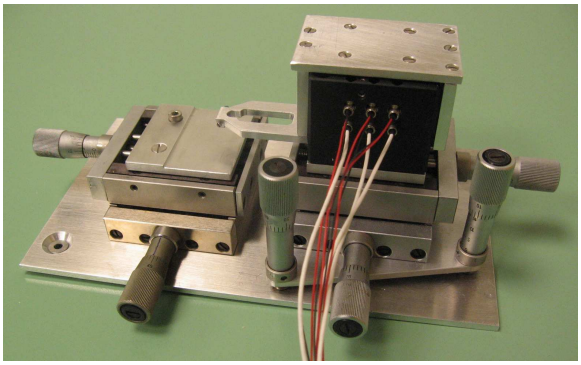

Figure 5.2: *Picture of the new AFM design for laser experiments.*

### 5.2.2 IR $CO_2$ Laser Experiment

The UTT had just bought a $CO_2$ laser. This was the chance to try an experiment with a laser-based IR SNOM.

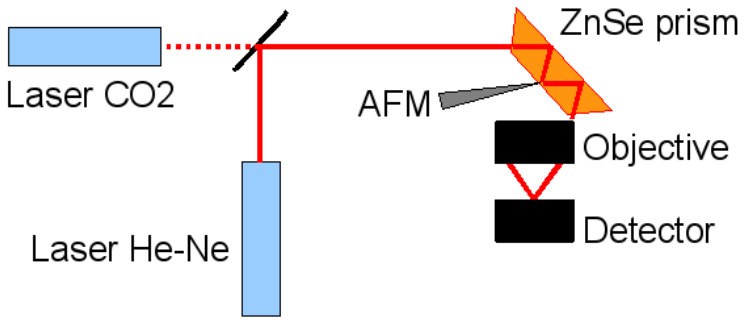


Figure 5.3: *Scheme of the experimental setup with the infrared $CO_2$ laser.*

Figure 5.3 illustrates the scheme of the proposed setup for this experiment. Since the $CO_2$ laser is invisible, it is usually combined with a visible laser by means of a beam splitter. Then the idea is to do what we had been doing until now: to use the total internal reflection with a ZnSe prism, frustrate the evanescent wave with a tip, capture the signal with an objective and send it to the detector. The detection is also to be done with a lock-in amplifier.

In fact, the tip was mounted directly on the scanner without a force sensor, this means that it was not vibrating. Then it was approached manually into the red spot at the prism surface. This spot is where the internal reflection happens and can be seen due to some surface diffusion. Then the detection is done with the lock-in amplifier synchronized with the IR laser pulsation.

The big difficulty in this experiment was that the detection part had

to be assembled. We had avoided this when conceiving the first prototype and that is why we had decided to use the commercial microscope. It is hard to match the detection volume where the signal is generated with a detector that has a $50\mu m$ cell. If the optics are moved in search for the signal, the image that should hit the detector is consequently moved away from its previously aligned position. If on the other hand, the optics stays still and the sample is moved in front of the objective, then the illumination conditions change. This is a dilemma. The solution previewed for the next experiment would be to solidarize the optics with the detector, and then scan the sample with the whole ensemble.

The whole AFM system had to be taken to the laboratory where the laser was. This proved the portability of our system: electronics rack, computer and AFM.

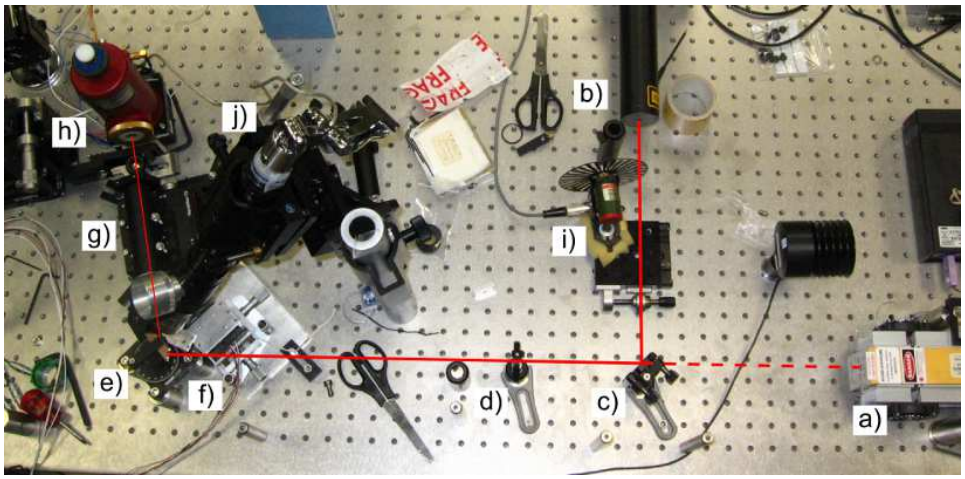


Figure 5.4: *Picture with scheme of the experimental setup with the infrared $CO_2$ laser: a) IR laser; b) red laser; c) beam splitter; d) pinhole; e) sample holder; f) AFM; g) optics; h) detector; i) chopper; j) camera.*

The laser has a control device that allows to operate in the continuous or in the pulsated modes. To start, the laser is combined and aligned with the red laser with the help of a beam splitter and two pinholes. Both beams are aligned when both are passing through the two well separated pinholes.

A detailed scheme is illustrated in figure 5.4. There is a webcam mounted on a telescope, to look at the interaction point. In figure 5.5 is illustrated the prism with the entrance point of the two lasers together on the left, and the second reflection point, where the tip will be approached. This point is to be aligned with the objective focus point. The trajectory of the beam inside the prism can also be seen.

The optics are two schwarzschild objectives attached to each other, one with the focal point on the sample and the other with the focal point on the

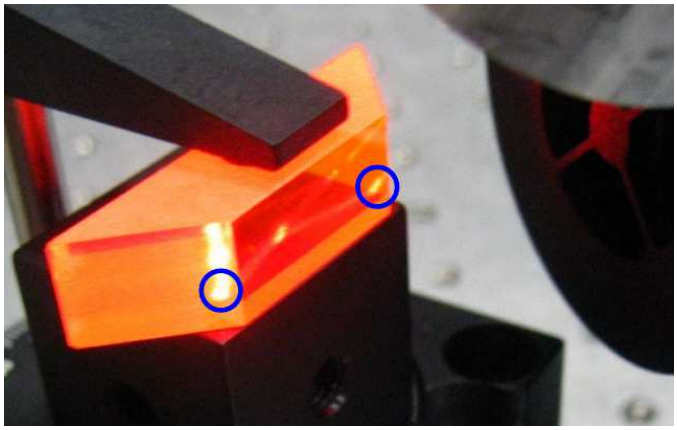

Figure 5.5: *Prism with entrance point of the two merged lasers and the second reflection, the future interaction point.*

Figure 5.6: *Projection on the sample of the green light source at the detector position.*

detector. These optics had to be aligned between sample and detector. A point-like light source was placed at the detector position. Then the image of this green light source was positioned on the sample like illustrated in figure 5.6.

Then the opposite was done by bringing a special optical fiber with the green light, into the red spot and looked for its image on the detector side like illustrated in figure 5.7. On the right side, the optical fiber over the red spot as viewed by the camera.

After the alignment procedures a tungsten wire was approached to the spot of the internal reflection and no signal was detected. The optics were again changed, this time with only one objective and the detector further away. More tests followed without success until the end of the limited time to realize the experiment.

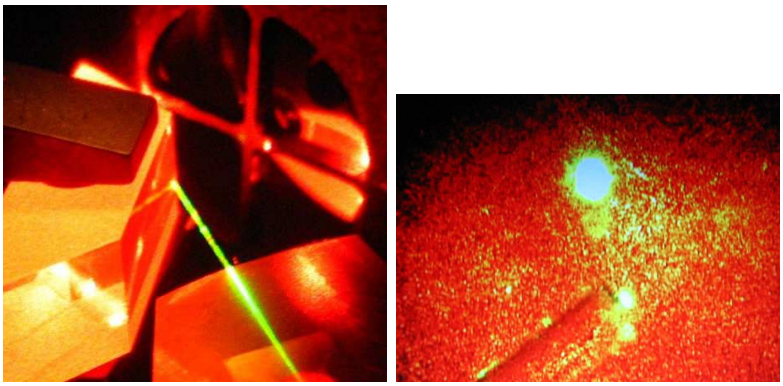

Figure 5.7: *Optical fiber with green light positioned over the red spot for detector alignment.*

# Conclusion

L'AFM fonctionne bien et les techniques pour opérer avec elle sont bien compris. L'intégration de l'AFM avec le microscope infrarouge a aussi été achevée et les expériences ont été effectuées.

Il y avait seulement l'accès au faisceau infrarouge, une fois tous les six mois en moyenne. Le rayonnement synchrotron a des modes de fonctionnement différents et un seul d'entre eux, le mode bouquet complet, est intéressant pour ces expériences, car elle offre le maximum de photons possible.

Un bon résultat serait tout simplement l'acquisition d'un signal de champ proche. Tout le reste a jusqu'ici bien fonctionné. On pourrait en effet être déjà détecter, mais malheureusement nous n'avons pas été capables de filtrer ou de le décoder.

En ce qui concerne la présente plusieurs questions se posent. Toutes les publications que nous avons suivi le traitement des sources monochromatiques et n'a donc jamais eu à faire face au fait que les longueurs d'onde différentes sont présentes dans le champ proche. Chaque amplitude d'oscillation du capteur de force est optimal pour une de ces longueurs d'onde [TKH05a]. Si l'on veut extraire de faon optimale toutes les longueurs d'onde, l'amplitude des oscillations du capteur de force serait éventuellement également être scannés dans une certaine plage tout en récoltant les données d'un seul point dans l'analyse.

De Wilde a utilisé le rayonnement thermique des corps de chauffe comme source infrarouge. Il n'est pas monochromatique et pourtant il obtient des images en intégrant l'ensemble du spectre détectable. Jusqu'à présent, il ne fonctionne pas spectroscopie mais les vagues images de surface, sur des échantillons de SiC avec des motifs en or, un échantillon suffisant pour la génération d'ondes de surface [WFC$^+$06].

Ce qui limite le succès des expériences? Est-ce l'intensité seule? Nous sommes très proches de la limite de détection du détecteur, mais il est difficile de savoir exactement o nous sommes.

Serait-ce un problème d'alignement que nous ne sommes pas encore au courant? Tout le système optique est délicate et complexe à la même époque, en sorte qu'un petit changement pourrait entraner des changements drastiques dans le résultat.

Afin de poursuivre cette recherche, une meilleure compréhension des phénomènes mis en jeu est désiré à l'aide de lasers. Ces sources sont beaucoup plus intense que le synchrotron infrarouge et permettrait la détection d'un signal.

Avec l'utilisation de lasers, d'autres techniques peuvent être utilisées que par ailleurs il n'était pas possible avec notre faisceau semaine. Un exemple est la détection hétérodyne qui implique la scission du faisceau d'éclairage et la recombinaison après l'échantillon. De cette faon, le S / N devient beaucoup plus importante en raison de filtrage du bruit par interférométrie. Un autre avantage des lasers intenses est la détection du signal de champ proche à $2\omega$, impossible avec l'intensité de rayonnement synchrotron disponibles aujourd'hui dans l'infrarouge.

# Conclusions

The AFM works well and the techniques for operating with it are understood. The integration of the AFM with the infrared microscope was also completed and experiments were done.

There was only access to the IR beam once every six months in average. The synchrotron has different operation modes and only one of them, the full bunch mode, is interesting for these experiments since it delivers the maximum amount of photons possible.

A good result would simply be the acquisition of a near-field signal. Everything else so far has worked well. We could indeed be already detecting it but unfortunately we have not been able to filter it or to decode it.

In respect to this several questions arise. All the publications that we have followed treat monochromatic sources and therefore never had to deal to the fact that different wavelengths are present in the near-field. Each oscillation amplitude of the force sensor is optimal for one of these wavelengths [TKH05a]. If we desire to optimally extract all the wavelengths, the oscillation amplitude of the force sensor would possibly also have to be scanned within a certain range while collecting data of one single point in the scan.

De Wilde was using the thermal radiation of the heated bodies as source of infrared. It is not monochromatic and nevertheless he obtains images by integrating all the detectable spectrum. So far, he is not performing spectroscopy but imaging the surface waves, on SiC samples with Gold patterns, an adequate sample for surface wave generation [WFC$^+$06].

What is limiting the success of the experiments? Is it the intensity alone? We are very close to the detection limit of the detector but it is hard to know where exactly we are.

Could it be a problem of alignment that we are not yet aware of? All the optical system is delicate and complex at the same time, in a way that a small change could lead to drastic changes in the result.

In order to continue this research, a better understanding of the involved phenomena is desired by using lasers. These sources are much more intense than the synchrotron infrared and would allow the detection of a signal.

With the use of lasers, other techniques can be used that otherwise it was not possible with our week beam. One example is the heterodyne detection

which implies the splitting of the illuminating beam and recombination after the sample. In this way, the S/N becomes much larger due to noise filtering by interferometry. Another advantage of the intense lasers is the detection of the near field signal at $2\omega$, impossible with the synchrotron intensity available today in the infrared.

# Bibliography


[Abb73] E. Abbe, *Beiträge zur theorie des mikroskops und der mikroskopischen wahrnehmung*, Archiv für Mikroskopische Anatomie **9** (1873), no. 1, 413–418.

[AGHR91] T. R. Albrecht, P. Grütter, D. Horne, and D. Rugar, *Frequency modulation detection using high-q cantilevers for enhanced force microscope sensitivity*, Journal of Applied Physics **69** (1991), no. 2, 668–673.

[BQG86] G. Binnig, C. F. Quate, and Ch. Gerber, *Atomic force microscope*, Phys. Rev. Lett. **56** (1986), no. 9, 930–933.

[BRGW82] G. Binnig, H. Rohrer, Ch. Gerber, and E. Weibel, *Surface studies by scanning tunneling microscopy*, Phys. Rev. Lett. **49** (1982), no. 1, 57–61.

[CGB+98] A. Cricenti, R. Generosi, C. Barchesi, M. Luce, M. Rinaldi, C. Coluzza, P. Perfetti, G. Margaritondo, D.T. Schaafsma, I.D. Aggarwal, J.M. Gilligan, and N.H. Tolk, *First experimental results with the free electron laser coupled to a scanning near-field optical microscope*, physica status solidi (a) **170** (1998).

[CGP+98] A. Cricenti, R. Generosi, P. Perfetti, J. M. Gilligan, N. H. Tolk, C. Coluzza, and G. Margaritondo, *Free-electron-laser near-field nanospectroscopy*, Applied Physics Letters **73** (1998), no. 2, 151–153.

[Che08] C. Julian Chen, *Introduction to scanning tunneling microscopy*, 2. ed. ed., Monographs on the physics and chemistry of materials, Oxford Univ. Press, Oxford [u.a.], 2008.

[Chr95] Douglas A. Christensen, *Analysis of near field tip patterns including object interaction using finite-difference time-domain calculations*, Ultramicroscopy **57** (1995), no. 2-3, 189 – 195, Near-Field Optics.

[CRB+06] N. Chevalier, N. Rochat, F. Bertin, A. Chabli, M. Silveira, M. Cotte, J. Susini, F. Comin, P. Royer, G. Lrondel, S. Blaize, Y. Sonnefraud, F. Martins, H. Seillier, and S. Huant, *Le rayonnement synchrotron infrarouge pour les techniques de champ proche optique*, GDR Ondes "Dispositifs et Composants en Champ Proche", 2006.

[DPGO05] A. Dazzi, R. Prazeres, F. Glotin, and J. M. Ortega, *Local infrared microspectroscopy with subwavelength spatial resolution with an atomic force microscope tip used as a photothermal sensor*, Opt. Lett. **30** (2005), no. 18, 2388–2390.

[DZS92] U. Dürig, O. Züger, and A. Stalder, *Interaction force detection in scanning probe microscopy: Methods and applications*, Journal of Applied Physics **72** (1992), no. 5, 1778–1798.

[FK96] Hiromitsu Furukawa and Satoshi Kawata, *Analysis of image formation in a near-field scanning optical microscope: effects of multiple scattering*, Optics Communications **132** (1996), no. 1-2, 170 – 178.

[FWA05a] F. Formanek, Y. De Wilde, and L. Aigouy, *Analysis of the measured signals in apertureless near-field optical microscopy*, Ultramicroscopy **103** (2005), no. 2, 133 – 139.

[FWA05b] ———, *Analysis of the measured signals in apertureless near-field optical microscopy*, Ultramicroscopy **103** (2005), no. 2, 133 – 139.

[FWLA04] F. Formanek, Y. De Wilde, and Y. Chen L. Aigouy, *Apertureless near-field scanning optical microscope working with or without laser source*, Scanning **I63** (2004), no. 26.

[GAS+00a] R. D. Grober, J. Acimovic, J. Schuck, D. Hessman, P. J. Kindleman, J. Hespanha, A. S. Morse, K. Karrai, I. Tiemann, and S. Manus, *Fundamental limits to force detection using quartz tuning forks*, Rev. Sci. Inst. **71** (2000), 2776.

[GAS+00b] Robert D. Grober, Jason Acimovic, Jim Schuck, Dan Hessman, Peter J. Kindlemann, Joao Hespanha, A. Stephen Morse, Khaled Karrai, Ingo Tiemann, and Stephan Manus, *Fundamental limits to force detection using quartz tuning forks*, Review of Scientific Instruments **71** (2000), no. 7, 2776–2780.

[GBSU95] M. J. Gregor, P. G. Blome, J. Schöfer, and R. G. Ulbrich, *Probe-surface interaction in near-field optical microscopy: The nonlinear bending force mechanism*, Appl. Phys. Lett. **68** (1995), 308.

[GC90] C. Girard and D. Courjon, *Model for scanning tunneling optical microscopy: A microscopic self-consistent approach*, Phys. Rev. B **42** (1990), no. 15, 9340–9349.

[GD96] Christian Girard and Alain Dereux, *Near-field optics theories*, Rep. Prog. Phys. **59** (1996), 657–699.

[Gie98] Franz J. Giessibl, *High-speed force sensor for force microscopy and profilometry utilizing a quartz tuning fork*, Applied Physics Letters **73** (1998), no. 26, 3956–3958.

[GSPH00] H. Göttlich, R. W. Stark, J. D. Pedarnig, and W. M. Heckl, *Noncontact scanning force microscopy based on a modified tuning fork sensor*, Rev. Sci. Inst. **74** (2000), 3104.

[HGM02] S. Hembacher, F. J. Giessibl, and J. Mannhart, *Evaluation of a force sensor based on a quartz tuning fork for operation at low temperatures and ultrahigh vacuum*, Applied Surface Science **188** (2002), no. 3-4, 445 – 449.

[Hil04] Rainer Hillenbrand, *Towards phonon photonics: scattering-type near-field optical microscopy reveals phonon-enhanced near-field interaction*, Ultramicroscopy **100** (2004), no. 3-4, 421 – 427, Proceedings of the Fifth International Conference on Scanning Probe Micrscopy, Sensors and Nanostructures.

[HKRF04] M. Heyde, M. Kulawik, H.-P. Rust, and H.-J. Freund, *Double quartz tuning fork sensor for low temperature atomic force and scanning tunneling microscopy*, Rev. Sci. Instrum. **75** (2004), 2446.

[Jac99] John David Jackson, *Classical electrodynamics*, 3rd ed. ed., Wiley, New York, NY, 1999.

[Kar06] K. Karrai, *Photonics: a cooling light breeze.*, Nature **444** (2006), no. 7115, 41–2 (eng).

[KG95] Khaled Karrai and Robert D. Grober, *Piezoelectric tip-sample distance control for near field optical microscopes*, Applied Physics Letters **66** (1995), no. 14, 1842–1844.

[KK00] Bernhard Knoll and Fritz Keilmann, *Enhanced dielectric contrast in scattering-type scanning near-field optical microscopy*, Optics Communications **182** (2000), 321–328.

[KNT+03] M. Kulawik, M. Nowicki, G. Thielsch, L. Cramer, H.-P. Rust, H.-J. Freund, T. P. Pearl, and P. S. Weiss, *A double lamellae dropoff etching procedure for tungsten tips attached to tuning*

*fork atomic force microscopy/scanning tunneling microscopy sensors*, Review of Scientific Instruments **74** (2003), no. 2, 1027–1030.

[KT00] K. Karrai and I. Tiemann, *Interfacial shear force microscopy*, Phys. Rev. B **62** (2000), 62.

[LA06] M. Labardi and M. Allegrini, *Noncontact friction force microscopy based on quartz tuning fork sensors*, Appl. Phys. Lett. **89** (2006), 174104.

[LBBC95] D. Van Labeke, F. Baida, D. Barchiesi, and D. Courjon, *A theoretical model for the inverse scanning tunneling optical microscope (istom)*, Optics Communications **114** (1995), no. 5-6, 470 – 480.

[Mar08] Frederico Martins, *From the parametric amplification in electric force microscopy to the scanning gate microscopy of quantum rings*, Ph.D. thesis, Université Joseph Fourier - Grenoble 1, 2008.

[MGCS04] Chris A. Michaels, Xiaohong Gu, D. Bruce Chase, and Stephan J. Stranick, *Near-field infrared imaging and spectroscopy of a thin film polystyrene/poly(ethyl acrylate) blend*, Appl. Spectrosc. **58** (2004), no. 3, 257–263.

[Mic00] *Microbeam analysis 2000 : Proceedings of the second conference of the international union of microbeam analysis societies held in kailua-koma, hawaii*, 2000.

[Min88] Marvin Minsky, *Memoir on inventing the confocal scanning microscope*, Scanning **10** (1988), 128–138.

[MJT+96] I. H. Munro, G. R. Jones, M. Tobin, DA Shaw, Y Levine, H Gerritsen, K van der Oord, and F Rommerts, *Confocal imaging using synchrotron radiation*, Journal of Electron Spectroscopy and Related Phenomena **80** (1996), 343 – 347, Proceedings of the 11th International Conference on Vacuum Ultraviolet Radiation Physics.

[Moe95] M. H. P. Moers, *Near-field optical microscopy*, Ph.D. thesis, University of Twente, 1995.

[Mom97] E. Momosaki, *A brief review of progress in quartz tuning fork resonators*, Proc. 1997 IEEE Interntl. Freq. Contr. Symp **56** (1997), 552–565.

[MWW87] Y. Martin, C. C. Williams, and H. K. Wickramasinghe, *Atomic force microscope–force mapping and profiling on a sub 100-[a-ring] scale*, Journal of Applied Physics **61** (1987), no. 10, 4723–4729.

[NPH95] Lukas Novotny, Dieter W. Pohl, and Bert Hecht, *Light confinement in scanning near-field optical microscopy*, Ultramicroscopy **61** (1995), no. 1-4, 1 – 9, Selected Papers from the 3rd International Conference on Near-Field Optics and Related Techniques.

[Oht98] M. Ohtsu, *Near-field nano/atom optics and technology*, Springer-Verlag, 1998.

[PNHH96] D. W. Pohl, L. Novotny, B. Hecht, and H. Heinzelmann, *Radiation coupling and image formation in scanning near-field optical microscopy*, Thin Solid Films **273** (1996), no. 1-2, 161 – 167, International Symposium on Ultra Materials for Pico-transfer.

[Rad06] J. Radojewski, *Moving from micro- to nanoworld in optical domain scanning probe microscopy*, Bulletin of the Polish Academy of Sciences **54** (2006).

[Ray79] J.W. Strutt Lord Rayleigh, *Investigations in optics with special reference to the spectroscope*, Phil. Mag. **8** (1879), 261–274.

[RCB+02] N. Rochat, A. Chabli, F. Bertin, M. Olivier, C. Vergnaud, and P. Mur, *Attenuated total reflection spectroscopy for infrared analysis of thin layers on a semiconductor substrate*, Journal of Applied Physics **91** (2002), no. 8, 5029–5034.

[RGEH05] Jan Renger, Stefan Grafström, Lukas M. Eng, and Rainer Hillenbrand, *Resonant light scattering by near-field-induced phonon polaritons*, Phys. Rev. B **71** (2005), no. 7, 075410.

[RIS+99] J. Rychen, T. Ihn, P. Studerus, A. Herrmann, and K. Ensslin, *A low-temperature dynamic mode scanning force microscope operating in high magnetic fields*, Rev. Sci. Instrum. **70** (1999), 2765–2768.

[Rod09] M. Rodrigues, *Bringing light into the nanoworld. what can you do with an atomic force microscope on top of your synchrotron radiation sample holder?*, Ph.D. thesis, Université Joseph Fourier - Grenoble I, 2009.

[RvHRW99] W. H. J. Rensen, N. F. van Hulst, A. G. T. Ruiter, and P. E. West, *Atomic steps with tuning-fork-based noncontact atomic force microscopy*, Appl. Phys. Lett. **75** (1999), 1640.

[Sch05] *Detailed experience of synchrotron light extraction system with slotted mirror at the esrf*, 2005.

[SCZC07] Y. Seo, P. Cadden-Zimansky, and V. Chandrasekhar, *Low-temperature scanning force microscopy using a tuning fork transducer*, Korean Phys. Soc. **50** (2007), 378.

[SJH02] Y. Seo, W. Jhe, and C. S. Hwang, *Electrostatic force microscopy using a quartz tuning fork*, Appl. Phys. Lett. **80** (2002), 4324.

[SMS+01] B. C. Stipe, H. J. Mamin, T. D. Stowe, T. W. Kenny, and D. Rugar, *Noncontact friction and force fluctuations between closely spaced bodies*, Phys. Rev. Lett. **87** (2001), 96801.

[Suk04] S. V. Sukhov, *Role of multipole moment of the probe in apertureless near-field optical microscopy*, Ultramicroscopy **101** (2004), no. 2-4, 111 – 122.

[Syn28] E. H. Synge, *A suggested method for extending microscopic resolution into the ultra-microscopic region*, Philosophy Magazine **6** (1928), 356–362.

[TKH04] T. Taubner, F. Keilmann, and R. Hillenbrand, *Nanomechanical resonance tuning and phase effects in optical near-field interaction*, Nano Letters **4** (2004), 1669–1672.

[TKH05a] ———, *Effect of tip modulation on image contrast in scattering-type near-field optical microscopy*, JKPS **47** (2005), 213.

[TKH05b] Thomas Taubner, F. Keilmann, and R. Hillenbrand, *Nanoscale-resolved subsurface imaging by scattering-type near-field optical microscopy*, Opt. Express **13** (2005), no. 22, 8893–8899.

[Vis93] K. Visscher, *Optical micromanipulation and confocal microscopy*, Ph.D. thesis, Universiteit van Amsterdam, 1993.

[VMS+04] D. Vobornik, G. Margaritondo, J. S. Sanghera, P. Thielen, I. D. Aggarwal, B. Ivanov, J. K. Miller, R. Haglund, N. H. Tolk, A. Congiu-Castellano, M. A. Rizzo, D. W. Piston, F. Somma, G. Baldacchini, F. Bonfigli, T. Marolo, F. Flora, R. M. Montereali, A. Faenov, T. Pikuz, G. Longo, V. Mussi, R. Generosi,

M. Luce, P. Perfetti, and A. Cricenti, *Infrared near-field microscopy with the vanderbilt free electron laser: overview and perspectives*, Infrared Physics & Technology **45** (2004), no. 5-6, 409–416.

[Wal85] F.L. Walls, *Precision frequency control*, Academic Press (Orlando, Fla), 1985.

[WBG91] O. Wolter, Th. Bayer, and J. Greschner, *Micromachined silicon sensors for scanning force microscopy*, vol. 9, AVS, 1991, pp. 1353–1357.

[WFA03] Y. De Wilde, F. Formanek, and L. Aigouy, *Apertureless near-field scanning optical microscope based on a quartz tuning fork*, Review of Scientific Instruments **74** (2003), no. 8, 3889–3891.

[WFC+06] Yannick De Wilde, Florian Formanek, Remi Carminati, Boris Gralak, Paul-Arthur Lemoine, Karl Joulain, Jean-Philippe Mulet, Yong Chen, and Jean-Jacques Greffet, *Thermal radiation scanning tunnelling microscopy*, nature **444** (2006).

[Wic89] H. Kumar Wickramasinghe, *Scanned-probe microscopes*, J-SCI-AMER **261** (1989), no. 4, 74–81.

[Zan88] A. Zangwill, *Physics at surfaces*, Cambridge University Press, Cambridge, 1988.

# List of Figures

# Appendix A

# Technical Drawings

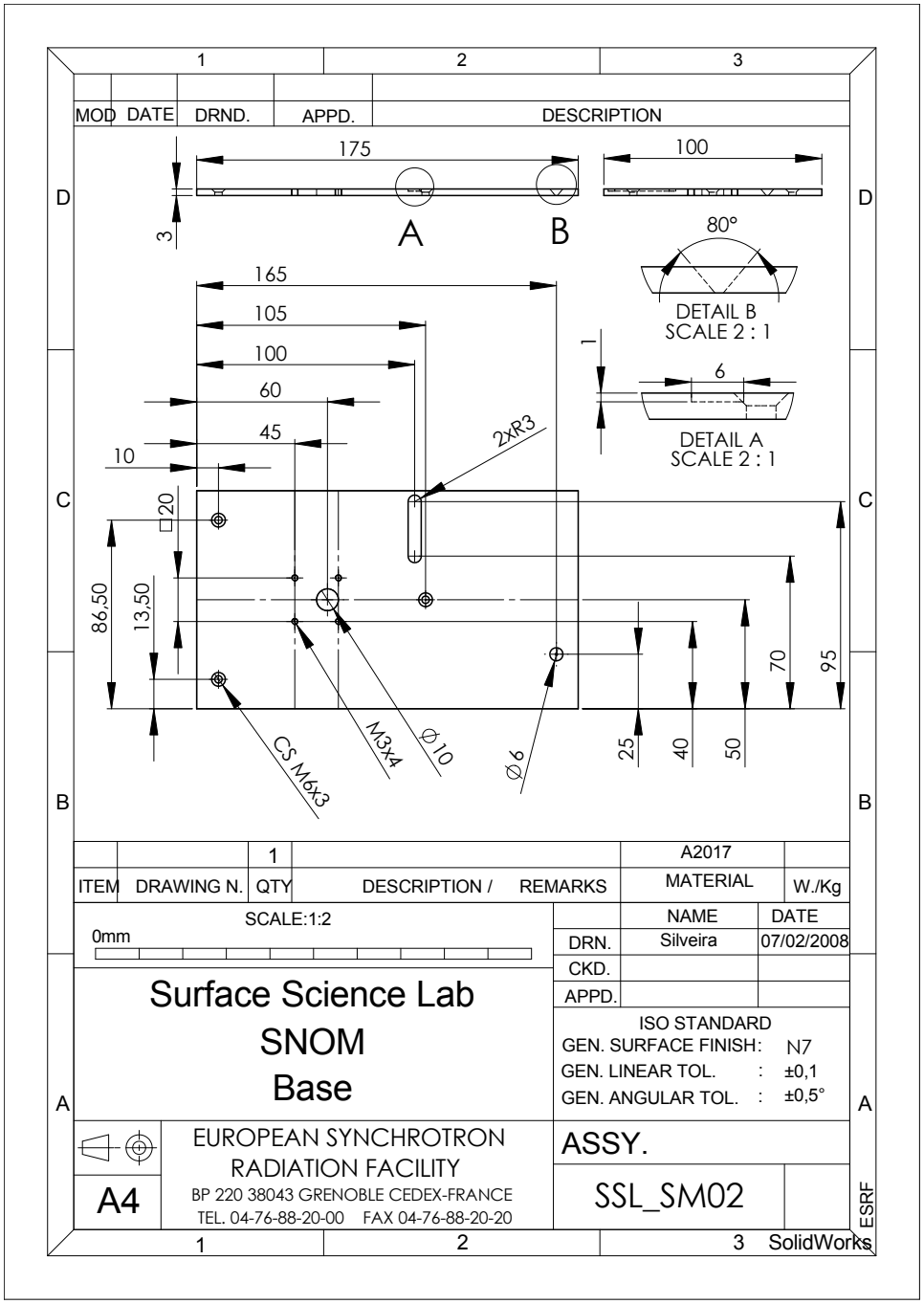
MOD DATE DRND. APPD. DESCRIPTION
175
100
3
A
B
80°
DETAIL B
SCALE 2 : 1
165
105
100
60
45
10
2xR3
1
6
DETAIL A
SCALE 2 : 1
□20
86,50
13,50
70
95
25
40
50
CS M6x3
M3x4
Ø10
Ø6
ITEM DRAWING N. QTY DESCRIPTION / REMARKS
A2017
MATERIAL
W./Kg
SCALE:1:2
0mm
NAME DATE
DRN. Silveira 07/02/2008
CKD.
APPD.
ISO STANDARD
GEN. SURFACE FINISH: N7
GEN. LINEAR TOL. : ±0,1
GEN. ANGULAR TOL. : ±0,5°
Surface Science Lab
SNOM
Base
EUROPEAN SYNCHROTRON
RADIATION FACILITY
BP 220 38043 GRENOBLE CEDEX-FRANCE
TEL. 04-76-88-20-00 FAX 04-76-88-20-20
ASSY.
SSL_SM02
A4
ESRF
SolidWorks

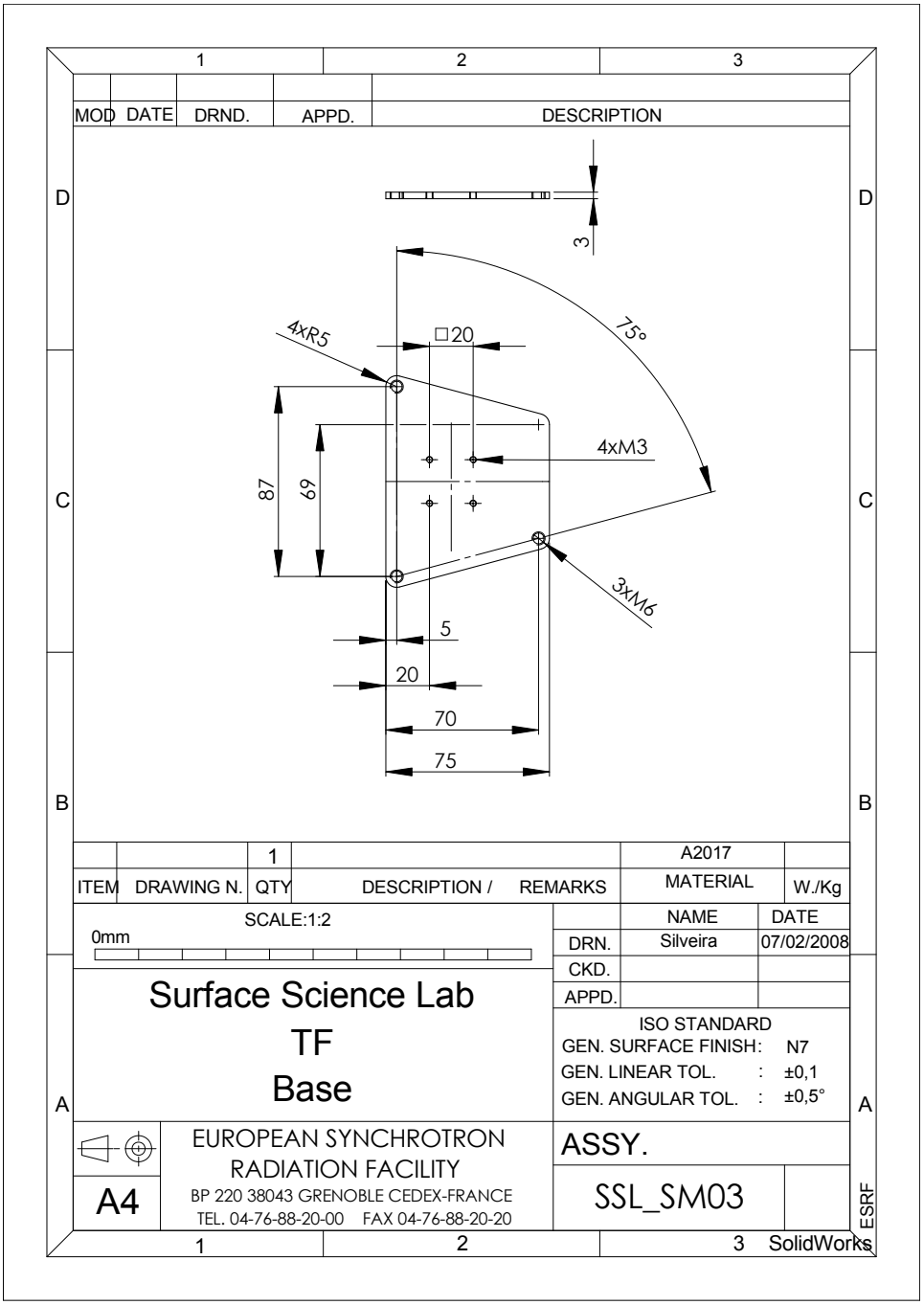
MOD DATE DRND. APPD. DESCRIPTION
3
75°
4xR5
□20
4xM3
87
69
3xM6
5
20
70
75
ITEM DRAWING N. QTY DESCRIPTION / REMARKS
1
A2017
MATERIAL
W./Kg
SCALE:1:2
0mm
NAME DATE
DRN. Silveira 07/02/2008
CKD.
APPD.
ISO STANDARD
GEN. SURFACE FINISH: N7
GEN. LINEAR TOL. : ±0,1
GEN. ANGULAR TOL. : ±0,5°
Surface Science Lab
TF
Base
EUROPEAN SYNCHROTRON
RADIATION FACILITY
BP 220 38043 GRENOBLE CEDEX-FRANCE
TEL. 04-76-88-20-00 FAX 04-76-88-20-20
ASSY.
A4
SSL_SM03
ESRF
SolidWorks

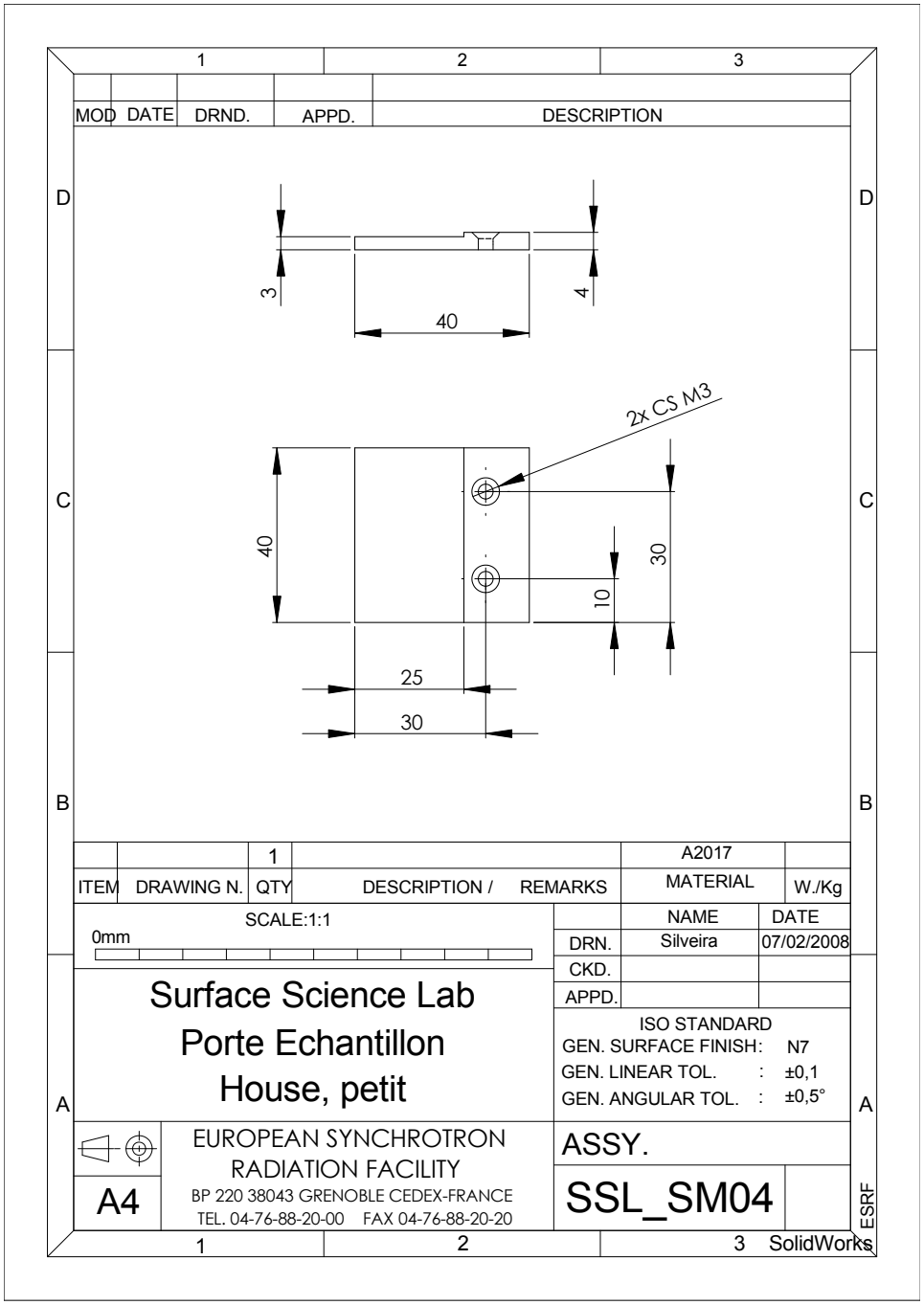
1
2
3
MOD DATE DRND. APPD. DESCRIPTION
D
C
B
A
3
4
40
2x CS M3
40
30
10
25
30
1
A2017
ITEM DRAWING N. QTY DESCRIPTION / REMARKS MATERIAL W./Kg
SCALE:1:1
0mm
NAME DATE
DRN. Silveira 07/02/2008
CKD.
APPD.
Surface Science Lab
Porte Echantillon
House, petit
ISO STANDARD
GEN. SURFACE FINISH: N7
GEN. LINEAR TOL. : ±0,1
GEN. ANGULAR TOL. : ±0,5°
EUROPEAN SYNCHROTRON
RADIATION FACILITY
BP 220 38043 GRENOBLE CEDEX-FRANCE
TEL. 04-76-88-20-00 FAX 04-76-88-20-20
ASSY.
A4
SSL_SM04
ESRF
SolidWorks

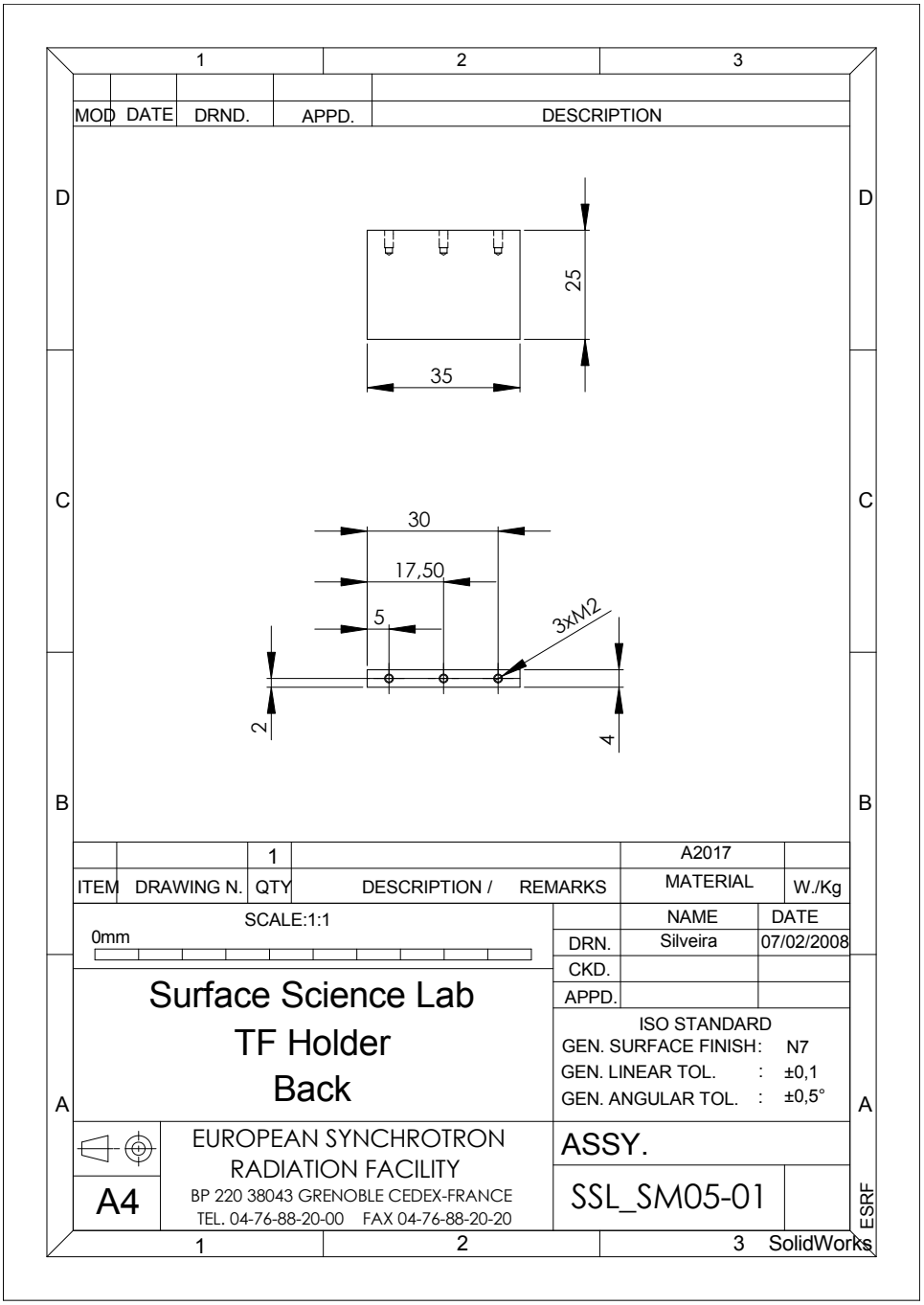
1
2
3
MOD DATE DRND. APPD. DESCRIPTION
D
C
B
A
25
35
30
17,50
5
3xM2
2
4
1
A2017
ITEM DRAWING N. QTY DESCRIPTION / REMARKS MATERIAL W./Kg
SCALE:1:1
0mm
NAME DATE
DRN. Silveira 07/02/2008
CKD.
APPD.
Surface Science Lab
TF Holder
Back
ISO STANDARD
GEN. SURFACE FINISH: N7
GEN. LINEAR TOL. : ±0,1
GEN. ANGULAR TOL. : ±0,5°
EUROPEAN SYNCHROTRON
RADIATION FACILITY
BP 220 38043 GRENOBLE CEDEX-FRANCE
TEL. 04-76-88-20-00 FAX 04-76-88-20-20
ASSY.
A4
SSL_SM05-01
ESRF
SolidWorks

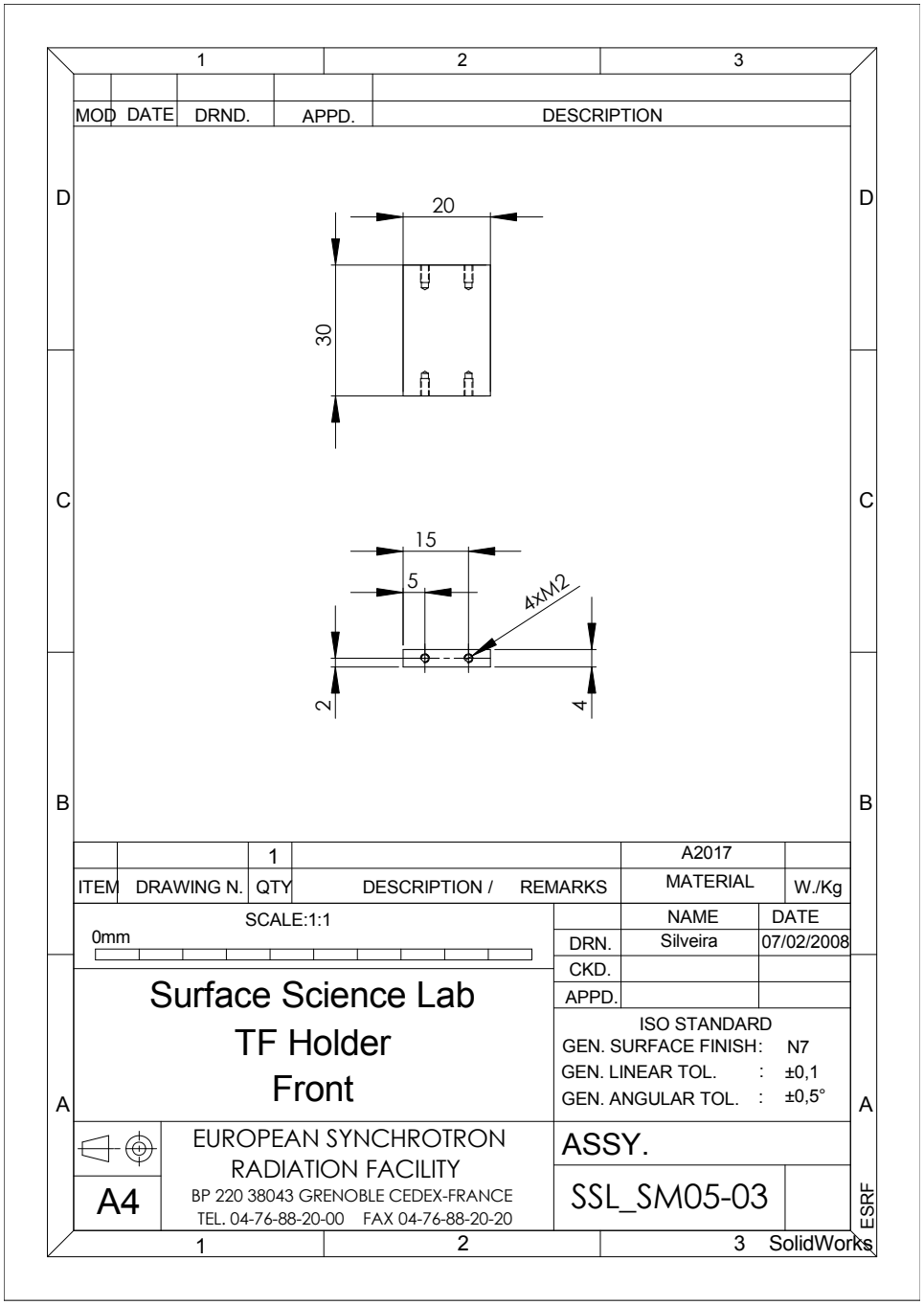
1
2
3
MOD DATE DRND. APPD. DESCRIPTION
D
C
B
A
20
30
15
5
4xM2
2
4
1
A2017
ITEM DRAWING N. QTY DESCRIPTION / REMARKS MATERIAL W./Kg
SCALE:1:1
0mm
NAME DATE
DRN. Silveira 07/02/2008
CKD.
APPD.
Surface Science Lab
TF Holder
Front
ISO STANDARD
GEN. SURFACE FINISH: N7
GEN. LINEAR TOL. : ±0,1
GEN. ANGULAR TOL. : ±0,5°
EUROPEAN SYNCHROTRON
RADIATION FACILITY
BP 220 38043 GRENOBLE CEDEX-FRANCE
TEL. 04-76-88-20-00 FAX 04-76-88-20-20
ASSY.
A4
SSL_SM05-03
ESRF
SolidWorks

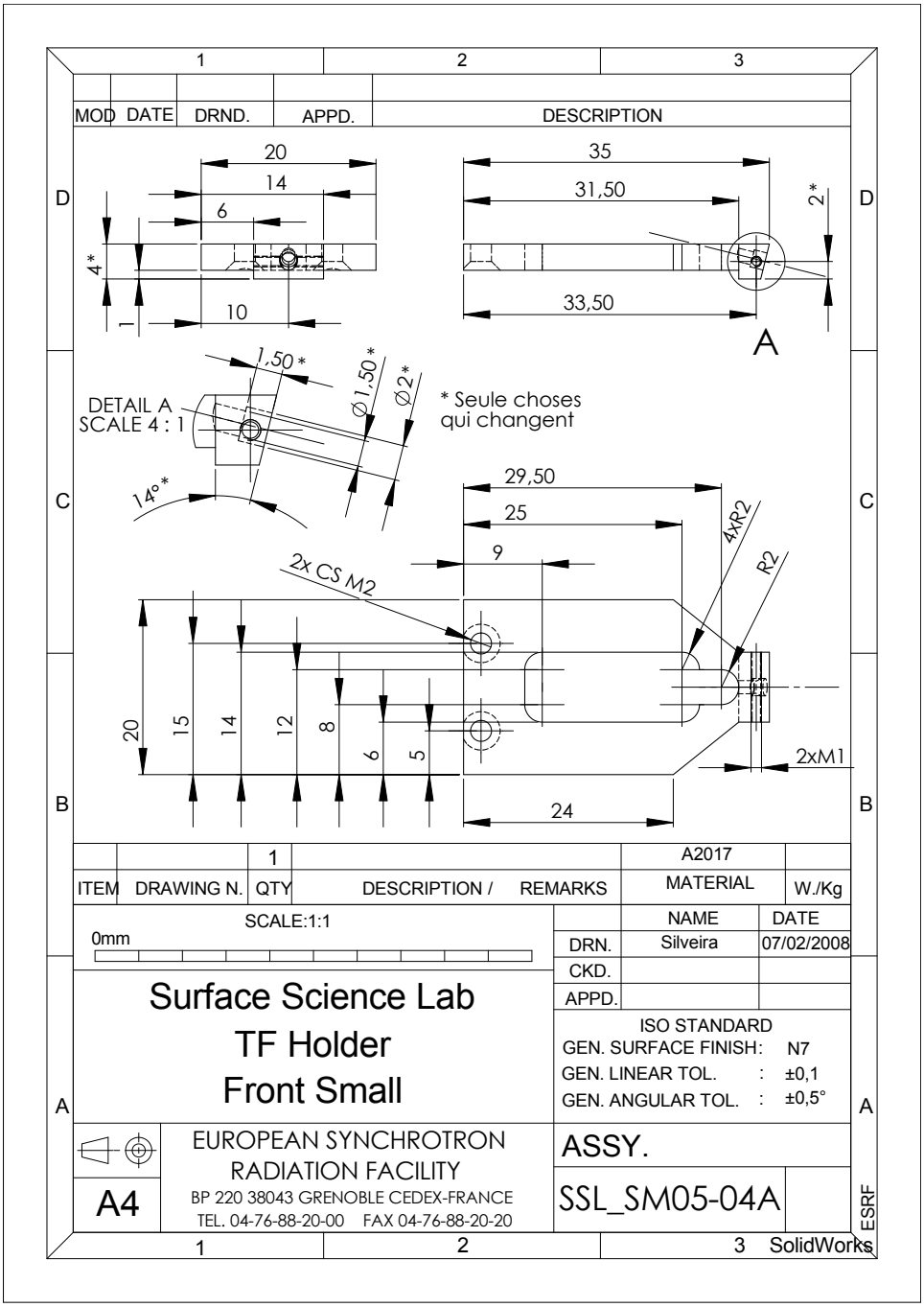
MOD DATE DRND. APPD. DESCRIPTION
20
14
6
4*
1
10
35
31,50
2*
33,50
A
1,50*
Ø1,50*
Ø2*
DETAIL A
SCALE 4 : 1
* Seule choses
qui changent
14°*
29,50
25
9
4xR2
R2
2x CS M2
20
15
14
12
8
6
5
2xM1
24
ITEM DRAWING N. QTY DESCRIPTION / REMARKS
A2017
MATERIAL
W./Kg
SCALE:1:1
0mm
NAME DATE
DRN. Silveira 07/02/2008
CKD.
APPD.
Surface Science Lab
TF Holder
Front Small
ISO STANDARD
GEN. SURFACE FINISH: N7
GEN. LINEAR TOL. : ±0,1
GEN. ANGULAR TOL. : ±0,5°
EUROPEAN SYNCHROTRON
RADIATION FACILITY
BP 220 38043 GRENOBLE CEDEX-FRANCE
TEL. 04-76-88-20-00 FAX 04-76-88-20-20
ASSY.
A4
SSL_SM05-04A
ESRF
SolidWorks

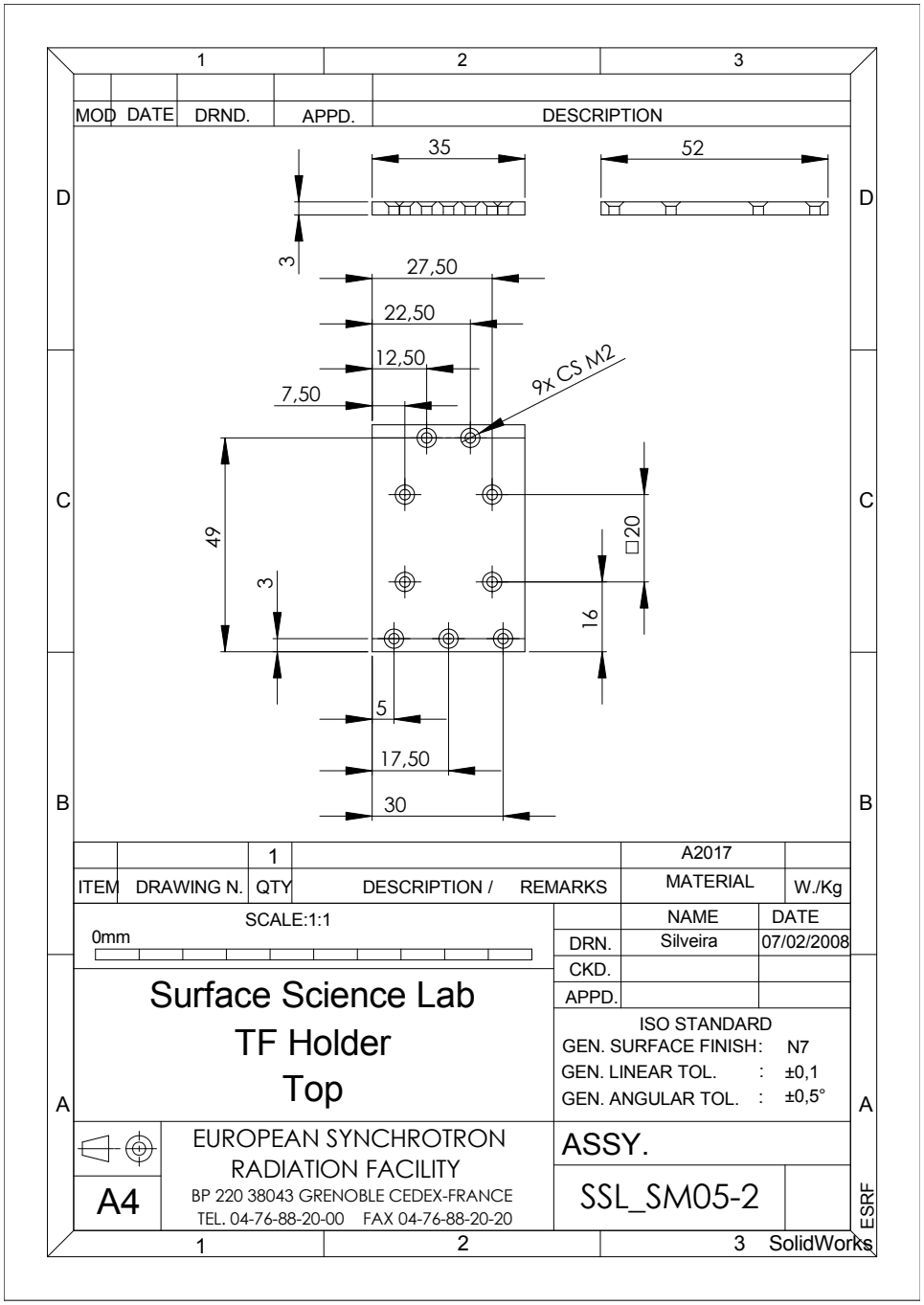
MOD DATE DRND. APPD. DESCRIPTION
35
52
3
27,50
22,50
12,50
7,50
9x CS M2
49
3
□20
16
5
17,50
30
ITEM DRAWING N. QTY DESCRIPTION / REMARKS
1
A2017
MATERIAL
W./Kg
SCALE:1:1
0mm
NAME DATE
DRN. Silveira 07/02/2008
CKD.
APPD.
Surface Science Lab
TF Holder
Top
ISO STANDARD
GEN. SURFACE FINISH: N7
GEN. LINEAR TOL. : ±0,1
GEN. ANGULAR TOL. : ±0,5°
EUROPEAN SYNCHROTRON
RADIATION FACILITY
BP 220 38043 GRENOBLE CEDEX-FRANCE
TEL. 04-76-88-20-00 FAX 04-76-88-20-20
ASSY.
A4
SSL_SM05-2
ESRF
SolidWorks